PHENOMENOLOGY OF PURE-GAUGE HIDDEN VALLEYS AT HADRON COLLIDERS

BY JOSE E. JUKNEVICH

A dissertation submitted to the
Graduate School—New Brunswick
Rutgers, The State University of New Jersey
in partial fulfillment of the requirements
for the degree of
Doctor of Philosophy
Graduate Program in Physics and Astronomy
Written under the direction of
Professor Matthew J. Strassler
and approved by

_____

_____

_____

_____

_____

New Brunswick, New Jersey
October, 2010

ABSTRACT OF THE DISSERTATION

Phenomenology of Pure-Gauge Hidden Valleys at Hadron Colliders

by Jose E. Juknevich

Dissertation Director: Professor Matthew J. Strassler

Expectations for new physics at the LHC have been greatly influenced by the Hierarchy problem of electroweak symmetry breaking. However, there are reasons to believe that the LHC may still discover new physics, but not directly related to the resolution of the Hierarchy problem. To ensure that such a physics does not go undiscovered requires precise understanding of how new phenomena will reveal themselves in the current and future generation of particle-physics experiments. Given this fact it seems sensible to explore other approaches to this problem; we study three alternatives here.

In this thesis I argue for the plausibility that the standard model is coupled, through new massive charged or colored particles, to a hidden sector whose low energy dynamics is controlled by a pure Yang-Mills theory, with no light matter. Such a sector would have numerous metastable "hidden glueballs" built from the hidden gluons. These states would decay to particles of the standard model. I consider the phenomenology of this scenario, and find formulas for the lifetimes and branching ratios of the most important of these states. The dominant decays are to two standard model gauge bosons or to fermion-antifermion pairs, or by radiative decays with photon or Higgs emission, leading to jet- and photon-rich signals, and some occasional leptons. The presence of effective operators of different mass dimensions, often competing with each other, together with a great diversity of states, leads to a great variability in the lifetimes and decay modes of the hidden glueballs. I find that most of the operators considered in this work are not heavily constrained by precision electroweak physics, therefore leaving plenty of room in the parameter space to be explored by the future experiments at the LHC. Finally, I

discuss several issues on the phenomenology of the new massive particles as well as an outlook for experimental searches.

Acknowledgements

First, I would like to thank my advisor Matthew Strassler for his guidance, help and support during these years. His unique way of approaching physics has opened my mind to new possibilities. I am very grateful to Prof. Emanuel Diaconescu for his support during my first years at Rutgers and to Dmitry Melnikov for many interesting physics discussions. Thanks go also to all of the Professors at the NHETC from whom I have learned many valuable lessons, through courses and collaborations. From my first steps in theoretical physics I have had the guidance of my M.S. advisor Gerardo Aldazabal; he has always been there when I needed him. I would also like to thank Diane Soyak for all her support, and Prof. Ron Ransome for his constant help through my graduate studies.

I would like thank my fellow students and friends at Rutgers: Evgeny, Haile, Iskander, Sam, Korneel and Jeff for the stimulating discussions, and for all the good moments we have had in the last five years.

My time at Rutgers was made enjoyable in large part due to the many friends that became a part of my life. I am very grateful to my friends in New Jersey: Luca, Merce, Stacey, Greg and Vale, the Mosteiro family, Alberto, Roberto, Marcos, Loreto, Silvia and Nuria. They have changed my life in the US. My deepest gratitude goes my housemates and friends Gonza, Nachi and Gabi for their support through good and bad times during my last five years; this dissertation is simply impossible without them. I am also indebted to my best friends in Bahia Blanca, Seba and Leo, for all the good times and wonderful asados. Lastly, I would like to thank my family for all their love and encouragement. I would not have been able to make it without the support and love from my parents.

Dedication

Para Mamá y Papá.

Por enseñarme las cosas importantes de la vida.

Table of Contents

List of Figures

Chapter 1
Introduction and overview

The last century has seen revolutionary discoveries in particle physics, where a vast number of ambitious experiments have been conducted in concordance with major theoretical breakthroughs. The Standard Model (SM) has emerged as the best construct for explaining the range and behavior of particle interactions, as it has ability to explain a wide range of observed phenomena down to distances of order of 10^{-16} centimeters. Its electroweak sector has been probed to better than 1% level by precision experiments at low energy as well as at the Z-pole by LEP and SLC, severely constraining possible extensions of the SM at the TeV scale [1].

Yet, there are high hopes that new phenomena beyond the Standard Model are awaiting to be discovered already at the TeV scale. The reason is founded on the principle of naturalness, according to which the parameters of a low energy effective theory should not be much smaller than the contributions that come from running them up to the cutoff. Applying this principle to the Standard Model means that despite its incredible precision this theory cannot be complete due to an instability in the Higgs sector: radiative corrections to the mass parameter in the Higgs potential tend to scale with the largest mass scale in the theory M, with M being the Planck scale or any other high energy scale. If M is too large, the Higgs mass must be fine-tuned to an accuracy of order $(M_W/M)^2$ to explain the weak scale. In the absence of highly unnatural fine-tuning of the parameters in the underlying theory, the stabilization of the electroweak scale would then suggest the existence of new particles at the TeV scale.

Our best hope for the resolution of the hierarchy problem is now at the Large Hadron Collider (LHC) at the CERN laboratory in Geneva. With the LHC, particle physics enters a new era of potential discovery, one which may provide insights into the many puzzles of the SM. Given the immense challenges of hadron collider physics, and the degree to which the future of particle physics rests on the LHC, it is important to ensure that the LHC community is fully prepared for whatever might appear in the data. This requires consideration of a wide variety of models and signatures in advance of the experimental program.

Most of the effort for searches of physics beyond the Standard Model (BSM) has focused on "minimal" models which solve the hierarchy problem. The most favored solution is presently

Supersymmetry (SUSY), with others including the little Higgs, warped extra dimensions and technicolor. However, experience has taught us that the most striking experimental discoveries may a priori be unrelated to the fundamental questions. We have also learned that BSM physics may be especially difficult to discover, either because SM backgrounds are large or because special discriminating variables are needed to extract a signal from backgrounds. Therefore, it is prudent that we explore as many scenarios for BSM physics as possible, with particular emphasis on models with varied experimental signatures, to ensure that their signatures would not be missed at the LHC.

Among the extensions of the SM not directly tied to electroweak symmetry breaking, those with an additional $U(1)$ factor in the gauge group, associated with a heavy neutral gauge boson Z', have often been considered in direct and indirect searches for new physics, and in the studies of possible early discoveries at the LHC (for recent reviews and references, see e.g. [2–4]). While not prescribed by compelling theoretical or phenomenological arguments, these extensions naturally arise from Grand Unified Theories (GUTs) based on groups of rank larger than four and from higher-dimensional constructions such as string compactifications. Z' bosons also appear in little Higgs models, composite Higgs models, technicolor models and other more or less plausible scenarios for physics at the Fermi scale.

One likely possibility for new non-minimal physics involves the presence of a hidden sector with TeV-scale couplings to the standard model. A large fraction of these models fall within the "hidden valley scenario" [6–11]. In the hidden valley scenario, a new hidden sector (the "hidden valley sector", or "v-sector" for short) is coupled to the SM in some way at or near the TeV scale, in such a way that the cross sections for SM visible particles disappearing into the hidden sector are small enough to evade the current experimental limits, and yet large enough to be observable at LHC. Typically, the valley particles "v-particles" are charged under a valley group G_v and neutral under the SM group G_{SM} , and the SM particles are neutral under G_v. The v-sector's dynamics also generates a mass gap. Such a mass gap,[1] independent of the dynamics leading to that gap, ensures that there are particles that are stable or metastable within the v-sector. These can only decay, if at all, via their very weak interactions with the SM. A common choice is to have a coupling via a Z' or via loops of heavy particles carrying both G_{SM} and G_v charges. Processes that access the hidden valley are often quite unusual compared to those in minimal supersymmetric or other well-studied models. Production of v-sector particles commonly leads to final states with a high multiplicity of SM particles. Also,

[1] or more generally a mass "ledge" where one or more new particles in the hidden sector, unable to decay within its own sector, is forced to decay via its weak coupling to the SM sector

a hidden valley often leads to particles that decay with macroscopic decay distances. The resulting phenomenological signatures can be difficult, or at least subtle, for detection at the Tevatron or LHC; see for example [6, 7, 11].

Hidden valleys have arisen in bottom-up models such as the twin Higgs and folded supersymmetry models [12, 13] that attempt to address the hierarchy problem, and in a recent attempt to explain the various anomalies in dark-matter searches [17] which requires a dark sector with a new force and a 1 GeV mass scale. They are also motivated by top-down model building: hidden sectors that are candidate hidden valleys arise in many string theory models, see for example [18]. In recent years string theorists have found many models that apparently have the minimal supersymmetric standard model as the chiral matter of the theory, but which typically have extra vector-like matter and extra gauge groups. The non-minimal particles and forces which arise in these various models may very well be visible at the LHC [6].

Interestingly enough, the case in which the hidden sector consists of some new vectorlike particles X and $\bar{X}$ that couple to a new confining gauge group $SU(n_v)$ leads to a surprisingly exotic phenomenology, if the following condition is satisfied:

$$M_X \gg \Lambda_v, \tag{1.1}$$

where M_X is the X mass and Λ_v is the scale where the $SU(n_v)$ gauge coupling gets strong. The reason is that, once produced, the X particles are eternally bound by an $SU(n_v)$ confining string, leading to a quite unusual, "quirky" phenomenology. By this reason, the X particles have been dubbed "quirks". This model was first considered in [47, 48], and more recently in [49]. In [6], this model was also mentioned as an example of a hidden valley model.

In this dissertation we attempt to continue this effort by exploiting the ideas of hidden valleys and quirks in order to extract concrete predictions for a variety of experiments at the LHC. A full study of all classes of hidden valleys is not feasible, and would not be particularly useful, given that many models are less likely to be found than others. Therefore in this thesis we focus on a hidden valley that at low energy is a pure-Yang-Mills theory, a theory that has its own gluons ("v-gluons") and their bound states ("v-glueballs") [19]. This scenario easily arises in models; for example, in many supersymmetric v-sectors, supersymmetry breaking and associated scalar expectation values may lead to large masses for all matter fields.

In these theories there are two interesting subjects to consider, which will comprise the bulk of this thesis. The first subject is determining under what circumstances hidden valleys can give signals that might result interesting and often difficult for the LHC experiments to detect, so as to assure no phenomena are overlooked. The questions we will attempt to answer are of

phenomenological origin: What new physics are we looking for? What are their mass scales? How do they couple to SM fields? and what are their signatures? To answer these questions, we will need to construct the low-energy effective action coupling the two sectors. Then we will use it to compute formulas for the partial widths of various decay modes of the v-glueballs, concentrating on the lighter v-glueball states, which we expect to be produced most frequently. This is accomplished in chapters 2 and 3 in two different hidden valley models.

The "pure glue" hidden valleys are phenomenologically interesting candidates for what new phenomena may lie at the TeV scale, which might represent our first indication of an even richer structure at even higher energies. They have a number of attractive features from both theoretical and experimental point of view, as well as prospects for rich LHC phenomenology. Hidden valley confinement can indeed lead to a very rich spectrum of accessible v-glueball physics, as we shall discuss below. But because the dominant bridge between the SM and the new physics is provided by the very weak interactions induced by TeV scale mediator fields, the new physics is not in conflict with existing experiments, and will be more stringently tested in the near future. Furthermore, assuming that the mediators transform in vectorlike representation of SM gauge group, one can naturally evade precision electroweak tests.

While pure glue hidden valleys involve very modest additions to the SM, as measured by either the fundamental particle content or complexity of Lagrangian, it can naturally give rise to a remarkable array of distinct experimental behaviors, including di-gauge-boson resonances, fermion pairs, radiative decays with photon and/or Higgs emission and long-lived neutral states, leading to jet- and photon-rich signals and perhaps displaced vertices. In this thesis we show how such signals can arise in the hidden valley scenario which has very few parameters and need not be tuned to avoid exclusion. Some of these signals have appeared previously in other scenarios, but often within models which are tightly constrained already by experiments. We will also see that there are some qualitatively distinct signals that have not been discussed before, such as displaced vertices coexisting with prompt diphoton resonances.

The second subject is related to the question of whether the aforementioned signatures are likely to be detectable at the LHC. To discover a promptly decaying v-glueball, the cleanest signature would be its decay to two photons, from which a resonance can be reconstructed. Late decaying v-glueballs are more complicated, since displaced jet pairs have no physics background but suffer from various detector and triggering issues, and detection of displaced photon pairs is often difficult and very dependent upon details of the detector. In either case, a full study of signal and background is subtle because the dynamics of the production process (e.g. non-perturbative glueball emission) are not calculable either analytically or numerically, and cannot

be compared with any known physical process. Besides, there is little that a theorist can do to study backgrounds from displaced vertices. So in this work we will limit ourselves to some discussion of the signal rates and of the most likely strategies for discovery.

This thesis is aimed at highlighting some of the generic features of the rich phenomenology in the pure-gauge hidden valley scenario as well as demonstrating consistency with all present experimental data, both in the form of exclusion from direct searches as well as the non-observation of any virtual effect.

This thesis focuses on the papers [19,20,40] published during the course of graduate studies and on ongoing work [60]. Their results appear as follows:

- Chapter 2 is based on [19].
- Chapter 3 and section 5.2 is based on [20, 40]
- Section 4.6 is based on [40].
- Chapters 4 and 5 are based on [60] and contain work in progress.

The rest of this chapter contain a brief introduction to the theory of hidden valleys and quirks. In chapter 2 we will qualitatively describe the short distance physics in the hidden valley scenario with quirks, and set up an effective Lagrangian to compute the decay rates for some of the most important states. Next, in chapter 3 we will extend our results on pure gauge hidden valleys to include couplings of the quirks to the SM Higgs sector. We go on to discuss several issues on the phenomenology of bound states of quirks and their more salient features in chapter 4. Further details of the phenomenology as well as an outlook for experimental searches will be presented in chapter 5. Our conclusions will be summarized in chapter 6.

1.1 Hidden valleys

A hidden valley sector ("v-sector") is defined by the following properties, depicted in figure 1.1 [6]. First, like an ordinary hidden sector, it has its own gauge symmetries and matter particles, with the property that no light particles carry charges under both Standard Model gauge groups and under the v-sector gauge groups. A mass gap ensures that not all the particles in the v-sector decay to extremely-light, invisible particles. An energetic barrier resulting from the very weak interactions between the SM sector and the v-sector has prevented v-particle production at LEP. However, collisions of Standard Model particles at higher energy at the LHC may be able to go over the mountain to produce v-sector particles. Finally, massive long-lived v-sector particles can decay back to light standard model particles. These decays have

strongly suppressed rates but would be often observable at the LHC, sometimes with displaced vertices.

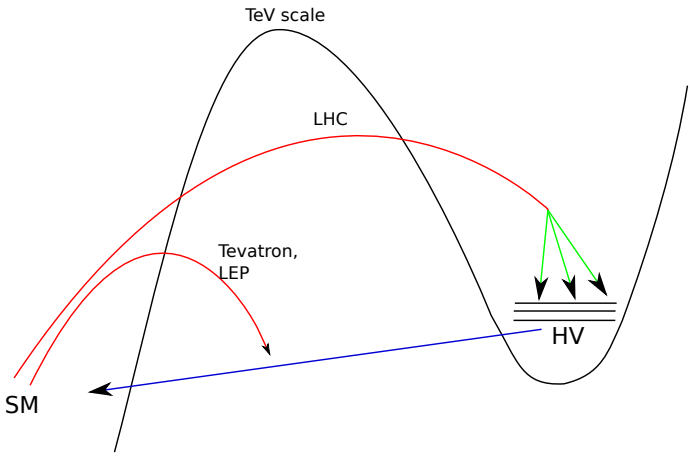

Figure 1.1: A despiction of a hidden valley. The mountain represents massive states which may connect the Standard Model sector to light states in the valley sector.

Among the representative hidden valley models are those whose gauge groups are strongly-interacting and confining, with the mass gap generated by the strong dynamics in the v-sector. A vast array of v-models are possible, as many as the imagination allows for (see figure 1.2) [14]. Some of the many choices for the type of v-sectors include, but are not limited to,

- QCD-like theory with F flavors, N colors
- QCD-like theory with only heavy fermions
- Pure-Yang-Mills theory
- Randall-Sundrum (RS) or Klebanov-Strassler (KS) throat
- Partially Higgsed $SU(N)$

The strong interactions cause the v-sector particles to confine at the scale Λ_v and form v-hadrons. A number of long-lived resonances will result. The strong-interactions also cause v-parton showering, following which, when the energy scale of a process is large enough compared to Λ_v, large numbers of v-hadrons may be simultaneously produced.

Finally, there are also many choices for the communicator fields, including many of the new heavy states that we have discussed in the introduction, such as

- Z'
- Higgs, or multiple Higgses

- Loops of heavy particles
- Heavy sterile neutrinos

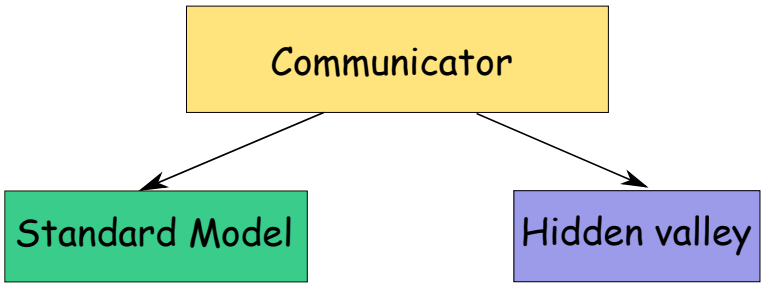

Figure 1.2: The class of models we are considering for a hidden sector.

The canonical example of a confining hidden valley, proposed by the authors of [6], is that of a QCD-like scenario, having only two light flavors with a $SU(N)$ gauge group. The dynamics of the model is determined by the confining scale Λ_v, where the strong coupling constant becomes strong. Light or heavy flavor is defined with respect to Λ_v : light quarks have masses $m_Q < \Lambda_v$ and heavy quarks have masses $m_v > \Lambda_v$. Production and decay processes of the hidden sector quarks ("v-quarks") can occur, for example, through a Z', whose charges are from an extra $U(1)_\chi$ gauge group. As in QCD, the v-quarks undergo a v-parton shower and form v-jets of v-hadrons. In the two light flavor model the v-hadrons are electrically neutral v-pions, $\pi_v^\pm$ and π_v^0, which are the analogue of SM $\pi^\pm$ and π^0 - the labels are simply meant to indicate the analogy with pions, they do not denote electric charge. Some of these v-hadrons can decay back to Standard Model particles, making a complex, high-multiplicity final state. This situation is illustrated in figure 1.3. Depending on parameters, the decays of the v-hadrons may be prompt or displaced.

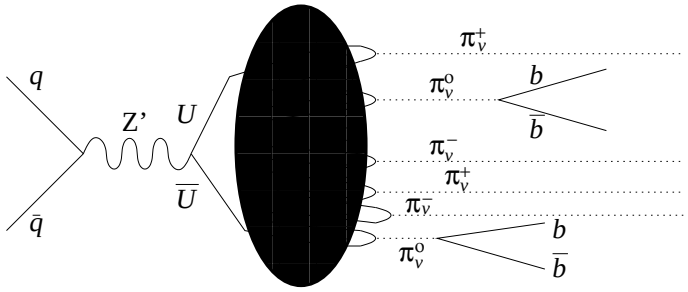

Figure 1.3: The production and hadronization of v-quarks.

This scenario was investigated by Strassler and Zurek with tools analogous to the ones used to simulate QCD [6]. It displays some rather startling features. For instance, a π_v could have a displaced decay in the muon spectrometer in the ATLAS detector, resulting in a large number

of charged hadrons traversing the spectrometer, or it could decay in the hadronic calorimeter producing a jet with no energy deposited in the electromagnetic calorimeter and no associated tracks in the inner detector. Experimental studies for these scenarios are currently under way, by the D0, CDF, LHCb, ATLAS and CMS collaborations.

This is just one simple model with two light flavors. However, the number of possibilities is huge, and it is possible to think of other simple variants. For example, in the case of one light flavor instead of two, the phenomenology is widely different. In this case, the light degrees of freedom are the η_v (pseudoscalar) and the ρ_v (pseudovector), with masses of order $m_v \simeq \Lambda_v$. It was shown in [6] that the ρ_v will decay democratically to all SM flavors. As a result, it may be possible to tag such events using multiple leptons from the decay of the vector. This aids the task of extracting a signal from the background.

However, in the case of hidden valleys with many light flavors, detection may be especially difficult [10]. These models predict a high multiplicity of v-hadrons, which in turn implies that the number of jets in their decay products will be especially large. So for jets produced in v-hadron decays, QCD backgrounds will be large and unknown, and any signal will be tough to extract.

The limit where there are no light v-quarks, but only a hidden sector with a low confinement scale is particularly interesting. In this case, the lightest states in the v-sector are glueballs of $SU(N)$ ("v-glueballs"). The v-color interactions ensure that all the heavy v-hadrons annihilate efficiently into v-glueballs. These can then decay back into SM states via their coupling to electroweak boson or the Higgs.

1.2 Quirks

Theories with an extra confining gauge group $SU(n_v)$ sector and some heavy matter fields charged under both SM and $SU(n_v)$ gauge group such that there is a large hierarchy between the masses of the matter fields, M_X, and the confining scale, Λ_v, give rise to very unusual dynamics [6, 47–49]. For this reason the quarks (or scalar quarks) of such a sector have been dubbed quirks [49]. To understand this, let us first recall the dynamics of normal QCD. Consider two heavy quarks that are produced back-to-back in a hard process. As the two quarks fly away from each other and their distance approaches $\Lambda_{\rm QCD}^{-1}$, confining dynamics sets in and creates a gluonic flux tube extending between them. When the local energy density in the flux tube is high enough it is energetically favorable to pair create a light quark anti-quark pair, breaking the tube. This mechanism of soft hadronization allows the two heavy quarks to hadronize

separately.

In the quirk scenario, on the other hand, such a soft hadronization mechanism is absent because there are no quarks with mass less than or comparable to Λ_v (see figure 4). The energy density in the flux tube, or more simply, the tension of the $SU(n_v)$ string, cannot exceed Λ_v^2 which is far less than the M_Q per Compton wavelength needed to create a heavy quirk anti-quirk pair. The splitting of the $SU(n_v)$ string by a quirk anti-quirk pair is indeed exponentially suppressed as $\exp(-M^2/\Lambda^2)$ [16]. In fact, one may view the entire process as single production of a highly excited bound state, quirkonium. All of the kinetic energy that the quirks posses at production, $\sqrt{s} - 2M_Q$, which is typically of order M_Q, can be interpreted as quirkonium excitation energy. This energy is radiated away into glueballs of $SU(n_v)$ and hadrons. Eventually the two quirks annihilate into lighter states.

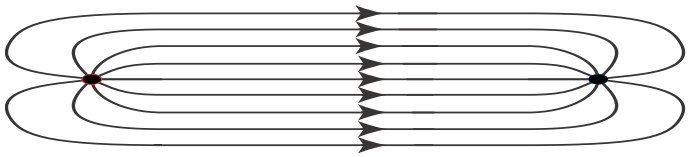

Figure 1.4: Pictorial diagram of quirk confinement. A flux tube of $SU(n_v)$ chromoelectric field forms between quirks. Since the mass of the quirks satisfies $M_X \gg \Lambda_v$, flux tube in $SU(n_v)$ are stable.

Because the quirks are very heavy, $M_Q \gg \Lambda_v$, the light degrees of freedom in the v-sector are glueballs of $SU(n_v)$. However, the standard model is uncharged under the new $SU(n_v)$ gauge group, and therefore a quirk loop is required to couple the sectors at low energies. As a result, effective couplings to the v-sector are highly suppressed at low energies. Specifically, the leading coupling between the standard model and the hiddden valley sector at low energies arises from a loop of virtual heavy quirks. This gives rise to dimension-8 effective operators of the form tr F^2tr G^2 and Ftr G^3, which mediate glueball decay, for example to photons or gluons.

The existence of additional gauge groups with matter in bifundamental representations is a hallmark of string theory model building. A quirk sector with vectorlike quirks and an extra gauge group $SU(n_v)$ sector can therefore arise naturally from string theory. It is also trivial to preserve gauge coupling unification in supersymmetric theories by assuming that the quirks come in complete GUT representations, e.g. $\mathbf{5} \oplus \bar{\mathbf{5}}$ and/or $\mathbf{10} \oplus \bar{\mathbf{10}}$ [15].

In fact, a quirk-like sector has already appeared in some supersymmetric extensions of the Standard Model motivated by the hierarchy problem. Such a sector was proposed in [15] to give additional loop contributions to the physical Higgs mass in supersymmetry. Scalar quirks appear in models of folded supersymmetry [13].

The collider phenomenology of quirks depends crucially on the length of the strings [49]. This is set by the scale where the kinetic energy is converted to potential energy of the string. Since the typical quirk pair production event is not close to threshold, the maximal length is

$$L = \frac{E}{\Lambda_v^2} \tag{1.2}$$

where $E = \sqrt{\hat{s}} - 2M$ is the kinetic energy of the quirks upon production. One can distinguish three different regimes.

- $100\text{eV} \lesssim \Lambda_\text{v} \lesssim 10\text{keV}$: In this case oscillations will be macroscopic. Since it takes many crossings before the quirks annihilate, one only observes the tracks of stable quirks in the detector.

- $10\text{keV} \lesssim \Lambda_\text{v} \lesssim 1\text{MeV}$: This is the case of mesoscopic strings. In this case one cannot resolve the oscillations, and the quirks look like a stable charged particle.

- $1\text{MeV} \lesssim \Lambda_\text{v} \lesssim 100\text{GeV}$: Here the strings are microscopic and the quirks get close enough to each other that they can annihilate. For $\Lambda_v \gtrsim \Lambda_\text{QCD}$ the annihilation is dominantly into gluons of $SU(n_v)$ gauge group, which at long distance become glueballs.

In the following we will be mostly interested in the case of microscopic strings where the quirks can annihilate producing visible signals.

So the overall picture in the quirk limit is that quirks are pair produced, and they fly away from each other, sometimes macroscopic distances before the string pulls them back together. They oscillate back and forth this way many times before the quirks can find each other and annihilate. Whether the annihilation occurs in the detector and whether the string oscillations are large enough to be visible will depend on the size of the confinement scale. We will see that the collider phenomenology will be very sensitive to the confinement scale in the hidden sector, leading to some remarkable, unstudied phenomena.

Chapter 2

A pure-glue hidden valley

In this chapter we consider a hidden valley that at low energy is a pure-Yang-Mills theory, a theory that has its own gluons ("v-gluons") and their bound states ("v-glueballs"). This scenario easily arises in models; for example, in many supersymmetric v-sectors, supersymmetry breaking and associated scalar expectation values may lead to large masses for all matter fields.

The spectrum of stable bound states in a pure Yang-Mills theory is known, to a degree, from lattice simulations [24]. The spectrum of such states for an $SU(3)$ gauge group is shown in figure 2.1. The spectrum includes many glueballs of mass of order the confinement scale Λ_v (actually somewhat larger), and various J^{PC} quantum numbers. All of the states shown are stable against decay to the other states, due to kinematics and/or conserved quantum numbers.

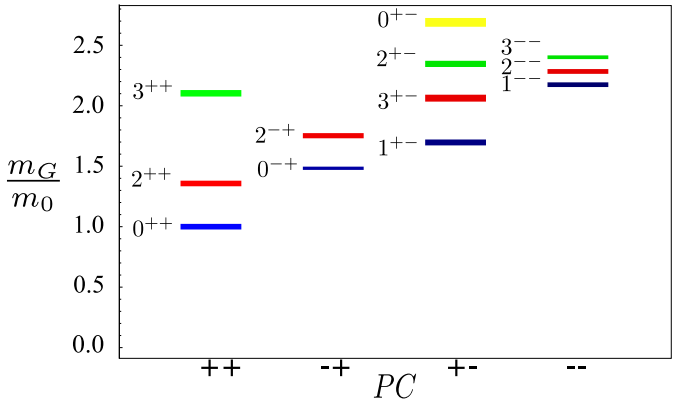

Figure 2.1: Spectrum of stable glueballs in pure glue $SU(3)$ theory [24].

In this work we will further specialize to the case where the coupling between the SM sector and the v-sector occurs through a multiplet of massive particles (which we will call X) charged under both SM-sector and v-sector gauge groups.[1] A loop of X particles[2] induces dimension-D

[1] Recently such states, considered long ago [47, 48], have been termed "quirks"; some of their very interesting dynamics, outside the regime we consider here, have been studied in [49].

[2] Much of the study covered in this and the next chapter was carried out before the proposal of [49] to name the X particles as "quirks". In most of the following discussion, the names "X particles" and "quirks" are used indistinctly.

operators of the form

$$\frac{1}{M^{D-4}}\mathcal{O}_s^{(D-d)}\mathcal{O}_v^{(d)} \tag{2.1}$$

where M is the mass of the heavy particle in the loop. Here we have split the dimension-D operator $\mathcal{O}^{(D)}$ into a Standard-Model part $\mathcal{O}_s^{(D-d)}$ of dimension $D-d$ and a hidden-valley part $\mathcal{O}_v^{(d)}$ of dimension d. All v-glueball states can decay through these operators.

By simple dimensional analysis, these operators yield partial decay widths of order $\Lambda_v^{2D-7}/M^{2D-8}$. We will see that the v-glueball decays are dominated by $D = 8$ operators. The next operators have $D = 10$, and their effects are typically suppressed by $\sim (\Lambda_v/M)^4$. The $D = 8$ operators induce lifetimes for the v-glueballs of order M^8/Λ^9, which can range anywhere from 10^{-20} seconds to much longer than a second, depending on the parameters. Implicitly our focus is on the case where the lifetimes are short enough that at least a few decays can be observed in an LHC detector. This typically requires lifetimes shorter than a micro-second, if the production cross-section is substantial.[3] However, our formulas will be valid outside this regime as well.

We will need to construct the $D = 8$ effective action coupling the two sectors. Then we will use it to compute formulas for the partial widths of various decay modes of the v-glueballs, concentrating on the lighter v-glueball states, which we expect to be produced most frequently.

Application of our formulas, particularly as relevant for the LHC, will be carried out in chapter 5. To put the present work in context, we now briefly review the results to be presented there. Although there are some irreducible uncertainties due to unknown glueball transition matrix elements and decay constants, we find that the various v-glueball states have lifetimes that probably span 3 or 4 orders of magnitude. We also find that the dominant v-glueball decays are to SM gauge-boson pairs, or radiative decays to another v-glueball and a photon (or perhaps a Z boson.) We will demonstrate that detection should be straightforward, if the mass M of the quirk X is small enough to give a reasonable cross-section, and Λ_v is large enough to ensure the v-glueballs decay promptly. Several v-glueballs form di-photon resonances, which should be easy to detect if their decays are prompt. Unlike [10], or especially [11], it appears that traditional cut-based analysis on ordinary events with jets and photons will be sufficient. For displaced decays, however, special experimental techniques are always needed. There are a number of different signatures, and the optimal search strategy is not obvious.

This chapter is organized as follows. In Sec. 2, we introduce our model and systematically describe the v-sector operators and the v-glueball states. In Sec. 3, we describe the effective

[3]To avoid any confusion, we emphasize again that these v-glueballs have extremely weak interactions with the standard model, and do not interact with the detector (in contrast to R-hadrons, which are made from QCD-colored constituents and have nuclear-strength interactions.) They can only be detected directly through their decay to standard model particles.

action coupling the two sectors and the SM matrix elements relevant for the decays. Our main results for the decay modes and their branching fractions appear in Sec. 4. We conclude in Sec. 5 with some final comments and perspective. Additional results appear in the Appendix.

2.1 The model and the hidden valley sector

2.1.1 Description of the Model

Consider adding to the standard model (SM) a new gauge group G, with a confinement scale Λ_v in the 1–1000 GeV range. We will refer to this sector as the "hidden valley", or the "v-sector" following [6]. What makes this particular confining hidden valley special is that it has no light charged matter; its only light fields are its gauge bosons, which we will call "hidden gluons" or "v-gluons". At low energy, confinement generates (meta)stable bound states, "v-glueballs", from the v-gluons. The SM is coupled to the hidden valley sector only through heavy fields X_r, in vector-like representations of both the SM and G, with masses of order the TeV scale. These states can be produced directly at the LHC, but because of v-confinement they cannot escape each other; they form a bound state which relaxes toward the ground state and eventually annihilates. The products of the annihilation are often v-glueballs. (Other annihilations lead typically to a hard pair or trio of standard model particles.) Thereafter, the v-glueballs decay, giving a potentially visible signal.

For definiteness, we take the gauge group G to be $SU(n_v)$, and the particles X_r to transform as a fundamental representation of $SU(n_v)$ and in complete $SU(5)$ representations of the Standard Model, typically $\mathbf{5}+\bar{\mathbf{5}}$ and/or $\mathbf{10}+\overline{\mathbf{10}}$. We label the fields and their masses as shown[4] in table 3.1. In this work, we will calculate their effects as a function of m_r. The approximate

Field	$SU(3)$	$SU(2)$	$U(1)$	$SU(n_v)$	Mass
$X_{\bar{d}}$	$\mathbf{3}$	$\mathbf{1}$	$\frac{1}{3}$	$\mathbf{n_v}$	$m_{\bar{d}}$
X_ℓ	$\mathbf{1}$	$\mathbf{2}$	$-\frac{1}{2}$	$\mathbf{n_v}$	m_ℓ
$X_{\bar{u}}$	$\overline{\mathbf{3}}$	$\mathbf{1}$	$-\frac{2}{3}$	$\mathbf{n_v}$	$m_{\bar{u}}$
X_q	$\mathbf{3}$	$\mathbf{2}$	$\frac{1}{6}$	$\mathbf{n_v}$	m_q
X_e	$\mathbf{1}$	$\mathbf{1}$	$\mathbf{1}$	$\mathbf{n_v}$	m_e

Table 2.1: The new fermions X_r that couple the hidden valley sector to the SM sector.

global $SU(5)$ symmetry of the SM gauge couplings suggests that the masses $m_{\bar{d}}$ and m_ℓ should

[4]In this work, we normalize hypercharge as $Y = T_3 - Q$, where T_3 is the third component of weak isospin.

be roughly of the same order of magnitude, and similarly for the masses $m_q, m_{\bar{u}}, m_e$. It is often more convenient to express the answer as a function of the (partially redundant) dimensionless parameters

$$\rho_r \equiv m_r/M \ . \tag{2.2}$$

Here M is a mass scale that can be chosen arbitrarily; depending on parameters, it is usually most natural to take it to be the mass of the lightest X_r particle.

Integrating out these heavy particles generates an effective Lagrangian $\mathcal{L}_{\rm eff}$ that couples the v-gluons and the SM gauge bosons. The terms in the effective Lagrangian are of the form (2.1), with operators $\mathcal{O}_v^{(d)}$ constructed from the gauge invariant combinations[5] tr $\mathcal{F}_{\mu\nu}\mathcal{F}_{\alpha\beta}$ and tr $\mathcal{F}_{\mu\nu}\mathcal{F}_{\alpha\beta}\mathcal{F}_{\delta\sigma}$, contracted according to different irreducible representations of the Lorentz group.

The interactions in the effective action then allow the v-glueballs in figure 2.1, which cannot decay within the v-sector, to decay to final states containing SM particles and at most one v-glueball. This is analogous to the way that the Fermi effective theory, which couples the quark sector to the lepton sector, permits otherwise stable QCD hadrons to decay weakly to the lepton sector. As is also true for leptonic and semileptonic decays of QCD hadrons, our calculations for v-hadrons decaying into SM particles simplify because of the factorization of the matrix elements into a purely SM part and a purely hidden-sector part. To compute the v-glueball decays, we will only need the following factorized matrix elements, involving terms in the effective action of dimension eight:

$$\langle SM|\mathcal{O}_s^{(8-d)}|0\rangle\langle 0|\mathcal{O}_v^{(d)}|\Theta_\kappa\rangle \ , \tag{2.3}$$

$$\langle SM|\mathcal{O}_s^{(8-d)}|0\rangle\langle \Theta_{\kappa'}|\mathcal{O}_v^{(d)}|\Theta_\kappa\rangle \ . \tag{2.4}$$

Here d is the mass dimension of the operator in the v-sector, $\langle SM|$ schematically represents a state built from Standard Model particles, and $|\Theta_\kappa\rangle$ and $|\Theta_{\kappa'}\rangle$ refer to v-glueball states with quantum numbers κ, which include spin J, parity P and charge-conjugation C. We will see later that we only need to consider $d = 4$ and 6; there are no dimension $D = 8$ operators in $\mathcal{L}_{\rm eff}$ for which $d = 5$, since there are no appropriate dimension-three SM operators to compensate. The SM part $\langle SM|\mathcal{O}_s^{(8-d)}|0\rangle$ can be evaluated by the usual perturbative methods of quantum field theory, but a computation of the hidden-sector matrix elements $\langle 0|\mathcal{O}_v^{(d)}|\Theta_\kappa\rangle$ and $\langle \Theta_{\kappa'}|\mathcal{O}_v^{(d)}|\Theta_\kappa\rangle$ requires the use of non-perturbative methods.

[5]Here we represent the v-gluon fields as $\mathcal{F}_{\mu\nu} = \mathcal{F}^a_{\mu\nu}\, T^a$, where T^a denote the generators of the $SU(n_v)$ algebra with a common normalization tr $T^a T^b = \frac{1}{2}\,\delta^{ab}$.

2.1.2 Classification of v-glueball states

In this section we shall classify the nonvanishing v-sector matrix elements. A v-glueball state Θ_κ with quantum numbers J^{PC} can be created by certain operators $\mathcal{O}_v^{(d)}$ acting on the vacuum $|\,0\rangle$. We wish to know which matrix elements, $\langle 0|\mathcal{O}_v^{(d)}|\Theta_\kappa\rangle$ and $\langle\Theta'_\kappa|\mathcal{O}_v^{(d)}|\Theta_\kappa\rangle$, are nonvanishing. This is equivalent to finding how the operators in various Lorentz representations are projected onto states with given quantum numbers J^{PC}. Their classification was carried out in [46]. At mass dimension $d = 4$ there are four different operators transforming in irreducible representations of the Lorentz group. These are shown[6] in table 2.2. From now on, we denote the operators $\mathcal{O}_v^\xi$, where ξ runs over different irreducible operators $\xi = S, P, T, L, \cdots$.

Operator $\mathcal{O}_v^\xi$	J^{PC}
$S = \mathrm{tr}\ \mathcal{F}_{\mu\nu}\mathcal{F}^{\mu\nu}$	0^{++}
$P = \mathrm{tr}\ \mathcal{F}_{\mu\nu}\tilde{\mathcal{F}}^{\mu\nu}$	0^{-+}
$T_{\alpha\beta} = \mathrm{tr}\ \mathcal{F}_{\alpha\lambda}\mathcal{F}_\beta{}^\lambda - \frac{1}{4}\, g_{\alpha\beta} S$	2^{++}, 1^{-+}, 0^{++}
$L_{\mu\nu\alpha\beta} = \mathrm{tr}\ \mathcal{F}_{\mu\nu}\mathcal{F}_{\alpha\beta} - \frac{1}{2}\,(g_{\mu\alpha}T_{\nu\beta} + g_{\nu\beta}T_{\mu\alpha} - g_{\mu\beta}T_{\nu\alpha} - g_{\nu\alpha}T_{\mu\beta})$ $-\frac{1}{12}\,(g_{\mu\alpha}g_{\nu\beta} - g_{\mu\beta}g_{\nu\alpha})S + \frac{1}{12}\,\epsilon_{\mu\nu\alpha\beta}P$	2^{++}, 2^{-+}

Table 2.2: The dimension $d = 4$ operators, and the states that can be created by these operators [46]. We denote $\tilde{\mathcal{F}}_{\mu\nu} = \frac{1}{2}\,\epsilon_{\mu\nu\alpha\beta}\mathcal{F}^{\alpha\beta}$.

The study of irreducible representations of dimension-six operators is more involved. A complete analysis in terms of electric and magnetic gluon fields, $\vec{E}_a$ and $\vec{B}_a$, was also presented in [46], with a detailed description of the operators and the states contained in their spectrum. There are only two such operators of relevance for our work, which we denote $\Omega_{\mu\nu}^{(1)}$ and $\Omega_{\mu\nu}^{(2)}$ as shown in table 2.3. The other dimension-six operators simply cannot be combined with any SM operator to make a dimension-eight interaction.

2.1.3 Matrix elements

As we saw, the matrix elements are factorized into a purely SM part and a purely v-sector part. We will first consider the v-sector matrix elements relevant to v-glueball transitions, $\langle 0|\mathcal{O}_v^\xi|\Theta_\kappa\rangle$

[6] As explained in [46], when an operator $\mathcal{O}_v^\xi$ is conserved and the associated symmetry is not spontaneously broken, some states must decouple. For example, with

$$\langle 0|\,T_{\mu\nu}\,|\,1^{-+}\rangle = (p_\mu\epsilon_\nu + p_\nu\epsilon_\mu)\mathbf{F}^{\mathbf{T}}_{\mathbf{1}^{-+}}\ ,$$

the conservation of $T_{\mu\nu}$ requires $\mathbf{F}^{\mathbf{T}}_{\mathbf{1}^{-+}} = 0$, and thus T does not create a 1^{-+} state. Similarly

$$\langle 0|\,T_{\mu\nu}\,|\,0^{++}\rangle = (ap^2 g_{\mu\nu} + bp_\mu p_\nu)\mathbf{F}^{\mathbf{T}}_{\mathbf{0}^{++}},$$

where a and b are some functions of p^2, must vanish for $T_{\mu\nu}$ conserved and traceless. Note that the trace anomaly complicates this discussion, but its effect in this model is minimal; see Sec. 3.1 below.

Operator $\mathcal{O}_v^\xi$	J^{PC}
$\Omega_{\mu\nu}^{(1)} = \text{tr } \mathcal{F}_{\mu\nu}\mathcal{F}_{\alpha\beta}\mathcal{F}^{\alpha\beta}$	1^{--}, 1^{+-}
$\Omega_{\mu\nu}^{(2)} = \text{tr } \mathcal{F}_{\mu}^{\alpha}\mathcal{F}_{\alpha}^{\beta}\mathcal{F}_{\beta\nu}$	1^{--}, 1^{+-}

Table 2.3: The important $d = 6$ operators. The states that can be created by these operators are shown [46].

and $\langle\Theta_{\kappa'}|\mathcal{O}_v^\xi|\Theta_\kappa\rangle$, where $|\Theta_\kappa\rangle$ and $|\Theta_{\kappa'}\rangle$ refer to v-glueball states with given quantum numbers and $\mathcal{O}_v^\xi$ is any of the operators in tables 2.2 and 2.3.

It is convenient to write the most general possible matrix element in terms of a few Lorentz invariant amplitudes or form factors. For the annihilation matrix elements we will write

$$\langle 0|\mathcal{O}_v^\xi|\Theta_\kappa\rangle = \Pi_{\kappa,\mu\nu\ldots}^\xi \mathbf{F}_\kappa^\xi \ , \tag{2.5}$$

where $\mathbf{F}_\kappa^\xi$ is the decay constant of the v-glueball Θ_κ, and $\Pi_{\kappa,\mu\nu\ldots}^\xi$ is determined by the Lorentz representations of Θ_κ and $\mathcal{O}_v^\xi$. In table 2.4 we list $\Pi_{\kappa,\mu\nu\ldots}^\xi$ for each operator.

The decay constants $\mathbf{F}_\kappa^\xi$ depend on the internal structure of the v-glueball states and, with the exception of those that vanish due to conservation laws (see footnote 6), must be determined by non-perturbative methods, for instance, by numerical calculations in lattice gauge theory. Only the first three non-vanishing decay constants in table 2.4 have been calculated, for $SU(3)$ Yang-Mills theory [25], although the reported values are not expressed in a continuum renormalization scheme. The other decay constants have not been computed.

Likewise, the transition matrix elements $\langle\Theta_{\kappa'}|\mathcal{O}_v^\xi|\Theta_\kappa\rangle$ are of the form

$$\langle\Theta_{\kappa'}|\mathcal{O}_v^\xi|\Theta_\kappa\rangle = \Pi_{\kappa\kappa',\mu\nu\ldots}^\xi \mathbf{M}_{\kappa,\kappa'}^\xi, \tag{2.6}$$

where now $\mathbf{M}_{\kappa,\kappa'}^\xi$ is the transition matrix, which depends only on the transferred momentum. In table 2.5 we have listed $\Pi_{\kappa\kappa',\mu\nu\ldots}^\xi$ for the simplest cases considered later in this work. In several other cases more than one Lorentz structure $\Pi_{\kappa\kappa',\mu\nu\ldots}^\xi$ contributes to the transition element. In such cases, since none of these matrix elements are known from numerical simulation, we will usually simplify the problem by using the lowest partial-wave approximation for the amplitudes. More details will follow in Sec. 2.3.

Clearly, any numerical results arising from our formulas, as we ourselves will obtain in our LHC study [60], will be subject to some large uncertainties, due to the unknown matrix elements. Of course, with sufficient motivation, such as a hint of a discovery, many of these could be determined through additional lattice gauge theory computations.

Now we turn to the SM part of the matrix element, which can be treated perturbatively,

$\mathcal{O}_v^\xi\ (\Theta_\kappa)$	$\Pi^\xi_{\kappa,\mu\nu\cdots}$	$\mathbf{F}^\xi_\kappa$
$S\ (0^{++})$	$\mathbf{1}$	$\mathbf{F^S_{0^{++}}}$
$P\ (0^{-+})$	$\mathbf{1}$	$\mathbf{F^P_{0^{-+}}}$
$T_{\alpha\beta}\ (0^{++})$	$g_{\alpha\beta}-\frac{p_\alpha p_\beta}{p^2}$	0
$T_{\alpha\beta}\ (1^{-+})$	$p_\alpha\epsilon_\beta+p_\beta\epsilon_\alpha$	0
$T_{\alpha\beta}\ (2^{++})$	$\epsilon_{\alpha\beta}$	$\mathbf{F^T_{2^{++}}}$
$L_{\mu\nu\alpha\beta}\ (2^{++})$	$\epsilon_{\mu\alpha}\mathcal{P}_{\nu\beta}+\epsilon_{\nu\beta}\mathcal{P}_{\mu\alpha}-\epsilon_{\nu\alpha}\mathcal{P}_{\mu\beta}-\epsilon_{\mu\beta}\mathcal{P}_{\nu\alpha}$	$\mathbf{F^L_{2^{++}}}$
$L_{\mu\nu\alpha\beta}\ (2^{-+})$	$(\epsilon_{\mu\nu\rho\sigma}\epsilon^\sigma{}_\beta p^\rho p_\alpha-\epsilon_{\mu\nu\rho\sigma}\epsilon^\sigma{}_\alpha p^\rho p_\beta$ $+\epsilon_{\alpha\beta\rho\sigma}\epsilon^\sigma{}_\nu p^\rho p_\mu-\epsilon_{\alpha\beta\rho\sigma}\epsilon^\sigma{}_\mu p^\rho p_\nu)/p^2$	$\mathbf{F^L_{2^{-+}}}$
$\Omega^{(n)}_{\mu\nu}\ (1^{--})$	$m_{1^-}(p_\mu\epsilon_\nu-p_\nu\epsilon_\mu)$	$\mathbf{F^{\Omega^{(n)}}_{1^{--}}}$
$\Omega^{(n)}_{\mu\nu}\ (1^{+-})$	$m_{1^+}\epsilon_{\mu\nu\alpha\beta}(p^\alpha\epsilon^\beta-p^\beta\epsilon^\alpha)$	$\mathbf{F^{\Omega^{(n)}}_{1^{+-}}}$

Table 2.4: Annihilation matrix elements. ϵ_μ and $\epsilon_{\mu\nu}$ are the polarization vectors of $1^{--},1^{+-}$ and polarization tensor of $2^{++},2^{-+}$ respectively. $\mathcal{P}_{\alpha\beta}=g_{\alpha\beta}-2p_\alpha p_\beta/p^2$. m_{1^-},m_{1^+} are the masses of the $1^{--},1^{+-}$ states; their appearance merely reflects our normalization convention.

$\mathcal{O}_v^\xi\ (\Theta_\kappa\ \Theta_{\kappa'})$	$\Pi^\xi_{\kappa\kappa',\mu\nu\cdots}$	$\mathbf{M}^\xi_{\kappa\kappa'}$
$P\ (0^{-+},0^{++})$	$\mathbf{1}$	$\mathbf{M^P_{0^+0^-}}$
$\Omega^{(n)}_{\mu\nu}\ (1^{--},0^{++})$	$p_\mu\epsilon_\nu-p_\nu\epsilon_\mu$	$\mathbf{M^{\Omega^{(n)}}_{1^{--}0^{++}}}$
$\Omega^{(n)}_{\mu\nu}\ (1^{+-},0^{-+})$	$p_\mu\epsilon_\nu-p_\nu\epsilon_\mu$	$\mathbf{M^{\Omega^{(n)}}_{1^{+-}0^{-+}}}$
$\Omega^{(n)}_{\mu\nu}\ (1^{--},0^{-+})$	$\epsilon_{\mu\nu\alpha\beta}p^\alpha\epsilon^\beta$	$\mathbf{M^{\Omega^{(n)}}_{1^{--}0^{-+}}}$
$\Omega^{(n)}_{\mu\nu}\ (1^{+-},0^{++})$	$\epsilon_{\mu\nu\alpha\beta}p^\alpha\epsilon^\beta$	$\mathbf{M^{\Omega^{(n)}}_{1^{+-}0^{++}}}$
$P\ (1^{--},1^{+-})$	$\epsilon^+\cdot\epsilon^-$	$\mathbf{M^P_{1^{--}1^{+-}}}$
$L\ (1^{--},1^{+-})$	$\epsilon_{\mu\nu\rho\sigma}p^\rho\epsilon^{-\sigma}(p_\alpha\epsilon^+{}_\beta-p_\beta\epsilon^+{}_\alpha)+\mu\nu\leftrightarrow\alpha\beta-\text{traces}$	$\mathbf{M^L_{1^{--}1^{+-}}}$
$\Omega^{(n)}_{\mu\nu}\ (2^{-+},1^{+-})$	$p_\mu\epsilon_{\nu\alpha}\epsilon^\alpha-p_\nu\epsilon_{\mu\alpha}\epsilon^\alpha$	$\mathbf{M^{\Omega^{(n)}}_{2^{-+}1^{+-}}}$
$\Omega^{(n)}_{\mu\nu}\ (1^{+-},2^{++})$	$\epsilon_{\mu\nu\alpha\beta}\epsilon^{\alpha\lambda}\tilde{\epsilon}_\lambda p^\beta,\ \epsilon_{\mu\nu\alpha\beta}\epsilon^{\alpha\lambda}p_\lambda\tilde{\epsilon}^\beta$	$\mathbf{M^{\Omega^{(n)}}_{1^{+-}2^{++}}}$

Table 2.5: Transition matrix elements. Momentum of the final glueball $\Theta_{\kappa'}$ is denoted p^μ; ϵ^α and $\epsilon^{\alpha\beta}$ are polarization tensors of spin 1 and spin 2 states respectively. The bottom part of the table contains matrix elements in the lowest partial wave approximation.

since we will only consider v-glueballs with masses well above Λ_{QCD}.[7] In all of our calculations, the SM gauge-boson field-strength tensors, which appear in the operators, are replaced in the matrix element by the substitution $G_{\mu\nu}\leftrightarrow k_\mu\varepsilon_\nu-k_\nu\varepsilon_\mu$. For example, for a transition to two gauge bosons, we write[8]

$$\langle k_1,\varepsilon_1^a;k_2,\varepsilon_2^b|\text{tr }G_{\mu\nu}G_{\alpha\beta}|0\rangle=\delta^{ab}(k_\mu^1\varepsilon_\nu^1-k_\nu^1\varepsilon_\mu^1)(k_\alpha^2\varepsilon_\beta^2-k_\alpha^1\varepsilon_\beta^2),\tag{2.7}$$

where $k^{1(2)}$, $\varepsilon^{1(2)}$ are the gauge-bosons' momenta and polarizations respectively. Later in the

[7]We will do all our calculations at SM-tree level; loop corrections for v-glueball decays to ordinary gluons should be accounted for when precision is required.

[8]Note that one has to take into account a factor of 2 which comes from the two different ways of contracting each $G^a_{\mu\nu}$ operator with $|k_1,\varepsilon_1^a;k_2,\varepsilon_2^b\rangle$. This factor then cancels an explicit $\frac{1}{2}$ factor appearing in the normalization of the trace.

text we will sometimes use the following notation for the SM matrix elements

$$\langle SM|\mathcal{O}_s^\eta|0\rangle = h_\eta^{\mu\nu\cdots} \ , \tag{2.8}$$

where $h_\eta^{\mu\nu\cdots} = h_\eta^{\mu\nu\cdots}(k_1, k_2, \cdots)$ is a function of the momenta of the SM particles in the final state.

2.2 Effective Lagrangian

In this section we discuss the effective action $\mathcal{L}_{\text{eff}}$ linking the SM sector with the v-sector, and discuss the general form of the amplitudes controlling v-glueball decays. We will confirm that all the important decay modes are controlled by $D = 8$ operators involving the $d = 4$ and 6 operators listed in tables 2.2 and 2.3.

2.2.1 Heavy particles and the computation of $\mathcal{L}_{\text{eff}}$

The low-energy interaction of v-gluons and v-glueballs with SM particles is induced through a loop of heavy X-particles. In this section we present the one-loop effective Lagrangian that describes this interaction, to leading non-vanishing order in $1/M$, namely $1/M^4$, which we will see is sufficient for inducing all v-glueball decays. The relevant diagrams all have four external gauge boson lines, as depicted in figure 2.2. They give the amplitude for scattering of two v-gluons to two SM gauge bosons, of either strong (gluons g), weak (W and Z) or hypercharge (photon γ or Z) interactions (figure 2.2a), as well as the conversion of three v-gluons to a γ or Z (figure 2.2b).

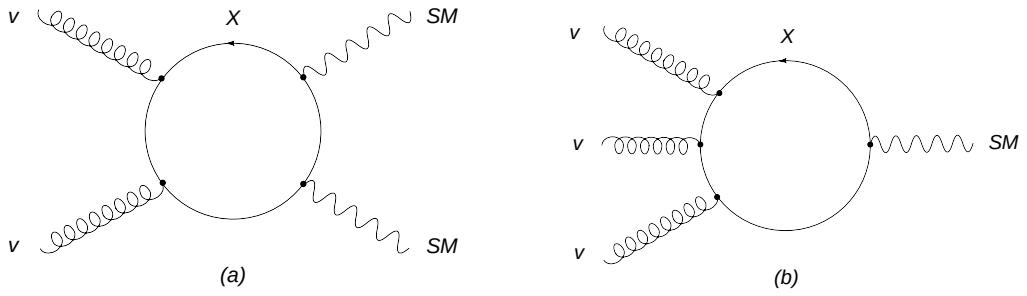

Figure 2.2: Diagrams contributing to the effective action

The dimension-eight operators appearing in the action can be found in studies of Euler-Heisenberg-like Lagrangians in the literature. Within the SM, effective two gluon - two photon, four gluon, and three gluon - photon vertices can be found in [42], [43] and [44] respectively. These results can be adapted for our present purposes.

We introduce now some notation, defining $G^1_{\mu\nu} \equiv B_{\mu\nu}$, $G^2_{\mu\nu} \equiv F_{\mu\nu}$ and $G^3_{\mu\nu} \equiv G_{\mu\nu}$, which are the field tensors of the $U(1)_Y$, $SU(2)$ and $SU(3)$ SM gauge groups. We denote their couplings g_i, $i = 1, 2, 3$, while g_v is the coupling of the new group $SU(n_v)$. In terms of the operators from tables 2.2 and 2.3, the effective Lagrangian reads

$$\begin{aligned}\mathcal{L}_{\text{eff}} = \frac{g_v^2}{(4\pi)^2 M^4}\left[g_1^2\chi_1 B^{\mu\nu}B^{\rho\sigma} + g_2^2\chi_2 \text{tr } F^{\mu\nu}F^{\rho\sigma} + g_3^2\chi_3 \text{tr } G^{\mu\nu}G^{\rho\sigma}\right] \\ \times\left(\frac{1}{60}\,S\,g_{\mu\rho}g_{\nu\sigma} + \frac{1}{45}\,P\,\epsilon_{\mu\nu\rho\sigma} + \frac{11}{45}\,T_{\mu\rho}g_{\nu\sigma} - \frac{1}{30}\,L_{\mu\nu\rho\sigma}\right) \\ + \frac{g_v^3 g_1}{(4\pi)^2 M^4}\,\chi\left(\frac{14}{45}\,B^{\mu\nu}\Omega^{(1)}_{\mu\nu} - \frac{1}{9}\,B^{\mu\nu}\Omega^{(2)}_{\mu\nu}\right). \quad (2.9)\end{aligned}$$

The coefficients χ_i and χ encode the masses of the heavy particles from table 3.1 and their couplings to the SM gauge groups. They are summarized in table 2.6.

	χ , χi
χ_1	$\frac{1}{3\rho_d^4} + \frac{1}{2\rho_l^4} + \frac{4}{3\rho_u^4} + \frac{1}{6\rho_q^4} + \frac{1}{\rho_e^4}$
χ_2	$\frac{1}{\rho_l^4} + \frac{3}{\rho_q^4}$
χ_3	$\frac{1}{\rho_d^4} + \frac{1}{\rho_u^4} + \frac{2}{\rho_q^4}$
χ	$\frac{1}{\rho_d^4} - \frac{1}{\rho_l^4} - \frac{2}{\rho_u^4} + \frac{1}{\rho_q^4} + \frac{1}{\rho_e^4}$

Table 2.6: The coefficients χ arise from a sum over the SM charges of X particles running in the loop. The χ_i, $i = 1, 2, 3$, arise from the diagram in figure 2.2(a) with two external SM gauge bosons of group i, while χ is determined by the diagram 2.2(b) with a single hypercharge-boson on an external line. The ρ_r are defined in (2.2).

The effective Lagrangian (2.9) can be compactly written as

$$\mathcal{L}_{\text{eff}} = \sum_{i=1}^{3}\sum_{\xi}\frac{g_v^{\frac{d_\xi}{2}}\,g_i^{4-\frac{d_\xi}{2}}}{(4\pi)^2 M^4}\,\Xi^i_\xi \mathcal{O}_s^{\eta(\xi,i)}\cdot\mathcal{O}_v^\xi, \quad (2.10)$$

where the sum is over operators and different ways to contract Lorentz indices. The notation $\eta(\xi, i)$ is to make explicit that for each ξ and i there is at most one SM operator $\mathcal{O}_s^\eta$ multiplying $\mathcal{O}_v^\xi$ in the effective Lagrangian (see table 2.7).

The mass dimension of $\mathcal{O}_v^\xi$ is denoted d_ξ, and the Ξ^i_ξ are dimensionless coefficients given by

$$\Xi^i_\xi = \begin{cases} \chi^i C_\xi & d_\xi = 4 \\ \chi C_\xi & d_\xi = 6\ . \end{cases} \quad (2.11)$$

The C_ξ are coefficients that depend only on the v-sector operators and the SM operator with which they are contracted; they are also given in table 2.7.

These values for the C_ξ are valid around the scale M, and they will be altered by perturbative renormalization between this scale and a lower scale closer to the glueball masses, at which the nonperturbative matrix elements are evaluated.[9] These renormalization effects (which will impact v-glueball lifetimes but cancel out of most branching fractions) can be computed, but are only useful to discuss once one has concrete values for the decay constants and matrix elements in a definite renormalization scheme, which at present is not available. We will not discuss them further here.

$\mathcal{O}_v^\xi$	C_ξ	$\mathcal{O}_s^\eta \cdot \mathcal{O}_v^\xi$	$\mathcal{O}_v^\xi$	C_ξ	$\mathcal{O}_s^\eta \cdot \mathcal{O}_v^\xi$
S	$\frac{1}{60}$	$(\text{tr } G^i_{\mu\nu} G^{i\mu\nu})\ S$	T	$\frac{11}{45}$	$(\text{tr } G^{i\mu\lambda} G^{i\nu}_{\lambda})\ T_{\mu\nu}$
P	$\frac{2}{45}$	$(\text{tr } G^i_{\mu\nu} \tilde{G}^{i\mu\nu})\ P$	$\Omega^{(1)}$	$\frac{14}{45}$	$G^{1\mu\nu}\ \Omega^{(1)}_{\mu\nu}$
L	$-\frac{1}{30}$	$(\text{tr } G^{i\mu\nu} G^{i\alpha\beta})\ L_{\mu\nu\alpha\beta}$	$\Omega^{(2)}$	$-\frac{1}{9}$	$G^{1\mu\nu}\ \Omega^{(2)}_{\mu\nu}$

Table 2.7: List of coefficients C_ξ and contractions of the operators $\mathcal{O}_v^\xi$ introduced in tables 2.2 and 2.3. $G^i_{\mu\nu}$ represents the field-strength tensor of the i^{th} SM group.

The coefficients χ and χ_i in table 2.6 determine the relative coupling of v-gluons to the electroweak-sector gauge bosons W^i_μ and B_μ for the $SU(2)$ and $U(1)_Y$ factors respectively. For applications it is convenient to convert these to the couplings to the photons γ, W and Z bosons. We introduce the following coefficients

$$\begin{aligned} \chi_\gamma \equiv \chi_1 + \chi_2/2, \qquad \chi_Z \equiv \frac{\sin^4\theta_W \chi_1 + \cos^4\theta_W \chi_2/2}{\cos^2\theta_W}, \\ \chi_W \equiv \chi_2, \qquad \chi_{\gamma Z} \equiv \frac{\cos^2\theta_W \chi_2 - 2\sin^2\theta_W \chi_1}{\cos\theta_W}, \qquad \chi_s \equiv \chi_3\ , \end{aligned} \tag{2.12}$$

where θ_W is the weak mixing angle. We will often use these coefficients instead of χ_i in the effective Lagrangian (2.9), with a corresponding substitution of field tensors and couplings.

2.2.2 Effective Lagrangian and renormalization group

The introduction of an effective Lagrangian is very helpful in the consideration of higher order corrections in strong interactions. These corrections lead to terms $\alpha_v \ln M$ which can be summed up in a simple way by applying the renormalization group technique. These renormalization effects(which will impact v-glueball lifetimes but cancel out of most branching fractions) can be computed as follows.

[9] Decays of v-glueballs to standard model gauge bosons are affected by the trace anomaly, but minimally, because both sectors' trace anomalies must be non-zero, and that of the SM is small at the scale of the v-glueball masses.

Let us first write the effective Lagrangian (2.9) as

$$\mathcal{L}_{\rm eff} = \sum_{\xi} C_\xi \mathcal{O}^\xi, \tag{2.13}$$

where

$$\mathcal{O}^\xi = \sum_{i=1}^{3} \frac{g_v^{\frac{d_\xi}{2}} g_i^{4-\frac{d_\xi}{2}}}{(4\pi)^2 M^4} \Xi_\xi'^i \mathcal{O}_s^{\eta(\xi,i)} \cdot \mathcal{O}_v^\xi, \tag{2.14}$$

with $\Xi_\xi'^i = \Xi_\xi^i / C_\xi$. Here the operators O_ξ must be treated on equal footing with the original terms in the Lagrangian, with the coefficients C_ξ considered as some new charges.

To lowest order in α_v the coefficients C_ξ can be read off table 2.7. These values arise from quirk loops and hence are valid at the scale M. To consider contributions of these operators to v-glueball matrix elements, one must use the renormalization group to evolve the coefficients down to a scale closer to the glueball masses, at which the nonperturbative matrix elements are evaluated. To do this, the anomalous dimensions of the operators O_ξ are required.

To calculate the anomalous dimension γ_ξ of an operator O_ξ, we add the operator to the Lagrangian with coupling C_ξ, shift $A \to A + a$, expand to $\mathcal{O}(a^2)$, calculate the functional determinant, and expand it in powers $G_{\mu\nu}$, looking for the appearance of O_ξ with a logarithmically divergent coefficient. Specifically, in the path integral picture,

$$\int \mathcal{D}a \exp\left[i(S+a) + iC_\xi \int O_\xi(A+a)dx^4\right] \to \exp\left[iZ^{-1}_{\xi\xi'} C_\xi \int O_{\xi'}(A)dx^4 + \cdots\right], \tag{2.15}$$

where, to lowest order,

$$Z^{-1}_{\xi\xi'} = 1 + \frac{\gamma_{\xi\xi'}}{2} \frac{g^2}{16\pi} \ln\left[\frac{M^2}{\mu^2}\right]. \tag{2.16}$$

The last expression defines the matrix of reduced anomalous dimensions.

The couplings $C_\xi(\mu)$ are found by solving the generalized Gell-Mann-Low equations,

$$\mu \frac{dC_\xi}{d\mu} = -\frac{\alpha_v}{2\pi} \gamma_{\xi\xi'} C_{\xi'}, \tag{2.17}$$

$$\mu \frac{d\alpha_v}{d\mu} = -\frac{b}{2\pi} \alpha_v^2, \tag{2.18}$$

with $b = (11/3)n_v$. The required anomalous dimensions for the operators shown in table 2.7 can be calculated using a systematic algorithm developed by Morozov [23]. The anomalous dimension for S was also obtained in [21, 22]. One finds that S, P, T, L, Ω^1, Ω^2 have reduced anomalous dimensions $\gamma_{SS} = 0$, $\gamma_{PP} = 0$, $\gamma_{TT} = b_0 = 11$, $\gamma_{LL} = 6$, $\gamma_{\Omega^1\Omega^1} = \gamma_{\Omega^2\Omega^2} = 23/2$ and $\gamma_{\Omega^1\Omega^2} = \gamma_{\Omega^2\Omega^1} = 1/2$, with all remaining coefficients equal to zero.

2.2.3 Decay amplitudes

Now, using (2.5), (2.8) and the couplings from (2.14), we obtain that the amplitude for a decay of a v-glueball into SM particles is given by

$$\mathcal{M} = \frac{g_v^{\frac{d_\xi}{2}} g_i^{4-\frac{d_\xi}{2}}}{(4\pi)^2 M^4} \Xi^i_\xi(\rho_{\bar{u}}, ..., \rho_e) \langle SM| \mathcal{O}^\eta_s |0\rangle \langle 0| \mathcal{O}^\xi_v |\Theta_\kappa\rangle = \\ = \frac{g_v^{\frac{d_\xi}{2}} g_i^{4-\frac{d_\xi}{2}}}{(4\pi)^2 M^4} \Xi^i_\xi(\rho_{\bar{u}}, ..., \rho_e) f^i_{\xi,\eta}(p, q_1, q_2, ...) \mathbf{F}^\xi_\kappa, \quad (2.19)$$

where

$$f^i_{\xi,\,\eta}(p, k_1, k_2, ...) = h^{\mu\nu\cdots}_\eta(k_1, k_2, ...) \Pi^\xi_{\kappa,\,\mu\nu\cdots}(p)$$

encodes all the information about the matrix element that can be determined from purely perturbative computations and Lorentz or gauge invariance, and $\mathbf{F}^\xi_\kappa$ is the v-glueball decay constant. See Eq. (2.11) for the definition of Ξ and Eq. (2.2) and table 2.6 for the definition of ρ.

Similarly, using (2.6), (2.8) and (2.14), the amplitude for the decay of a v-glueball into another v-glueball and SM particles reads

$$\mathcal{M} = \frac{g_v^{\frac{d_\xi}{2}} g_i^{4-\frac{d_\xi}{2}}}{(4\pi)^2 M^4} \Xi^i_\xi(\rho_{\bar{u}}, ..., \rho_e) \langle SM| \mathcal{O}^\eta_s |0\rangle \langle \Theta_{\kappa'}| \mathcal{O}^\xi_v |\Theta_\kappa\rangle = \\ = \frac{g_v^{\frac{d_\xi}{2}} g_i^{4-\frac{d_\xi}{2}}}{(4\pi)^2 M^4} \Xi^i_\xi(\rho_{\bar{u}}, ..., \rho_e) f^i_{\kappa\kappa';\xi,\eta}(p, p', k_1, k_2, ...) \mathbf{M}^\xi_{\kappa\kappa'}(k). \quad (2.20)$$

Here $\mathbf{M}^\xi_{\kappa\kappa'}(k)$ is the glueball-glueball transition matrix, which for given masses of Θ_κ and $\Theta_{\kappa'}$ is a function of transferred momentum $k \equiv p' - p$, and

$$f^i_{\kappa\kappa';\,\xi,\eta} = \Pi^\xi_{\kappa\kappa',\,\mu\nu\cdots}(p, p') h^{\mu\nu\cdots}_\eta(k_1, k_2, ...).$$

2.3 Decay rates for lightest v-glueballs

In this section we will compute the decay rates for some of the v-glueballs in figure 2.1. Let us make a quick summary of the results to come.

The operators shown in tables 2.2 and 2.3 induce the dominant decay modes of the v-glueball states appearing in figure 2.1. In the $PC = ++$ sector, the lightest 0^{++} and 2^{++} v-glueballs will mostly decay directly to pairs of SM gauge bosons via S, T and L operators. Three-body decays $2^{++} \to 0^{++}$ plus two SM gauge bosons are also possible, but are strongly suppressed by phase space. In the $PC = -+$ sector the lightest states are the 0^{-+} and 2^{-+} v-glueballs. These will also decay predominantly to SM gauge boson pairs, via P and L operators respectively.

There are also C-changing $2^{-+} \to 1^{+-} + \gamma$ decays, induced by the $d = 6$ $D = 8$ operators $\Omega_{\mu\nu}$ (table 2.3), but the small mass-splitting found in the lattice computations [24] suggests these decays are probably very rare or absent. In the $PC = +-$ sector, the leading decays are two-body C-changing processes, because C-conservation forbids annihilation to pairs of gauge bosons, and because three-body decays are phase-space suppressed. In particular, the 1^{+-}, the lightest v-glueball in that sector, will decay to the lighter C-even states 0^{++}, 2^{++} and 0^{-+} by radiating a photon (or Z when it is possible kinematically). The same is true for the states in the $PC = --$ sector, with an exception that the lightest 1^{--} v-glueball can annihilate to a pair of SM fermions through an off-shell photon or Z. The latter decay is also induced by $\Omega^{\mu\nu}$ operators.

We shall study decays of the 0^{++}, 2^{++}, 0^{-+}, 2^{-+}, 1^{+-} and 1^{--} v-glueballs in some detail. Since for this set of v-glueballs the combination of J and P quantum numbers is unique, we shall often omit the C quantum number from our formulas to keep them a bit shorter, referring simply to the 0^+, 2^+, 0^-, 2^-, 1^+ and 1^- states. At the end we shall make some brief comments about the other states, the 3^{++}, 3^{+-}, 3^{--}, 2^{+-}, 2^{--} and 0^{+-}.

Of course the allowed decays and the corresponding lifetimes are dependent upon the masses of the v-glueballs. While the results of Morningstar and Peardon [24], understood as dimensionless in units of the confinement scale Λ, can be applied to any pure $SU(3)$ gauge sector, the glueball spectrum for $SU(4)$ or $SU(7)$ are not known. Fortunately, at least for $SU(n_v)$, the spectrum is expected to be largely independent of n_v. Still, the precise masses will certainly be different for $n_v > 3$, and for some v-glueballs this could have a substantive effect on their lifetimes and branching fractions.

For other gauge groups, however, the spectrum may be qualitatively different; in particular, the C-odd sector may be absent or heavy. We will briefly discuss this in our concluding section. The $0^{\pm+}$ and $2^{\pm+}$ states are expected to be present in any pure-gauge theory, with similar production and decay channels, and as such are the most model-independent. Fortunately, it turns out they are also the easiest to study theoretically, and, as we will see below and in our LHC study [60], the easiest to observe.

2.3.1 Light C-even sector decays

We begin with the C-even 0^{++}, 2^{++}, 0^{-+} and 2^{-+} v-glueballs, which can be created by dimension 4 operators. The first three have been studied in some detail in various contexts; see for example [25–31] and a recent review [37]. The dominant decays of these states are annihilations

$\Theta_\kappa \to G^a G^b$, where Θ_κ denotes a v-glueball state and G^a, G^b is a pair of SM gauge bosons: gg, $\gamma\gamma$, ZZ, W^+W^- or γZ. We will also consider radiative decays $\Theta_\kappa \to \Theta_{\kappa'} + \gamma/Z$, and three-body decays of the form $\Theta_\kappa \to G^a G^b \Theta'_\kappa$, and will see they are generally subleading for these states.

Annihilations are mediated by the dimension $d = 4$ operators in Eq. (3.5). In particular, we know from the previous discussion (see [46] and table 2.2 above) that the 0^{++} v-glueball can be annihilated (created) by the operator S. The 0^{-+} and 2^{-+} states are annihilated by the operators P and $L_{\mu\nu\alpha\beta}$ respectively. The tensor 2^{++} can be destroyed by both $T_{\mu\nu}$ and $L_{\mu\nu\alpha\beta}$.

Radiative two-body decays are induced by the dimension $d = 6$ operators in Eq. (3.6). However, the decays $\Theta_\kappa \to \Theta_{\kappa'} + \gamma/Z$ are forbidden if Θ_κ and $\Theta_{\kappa'}$ are both from the C-even subsector. For the spectrum in figure 2.1, appropriate for $n_v = 3$, the only kinematically allowed radiative decay is therefore $2^{-+} \to 1^{+-} + \gamma$; the $1^{+-} + Z$ final state is kinematically allowed only for very large Λ_v. For $n_v > 3$, the glueball spectrum is believed to be quite similar to $n_v = 3$, but the close spacing between these two states implies that the ordering of masses might be altered, so that even this decay might be absent for larger n_v.

Decays of the 0^{++} state.

The scalar state can be created or destroyed by the operator S.

Then, according to a general discussion in Sec. 2.2, the amplitude of the decay of the scalar to two SM gauge bosons G^a and G^b is given by the expression

$$\frac{\alpha_i \alpha_v}{M^4}\, \chi_i\, C_S \langle G^a, G^b | \text{tr}\; G_{\mu\nu} G^{\mu\nu} | 0 \rangle \, \langle 0 | S | 0^{++} \rangle, \tag{2.21}$$

where α_i and χ_i encode the couplings of the bosons a and b of a SM gauge group i to the loop, introduced in Sec. 2.2; see (2.14), (2.11) and table 2.6.

For the decay of the scalar to two gluons, (2.21) takes the form

$$\begin{aligned} \frac{\alpha_s \alpha_v}{M^4} \chi_s\, C_S \langle g_1^a g_2^b | \,\text{tr}\; G_{\mu\nu} G^{\mu\nu} | 0 \rangle \, \langle 0 |\, S |\, 0^{++} \rangle = \\ = \frac{\alpha_s \alpha_v}{M^4}\, \frac{\delta^{ab}}{2}\, \chi_s C_S \mathbf{F}^{\mathbf{S}}_{\mathbf{0}^{++}} 2 (k_\mu^1 \varepsilon_\nu^1 - k_\nu^1 \varepsilon_\mu^1)(k^{2\mu} \varepsilon^{2\nu} - k^{2\nu} \varepsilon^{2\mu}), \end{aligned} \tag{2.22}$$

where, according to our conventions, constant $\mathbf{F}^{\mathbf{S}}_{\mathbf{0}^{++}}$ denotes the matrix element $\langle 0 | S | 0^{++} \rangle$. We are using the notation $\alpha_s \equiv \alpha_3, \chi_s \equiv \chi_3$. The rate of the decay (accounting for a 1/2 from Bose statistics) is then given by

$$\Gamma_{0^+ \to gg} = \frac{\alpha_s^2 \alpha_v^2}{16\pi M^8} (N_c^2 - 1) \chi_s^2 C_S^2 m_{0^+}^3 (\mathbf{F}^{\mathbf{S}}_{\mathbf{0}^{++}})^2. \tag{2.23}$$

Here and below we make explicit the $SU(3)$-color origin of a factor of $8 = N_c^2 - 1$.

The branching ratios for the decays to the photons, Z and $W^\pm$ are

$$\frac{\Gamma_{0^+\to\gamma\gamma}}{\Gamma_{0^+\to gg}} = \frac{1}{2}\,\frac{\alpha^2}{\alpha_s^2}\frac{\chi_\gamma^2}{\chi_s^2}, \tag{2.24}$$

$$\frac{\Gamma_{0^+\to ZZ}}{\Gamma_{0^+\to gg}} = \frac{1}{2}\,\frac{\alpha_w^2}{\alpha_s^2}\frac{\chi_Z^2}{\chi_s^2}\,\left(1-4\frac{m_Z^2}{m_{0^+}^2}\right)^{1/2}\left(1-4\frac{m_Z^2}{m_{0+}^2}+6\frac{m_Z^4}{m_{0^+}^4}\right), \tag{2.25}$$

$$\frac{\Gamma_{0^+\to\gamma Z}}{\Gamma_{0^+\to gg}} = \frac{1}{4}\,\frac{\alpha\alpha_w}{\alpha_s^2}\frac{\chi_{\gamma Z}^2}{\chi_s^2}\,\left(1-\frac{m_Z^2}{m_{0^+}^2}\right)^3, \tag{2.26}$$

$$\frac{\Gamma_{0^+\to W^+W^-}}{\Gamma_{0^+\to gg}} = \frac{1}{4}\,\frac{\alpha_w^2}{\alpha_s^2}\frac{\chi_W^2}{\chi_s^2}\,\left(1-4\frac{m_W^2}{m_{0^+}^2}\right)^{1/2}\left(1-4\frac{m_W^2}{m_{0^+}^2}+6\frac{m_W^4}{m_{0^+}^4}\right), \tag{2.27}$$

The coefficients χ used here were defined in Eq. (2.12). Factors of $1/2$ in the above ratios come from the color factor $N_c^2-1=8$ and a difference in the normalization of abelian and non-abelian generators. An extra $1/2$ is required if the particles in the final state are not identical, such as W^+W^- and γZ.

Of course these are SM-tree-level results. There will be substantial order-α_s corrections to the gg final state, so the actual lifetimes will be slightly shorter and the branching fractions to other final states slightly smaller than given in these formulas.

Decays of the 0^{-+} state.

The decay of the pseudoscalar state 0^{-+} to two gauge bosons proceeds in a similar fashion. This decay is induced by the operator P:

$$\frac{\alpha_i\alpha_v}{M^4}\,\chi_i C_P \langle G^a, G^b|\,\mathrm{tr}\;G_{\mu\nu}\tilde{G}^{\mu\nu}|\,0\rangle\,\langle 0|\,P|0^{-+}\rangle. \tag{2.28}$$

The amplitude leads to the following two-gluon decay rate:

$$\Gamma_{0^-\to gg} = \frac{\alpha_s^2\alpha_v^2}{16\pi M^8}\,(N_c^2-1)\chi_s^2 C_P^2 m_{0^-}^3\,(\mathbf{F}^{\mathbf{P}}_{\mathbf{0}^{-+}})^2, \tag{2.29}$$

and the same branching fractions as for 0^{++}, except for the decays to ZZ and W^+W^-,

$$\frac{\Gamma_{0^-\to ZZ}}{\Gamma_{0^-\to gg}} = \frac{1}{2}\,\frac{\alpha_w^2}{\alpha_s^2}\frac{\chi_Z^2}{\chi_s^2}\,\left(1-4\frac{m_Z^2}{m_{0^-}^2}\right)^{3/2}, \tag{2.30}$$

$$\frac{\Gamma_{0^-\to W^+W^-}}{\Gamma_{0^-\to gg}} = \frac{1}{4}\,\frac{\alpha_w^2}{\alpha_s^2}\frac{\chi_W^2}{\chi_s^2}\,\left(1-4\frac{m_W^2}{m_{0^-}^2}\right)^{3/2}. \tag{2.31}$$

The 0^{-+} state can also decay to lower lying states by emitting a pair of gauge bosons, but these decays are suppressed. For instance, the amplitude for the decay of $0^{-+}\to 0^{++}gg$ is

$$\frac{\alpha_i\alpha_v}{M^4}\,\chi_i C_P \langle G^a, G^b\,|\,\mathrm{tr}\;G_{\mu\nu}\tilde{G}^{\mu\nu}|\,0\rangle\,\langle 0^{++}|\,P|0^{-+}\rangle\;. \tag{2.32}$$

The matrix element $\mathbf{M^P_{0^+0^-}} = \langle 0^{++}|P|0^{-+}\rangle$ is a function of the momentum transferred. Let us first treat it as approximately constant. Then we obtain the decay rate

$$\Gamma_{0^-\to 0^+ gg} = \frac{\alpha_s^2\alpha_v^2}{256\pi^3 M^8}\,(N_c^2-1)\chi_s^2 C_P^2 m_{0^-}^5 f(a)(\mathbf{M^P_{0^+0^-}})^2, \tag{2.33}$$

where f is the dimensionless function of the parameter $a = m_{0^+}^2/m_{0^-}^2$,

$$f(a) = \frac{1}{12}(1-a^2)(1+28a+a^2) + a(1+3a+a^2)\ln a, \tag{2.34}$$

We plot f in figure 2.3; it falls rapidly from 1/12 to 0, because of the rapid fall of phase space as the two masses approach each other. For the masses in figure 2.1, $a = 0.44$ and $f \approx 10^{-4}$. This is in addition to the usual $1/16\pi^2$ suppression of three-body decays compared to two-body decays. Thus the branching fraction for this decay is too small to be experimentally relevant, and our approximation that the matrix element is constant is inconsequential. This will be our general conclusion for three-body decays of the light v-glueball states, and in most cases we will not bother to present results for such channels.

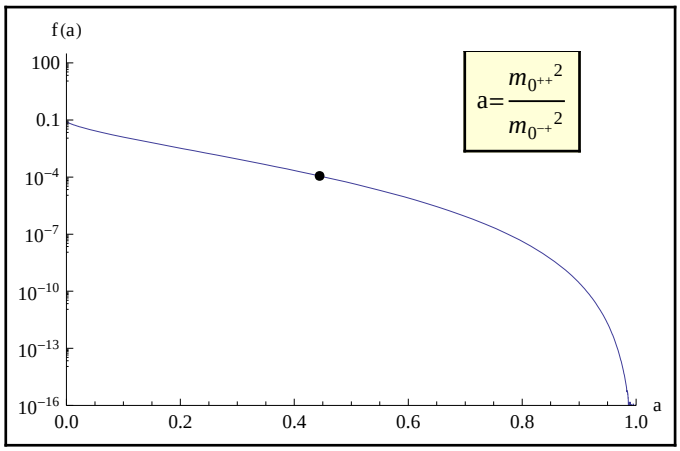

Figure 2.3: Kinematic suppression factor $f(a)$. Point corresponds to a value of a taken for v-glueball masses from the Morningstar and Peardon spectrum [24].

Decays of the 2^{++} state.

Decays of the 2^{++} glueball to two gauge bosons are induced by more than one operator in (2.9). In particular, the 2^{++} decays due to the $T_{\mu\nu}$ and $L_{\mu\nu\alpha\beta}$ operators. This corresponds to the amplitude

$$\frac{\alpha_i\alpha_v}{M^4}\,\chi_i\left[C_T\langle G^a,G^b|\,\mathrm{tr}\;G_{\mu\alpha}G_\nu{}^\alpha|\,0\rangle\,\langle 0|\,T^{\mu\nu}|2^{++}\rangle + \right.$$
$$\left. + C_L\langle G^a,G^b|\,\mathrm{tr}\;G_{\mu\nu}G_{\alpha\beta}|\,0\rangle\langle 0|\,L^{\mu\nu\alpha\beta}|2^{++}\rangle\right]. \tag{2.35}$$

The width of the decay to two gluons is

$$\Gamma_{2^+\to gg} = \frac{\alpha_s^2\alpha_v^2(N_c^2-1)}{160\pi M^8}\,\chi_s^2 m_{2^+}^3\left(\frac{1}{2}\,C_T^2(\mathbf{F^T_{2^{++}}})^2+\frac{4}{3}\,C_L^2(\mathbf{F^L_{2^{++}}})^2\right). \tag{2.36}$$

Here we used the following expressions for the matrix elements:

$$\langle 0|T^{\mu\nu}|2^{++}\rangle = \mathbf{F^T_{2^{++}}}\,\epsilon^{\mu\nu}, \tag{2.37}$$

$$\langle 0|L^{\mu\nu\alpha\beta}|2^{++}\rangle = \mathbf{F^L_{2^{++}}}\left[\mathcal{P}_{\mu\alpha}\epsilon_{\nu\beta}-\mathcal{P}_{\mu\beta}\epsilon_{\nu\alpha}+\mathcal{P}_{\nu\beta}\epsilon_{\mu\alpha}-\mathcal{P}_{\nu\alpha}\epsilon_{\mu\beta}\right], \tag{2.38}$$

where $\mathcal{P}_{\alpha\beta}$ is defined in the caption to table 2.4.

The branching fraction for the decay to two photons is again similar to (2.24). For two Z bosons in the final state, the width of the decay is equal to

$$\Gamma_{2^+\to ZZ} = \frac{\alpha_w^2\alpha_v^2}{40\pi M^8}\,\chi_Z^2 m_{2^+}^3(1-4\zeta_2)^{1/2}\left(\frac{1}{2}\,C_T^2 f_T(\zeta_2)(\mathbf{F^T_{2^{++}}})^2+\right.$$
$$\left.\frac{4}{3}\,C_L^2 f_L(\zeta_2)(\mathbf{F^L_{2^{++}}})^2+\frac{40}{3}\,C_T C_L f_{TL}(\zeta_2)\mathbf{F^T_{2^{++}}}\mathbf{F^L_{2^{++}}}\right), \tag{2.39}$$

where f_T, f_L, f_{TL} are the following functions of the parameter $\zeta_2 = m_Z^2/m_{2^+}^2$.

$$f_T(\zeta_2) = 1-3\zeta_2+6\zeta_2^2\ ,\ f_L(\zeta_2) = 1+2\zeta_2+36\zeta_2^2\ ,\ f_{TL}(\zeta_2) = \zeta_2(1-\zeta_2)\ . \tag{2.40}$$

The decay to W^+W^- is obtained from Eq. (2.39) by substituting $\chi_Z \to \chi_W$, $m_Z \to m_W$ and multiplying by 1/2. For the γZ final state, the decay rate is

$$\Gamma_{2^+\to\gamma Z} = \frac{\alpha\alpha_w\alpha_v^2}{80\pi M^8}\,\chi_{\gamma Z}^2 m_{2^+}^3(1-\zeta_2)^3\left(\frac{1}{2}\,C_T^2 g_T(\zeta_2)(\mathbf{F^T_{2^{++}}})^2+\right.$$
$$\left.\frac{4}{3}\,C_L^2 g_L(\zeta_2)(\mathbf{F^L_{2^{++}}})^2+\frac{20}{3}\,C_T C_L\zeta_2\mathbf{F^T_{2^{++}}}\mathbf{F^L_{2^{++}}}\right), \tag{2.41}$$

where

$$g_T(\zeta_2) = 1+\frac{1}{2}\,\zeta_2+\frac{1}{6}\,\zeta_2^2, \qquad g_L(\zeta_2) = 1+3\zeta_2+6\zeta_2^2. \tag{2.42}$$

As in the case of the 0^{-+}, we can ignore the three-body transitions $2^{++}\to 0^{++}+gg$, etc.

Decays of the 2^{-+} state.

The dominant decays of the 2^{-+} state occur due to the $L_{\mu\nu\alpha\beta}$ operator. The amplitude for such decays is given by

$$\frac{\alpha_i\alpha_v}{M^4}\,\chi_i C_L\langle G^a,G^b|\,\mathrm{tr}\;G_{\mu\nu}G_{\alpha\beta}|\,0\rangle\langle 0|\,L^{\mu\nu\alpha\beta}|\,2^{-+}\rangle. \tag{2.43}$$

The correct Lorentz structure that singles out the negative parity part of the operator $L_{\mu\nu\alpha\beta}$ is as follows:

$$\langle 0|L^{\mu\nu\alpha\beta}|\,2^{-+}\rangle = \mathbf{F^L_{2^{-+}}}\left(\epsilon_{\mu\nu\rho\sigma}\epsilon^{\sigma}{}_{\beta}n^\rho n_\alpha-\epsilon_{\mu\nu\rho\sigma}\epsilon^{\sigma}{}_{\alpha}n^\rho n_\beta+\right.$$
$$\left.+\epsilon_{\alpha\beta\rho\sigma}\epsilon^{\sigma}{}_{\nu}n^\rho n_\mu-\epsilon_{\alpha\beta\rho\sigma}\epsilon^{\sigma}{}_{\mu}n^\rho n_\nu\right), \tag{2.44}$$

where $n_\mu = p^\mu/m_{2^-}$ is a unit vector in the direction of the 4-momentum of the v-glueball.

The decay rate to two gluons is then given by

$$\Gamma_{2^-\to gg} = \frac{\alpha_s^2\alpha_v^2}{120\pi M^8}\,(N_c^2-1){\chi_s}^2 m_{2^-}^3 C_L^2(\mathbf{F^L_{2^{-+}}})^2 \tag{2.45}$$

and $\Gamma_{2^-\to\gamma\gamma}$ is provided by the same relation as (2.24). The widths of the decay to ZZ and γZ can be found from the ratios

$$\frac{\Gamma_{2^-\to ZZ}}{\Gamma_{2^-\to gg}} = \frac{1}{2}\,\frac{\alpha_w^2}{\alpha_s^2}\frac{\chi_Z^2}{\chi_s^2}\,\left(1-4\frac{m_Z^2}{m_{2^-}^2}\right)^{1/2}\left(1+2\frac{m_Z^2}{m_{2^-}^2}-24\frac{m_Z^4}{m_{2^-}^4}\right)\,, \tag{2.46}$$

$$\frac{\Gamma_{2^-\to\gamma Z}}{\Gamma_{2^-\to gg}} = \frac{1}{4}\,\frac{\alpha\alpha_w}{\alpha_s^2}\frac{\chi_{\gamma Z}^2}{\chi_s^2}\,\left(1-\frac{m_Z^2}{m_{2^-}^2}\right)^{3}\left(1+3\frac{m_Z^2}{m_{2^-}^2}+6\frac{m_Z^4}{m_{2^-}^4}\right)\,, \tag{2.47}$$

and the width for the decay to W^+W^- is again obtained by substituting in (2.46) $\chi_Z \to \chi_W$, $m_Z \to m_W$ and dividing the result by 2.

As before, we can neglect 3-body decays. However, there is a 2-body radiative decay that we should consider, although, as we will see, for the masses in figure 2.1 it is of the same order as the 3-body decays. For the $SU(3)$ spectrum in [24] (and possibly all pure glue $SU(n)$, $n\geq 3$) the 2^{-+} state is slightly heavier than the lightest state in the C-odd sector, the pseudovector 1^{+-}. Thus, we need at least to consider the decay $2^{-+}\to 1^{+-}+\gamma$. This decay is induced by the second type of operators (table 2.3) in the effective action (2.9). The amplitude of the decay reads

$$\frac{eg_v^3}{(4\pi)^2M^4}\,\chi\langle\gamma|\,G^{\mu\nu}\,|0\rangle\,\left(C_{\Omega^{(1)}}\langle 1^{+-}|\,\Omega^{(1)}_{\mu\nu}\,|2^{-+}\rangle + C_{\Omega^{(2)}}\langle 1^{+-}|\,\Omega^{(2)}_{\mu\nu}\,|2^{-+}\rangle\right)\,. \tag{2.48}$$

Unfortunately nothing quantitative is known about matrix elements like $\langle 1^{+-}|\Omega^{(n)}_{\mu\nu}\,|2^{-+}\rangle$. In fact each contains multiple Lorentz structures, constructed out of polarization tensors ϵ_α, $\epsilon_{\beta\gamma}$ and momenta p and q of the 1^{+-} and 2^{-+} v-glueballs, times functions of the momentum transfer, cf. [38]. Some simplification can be made if one takes into account the fact that masses of the v-glueballs are close, which we will assume below.

We start by writing the general expression for the amplitude (2.48):

$$\begin{aligned}\langle\,\gamma|\,G^{\mu\nu}\,|0\rangle\,\langle\,1^{+-}|\,\Omega^{(n)}_{\mu\nu}\,|\,2^{-+}\rangle = {}& 2\mathbf{M}^{\mathbf{\Omega^{(n)}}}_{\mathbf{2^{-+}1^{+-}}}(k\cdot p\,\varepsilon^\alpha\epsilon_{\alpha\beta}\epsilon^\beta - p\cdot\varepsilon\,k^\alpha\epsilon_{\alpha\beta}\epsilon^\beta)+\\ &+2\mathbf{M}^{\mathbf{\Omega^{(n)}}\prime}_{\mathbf{2^{-+}1^{+-}}}(k\cdot p\,\varepsilon\cdot\epsilon - k\cdot\epsilon p\cdot\varepsilon)\,\frac{p^\alpha\epsilon_{\alpha\beta}p^\beta}{m_{2^-}^2}+\\ &+2\mathbf{M}^{\mathbf{\Omega^{(n)}}\prime\prime}_{\mathbf{2^{-+}1^{+-}}}(k\cdot p\,\varepsilon^\alpha\epsilon_{\alpha\beta}p^\beta - p\cdot\varepsilon\,k^\alpha\epsilon_{\alpha\beta}p^\beta)\frac{q\cdot\epsilon}{m_{2^-}^2}\,,\end{aligned} \tag{2.49}$$

where $n=1,2$ and k, ε_α are the momentum and polarization of the photon. All contributions of the terms proportional to primed form-factors (which correspond to higher partial waves)

are suppressed by powers of $(m_{2^-} - m_{1^+})/(m_{2^-} + m_{1^+}) \simeq 0.017$, so we may neglect them.[10] Note, however, that if the mass splitting is much larger for $n_v > 3$, then there will be additional unknown quantities that will modify our result below.

We now find

$$\Gamma_{2^-\to 1^+ +\gamma} = \frac{\alpha\alpha_v^3}{960\pi M^8}\,\chi^2\,\frac{(m_{2^-}^2 - m_{1^+}^2)^3}{m_{2^-}^5 m_{1^+}^2}\times \\ \times\,(3m_{2^-}^4 + 34 m_{2^-}^2 m_{1^+}^2 + 3m_{1^+}^4)\left(\mathbf{M}^{\mathbf{\Omega}}_{\mathbf{2^{-+}1^{+-}}}\right)^2. \quad (2.50)$$

Here we introduced the notation

$$\mathbf{M}^{\mathbf{\Omega}}_{\mathbf{2^{-+}1^{+-}}} \equiv C_{\Omega^{(1)}}\mathbf{M}^{\mathbf{\Omega^{(1)}}}_{\mathbf{2^{-+}1^{+-}}} + C_{\Omega^{(2)}}\mathbf{M}^{\mathbf{\Omega^{(2)}}}_{\mathbf{2^{-+}1^{+-}}}. \quad (2.51)$$

Since the the form-factors $\mathbf{M}^{\mathbf{\Omega^{(n)}}}_{\mathbf{2^{-+}1^{+-}}}$ are unknown, we shall not distinguish between them and will use a collective notation, similar to (2.51), for them in the future. In the same manner we will use the notation

$$\Omega_{\mu\nu} \equiv C_{\Omega^{(1)}}\Omega^{(1)}_{\mu\nu} + C_{\Omega^{(2)}}\Omega^{(2)}_{\mu\nu}. \quad (2.52)$$

The factor $(m_{2^-}^2 - m_{1^+}^2)^3$ strongly suppresses the amplitude, given the spectrum of figure 2.1, and a rough estimate suggests it is of the same size as the three-body decays of the 2^- state, and consequently negligible. However this splitting is so small that it is sensitive to numerical uncertainties in the lattice calculation, and might well be different for other gauge groups. In particular, this decay channel might be closed, or might be more widely open than suggested by figure 2.1, depending on the mass spectrum.

Given the uncertainty on the spectrum and the unknown v-glueball mass scale, it is worth noting that the radiative decay of 2^{-+} to 1^{+-} can in principle occur through an emission of the Z boson. This decay is slightly more involved than the decay with photon emission considered above. Additional unknown form factors related to the finiteness of the Z mass further reduce the predictive power of any computation. But such a decay may be forbidden by kinematics, and if allowed it is probably of little importance for the discovery of v-glueballs. Its rate will almost certainly lie somewhere between 0 and $\tan^2\theta_W \sim 20\%$ of the rate for decays to a photon. There is no reason for the form factors $\mathbf{M}(k^2)$ to be enhanced at $k^2 \simeq m_Z^2$. Since the Z boson has only a few percent branching fraction to electrons and muons, the ratio of identifiable Z decays to photon decays is less than 2%. We therefore will not present formulas for this decay mode.

[10] Here we assume that the primed form-factors $\mathbf{M}$ are at most of the same order of magnitude as $\mathbf{M}^{\mathbf{\Omega^{(n)}}}_{\mathbf{2^{-+}1^{+-}}}$.

Again we emphasize that in obtaining the results (2.50) we made some assumptions and approximations, including $\Delta m \ll m_{2^-}$, and these results may require generalization in other calculations. However, we will adhere to similar simplifying approximations in the other radiative decays computed below.

2.3.2 Decays of the vector and pseudovector

In the C-odd sector, the lightest v-glueballs are the pseudovector 1^{+-} and vector 1^{--}. The lowest-dimension operators that can create or destroy 1^{--} and 1^{+-} v-glueballs are the $d = 6$ $\Omega_{\mu\nu}$ operators (table 2.3). Direct annihilation to non-abelian SM gauge bosons would require an operator in the effective action of dimension $D = 12$, and is hence negligible. Instead these operators, combined with a hypercharge field strength tensor to form an operator of dimension 8, induce radiative decays to C-even v-glueballs, and potentially, for the 1^{--} state, annihilation to SM fermions via an off-shell γ or Z. Three-body decays induced by the dimension 4 operators S, P, T, L, although quite uncertain because of the presence of many decay channels with many form factors, appear to be sufficiently suppressed by phase space that they can be disregarded.

Below, we will generally not write formulas for radiative decays by Z emission. As we discussed for the $2^- \to 1^+ + \gamma/Z$ decay, the ratio of leptonic Z bosons to photons is unlikely to reach 2%, even if there is no phase space suppression (which there typically is.) Moreover, decays to Z are described by a larger number of unknown form factors, making any attempt to predict the corresponding decay widths and branching ratios even more uncertain than for photon emission.

Decays of the 1^{+-} state.

Since the 1^{+-} is the lightest v-glueball in the C-odd sector, it can only decay, radiatively, to the lighter v-glueballs in the C-even sector.

According to table 2.5, the amplitude of the decay $1^{+-} \to 0^{++} + \gamma$ is given by[11]

$$\frac{e g_v^3}{(4\pi)^2 M^4}\,\chi \langle \gamma |\, G^{\mu\nu} \,| 0\rangle \,\langle 0^{++} |\, \Omega_{\mu\nu} \,| 1^{+-}\rangle = \frac{e g_v^3 \chi}{(4\pi)^2 M^4}\, 2 k_\mu \varepsilon_\nu \epsilon^{\mu\nu\alpha\beta} p_\alpha \epsilon_\beta \mathbf{M}^{\mathbf{\Omega}}_{\mathbf{1^{+-}0^{++}}}, \tag{2.53}$$

where ε_μ and ϵ_μ are the polarization vectors of the photon and the pseudovector v-glueball respectively; p_μ is the 4-momentum of the 0^{++}. The Levi-Civita tensor assures the final particles

[11] Similar amplitudes are used in the studies of vector and pseudovector mesons. See for example [32], [33] and [36].

are in a p-wave, as required by parity conservation. The decay rate of this process is

$$\Gamma_{1^{+}\to 0^{+}+\gamma} = \frac{\alpha\alpha_v^3}{24\pi M^8}\,\chi^2\,\frac{(m_{1^+}^2 - m_{0^+}^2)^3}{m_{1^+}^3}\,(\mathbf{M}^{\mathbf{\Omega}}_{\mathbf{1^{+-}0^{++}}})^2. \tag{2.54}$$

In the case of the decay to the pseudoscalar v-glueball $1^{+-} \to 0^{-+} + \gamma$, the amplitude is given by

$$\frac{eg_v^3}{(4\pi)^2 M^4}\,\chi\langle\,\gamma|\,G^{\mu\nu}|\,0\rangle\,\langle 0^{-+}|\,\Omega_{\mu\nu}|\,1^{+-}\rangle = \\ = \frac{eg_v^3}{(4\pi)^2 M^4}\,\chi\;2k^\mu\varepsilon^\nu(p_\mu\epsilon_\nu - p_\nu\epsilon_\mu)\mathbf{M}^{\mathbf{\Omega}}_{\mathbf{1^{+-}0^{-+}}}, \tag{2.55}$$

where p_μ is the 4-momentum of the 0^{-+}. The rate of the decay to the pseudoscalar is then

$$\Gamma_{1^{+}\to 0^{-}+\gamma} = \frac{\alpha\alpha_v^3}{24\pi M^8}\,\chi^2\,\frac{(m_{1^+}^2 - m_{0^-}^2)^3}{m_{1^+}^3}\,(\mathbf{M}^{\mathbf{\Omega}}_{\mathbf{1^{+-}0^{-+}}})^2. \tag{2.56}$$

The ratio of the decay rates to 0^{-+} and 0^{++} is

$$\frac{\Gamma_{1^{+}\to 0^{-}+\gamma}}{\Gamma_{1^{+}\to 0^{+}+\gamma}} = \left(\frac{m_{1^+}^2 - m_{0^-}^2}{m_{1^+}^2 - m_{0^+}^2}\right)^3 \left(\frac{\mathbf{M}^{\mathbf{\Omega}}_{\mathbf{1^{+-}0^{-+}}}}{\mathbf{M}^{\mathbf{\Omega}}_{\mathbf{1^{+-}0^{++}}}}\right)^2. \tag{2.57}$$

For the spectrum of figure 2.1, the factor involving the masses is about 0.39; the ratio of matrix elements is unknown, but if we guess that $\mathbf{M}^{\mathbf{\Omega}}_{\mathbf{1^{--}0^{\pm+}}} \sim 1/\mathbf{F}^{\mathbf{S,P}}_{\mathbf{0^{\pm+}}}$, as would be true for pion emission, and use the lattice results from [25], we would find this ratio to be slightly larger than 1. In any case, there is no sign of a significant suppression of one rate relative to the other.

Finally, in the case of the decay to the tensor v-glueball, the amplitude $1^{+-} \to 2^{++} + \gamma$ contains two independent form factors in the lowest partial wave approximation, denoted $\mathbf{M}^{\mathbf{\Omega}}_{\mathbf{1^{+-}0^{-+}}}$ and $\mathbf{M'}^{\mathbf{\Omega}}_{\mathbf{1^{+-}0^{-+}}}$,

$$\frac{eg_v^3}{(4\pi)^2 M^4}\,\chi\langle\,\gamma|\,G^{\mu\nu}|\,0\rangle\,\langle 2^{++}|\,\Omega_{\mu\nu}|\,1^{+-}\rangle = \\ = \frac{eg_v^3}{(4\pi)^2 M^4}\,\chi\;2k^\mu\varepsilon^\nu\epsilon_{\mu\nu\alpha\beta}\epsilon_{\beta\lambda}(\epsilon_\lambda p_\alpha\mathbf{M}^{\mathbf{\Omega}}_{\mathbf{1^{+-}0^{-+}}} + \epsilon_\alpha p_\lambda\mathbf{M'}^{\mathbf{\Omega}}_{\mathbf{1^{+-}0^{-+}}}) \tag{2.58}$$

and the corresponding decay rate is

$$\Gamma_{1^{+}\to 2^{+}+\gamma} = \frac{\alpha\alpha_v^3}{576\pi M^8}\,\chi^2\,\frac{(m_{1^+}^2 - m_{2^+}^2)^3}{m_{1^+}^5 m_{2^+}^2}\,\left(3m_{2^+}^4 + 34m_{1^+}^2m_{2^+}^2 + 3m_{1^+}^4\right)\times \\ \times\left[\left(\mathbf{M}^{\mathbf{\Omega}}_{\mathbf{1^{+-}2^{++}}} + \mathbf{M'}^{\mathbf{\Omega}}_{\mathbf{1^{+-}2^{++}}} f(m_{1^+}, m_{2^+})\right)^2 \right. \\ \left. + \left(\mathbf{M'}^{\mathbf{\Omega}}_{\mathbf{1^{+-}2^{++}}}\right)^2 g(m_{1^+}, m_{2^+})\right], \tag{2.59}$$

where f and g are the following functions of the v-glueball masses,

$$f(m_{1^+}, m_{2^+}) = \frac{\left(m_{2^+}^2 - m_{1^+}^2\right)\left(3m_{2^+}^2 + 7m_{1^+}^2\right)}{3m_{2^+}^4 + 34m_{1^+}^2m_{2^+}^2 + 3m_{1^+}^4}, \tag{2.60}$$

$$g(m_{1^+}, m_{2^+}) = 12\,\frac{\left(m_{2^+}^2 - m_{1^+}^2\right)^2 m_{1^+}^2(6m_{2^+}^4 + 8m_{1^+}^2m_{2^+}^2 + m_{1^+}^4)}{m_{2^+}^2\left(3m_{2^+}^4 + 34m_{1^+}^2m_{2^+}^2 + 3m_{1^+}^4\right)^2}. \tag{2.61}$$

Decays of the 1^{--} state.

The decays of the vector v-glueball are similar to the decays of the pseudovector, with a few additions. In contrast to the case of the 1^{+-}, the 1^{--} can annihilate through an off-shell vector boson to a SM fermion-antifermion pair. But the radiative decays to light v-glueballs in the C-even sector still typically dominate.

The radiative decay to the scalar, $1^{--} \to 0^{++}+\gamma$, is analogous to the decay $1^{--} \to 0^{++}+\gamma$; see table 2.5 and (2.56). Thus, its rate is

$$\Gamma_{1^-\to 0^+ +\gamma} = \frac{\alpha\alpha_v^3}{24\pi M^8}\,\chi^2\,\frac{(m_{1^-}^2 - m_{0^+}^2)^3}{m_{1^-}^3}\,(\mathbf{M}^{\mathbf{\Omega}}_{\mathbf{1^{--}0^{++}}})^2. \tag{2.62}$$

The decay to the pseudoscalar is analogous to the decay (3.17) and has the rate

$$\Gamma_{1^-\to 0^- +\gamma} = \frac{\alpha\alpha_v^3}{24\pi M^8}\,\chi^2\,\frac{(m_{1^-}^2 - m_{0^-}^2)^3}{m_{1^-}^3}\,(\mathbf{M}^{\mathbf{\Omega}}_{\mathbf{1^{--}0^{-+}}})^2. \tag{2.63}$$

The amplitude of the decay to the 2^{++} state is similar to the amplitude (2.49) of the decay $2^{-+} \to 1^{+-} + \gamma$. However, in this case the masses of the two states are not close, and our approximation which allowed us to ignore the contribution of three additional form factors is not valid. We therefore restrict ourselves to just demonstrating the general expression for the amplitude.

$$\begin{aligned}\frac{eg_v^3\chi}{(4\pi)^2M^4}\langle\,\gamma|\,G^{\mu\nu}\,|\,0\rangle\langle 2^{++}|\,\Omega_{\mu\nu}|\,1^{--}\rangle &= 2\mathbf{M}^{\mathbf{\Omega}}_{\mathbf{1^{--}2^{++}}}(k\cdot p\,\varepsilon^\alpha\epsilon_{\alpha\beta}\epsilon^\beta - p\cdot\varepsilon\,k^\alpha\epsilon_{\alpha\beta}\epsilon^\beta)\\ &+ 2\mathbf{M}^{\mathbf{\Omega'}}_{\mathbf{1^{--}2^{++}}}(k\cdot q\,\varepsilon\cdot\epsilon - k\cdot\epsilon q\cdot\varepsilon)\,\frac{q^\alpha\epsilon_{\alpha\beta}q^\beta}{m_{1^-}^2} +\\ &+ 2\mathbf{M}^{\mathbf{\Omega''}}_{\mathbf{1^{--}2^{++}}}(k\cdot q\,\varepsilon^\alpha\epsilon_{\alpha\beta}q^\beta - q\cdot\varepsilon\,k^\alpha\epsilon_{\alpha\beta}q^\beta)\frac{p\cdot\epsilon}{m_{1^-}^2}.\end{aligned} \tag{2.64}$$

A complete formula for the decay rate is not very useful, given the large number of unknown form factors that enter.

The 1^{--} state is also massive enough to decay to the 2^{-+} state. This decay has an amplitude similar to the decay $1^{+-} \to 2^{++} + \gamma$, given in (2.58). One can find the decay rate

$$\begin{aligned}\Gamma_{1^-\to 2^- +\gamma} = \frac{\alpha\alpha_v^3}{576\pi M^8}\,\chi^2\,\frac{(m_{1^-}^2 - m_{2^-}^2)^3}{m_{1^-}^5 m_{2^-}^2}\,\left(3m_{2^-}^4 + 34m_{1^-}^2m_{2^-}^2 + 3m_{1^-}^4\right)\times\\ \times\left[\left(\mathbf{M}^{\mathbf{\Omega}}_{\mathbf{1^{--}2^{-+}}} + \mathbf{M'}^{\mathbf{\Omega}}_{\mathbf{1^{--}2^{-+}}} f(m_{1^-},m_{2^-})\right)^2\right.\\ \left. + \left(\mathbf{M'}^{\mathbf{\Omega}}_{\mathbf{1^{--}2^{-+}}}\right)^2 g(m_{1^-},m_{2^-})\right],\end{aligned} \tag{2.65}$$

where functions f and g are defined by (2.60) and (2.61) respectively.

Now we consider the decay of the 1^{--} to SM fermion pairs through an off-shell γ or Z. For large m_{1^-} we can neglect the Z mass and treat the radiated particle as an off-shell hypercharge

boson. The amplitude reads

$$\frac{\alpha g_v^3}{2\pi M^4}\,\frac{\chi}{\cos^2\theta_W}\,\langle f,\bar{f}|Y_L\bar{\psi}_L\gamma^\mu\psi_L+Y_R\bar{\psi}_R\gamma^\mu\psi_R|\,0\rangle\,\frac{1}{p^2}\,\langle 0|p^\nu\Omega_{\nu\mu}|1^{--}\rangle. \tag{2.66}$$

Here Y_L and Y_R are left and right hypercharges of the emitted fermions. The matrix element of $\Omega_{\mu\nu}$ can be read off from table 2.4. The width (ignoring the fermion masses) is given by

$$\Gamma_{1^-\to\bar{f}f}=\frac{2\alpha^2\alpha_v^3}{3M^8}\,\frac{\chi^2}{\cos^4\theta_W}\,(Y_L^2+Y_R^2)\,m_{1^-}^3\,(\mathbf{F}^{\mathbf{\Omega}}_{\mathbf{1}^{--}})^2. \tag{2.67}$$

For quarks a factor of 3 must be included to account for color.

The above result is valid for $m_{1^-}\gg m_Z$. For smaller m_{1^-} one must account for the non-zero Z mass through the substitution

$$\frac{(Y_L^2+Y_R^2)}{\cos^4\theta_W}\to\left(Q-\frac{Q\cos^2\theta_W-Y_L}{\cos^2\theta_W}\,\frac{m_{1^-}^2}{m_{1^-}^2-m_Z^2}\right)^2+ \\ +Y_R^2\left(1+\frac{\sin^2\theta_W}{\cos^2\theta_W}\,\frac{m_{1^-}^2}{m_{1^-}^2-m_Z^2}\right)^2, \tag{2.68}$$

which accounts for a finite mass of the Z-boson. Here $Q=T_3+Y$ is the charge of f. A quick check shows that this rate, whose ratio to radiative decays is (for large m_{1^-})

$$\frac{\Gamma_{1^-\to\gamma^*/Z^*\to f\bar{f}}}{\Gamma_{1^-\to 0^+\gamma}}=\frac{16\pi\alpha}{\cos^4\theta_W}\,(Y_L^2+Y_R^2)\left(\frac{m_{1^-}^2}{m_{1^-}^2-m_{0^+}^2}\right)^3\left(\frac{\mathbf{F}^{\mathbf{\Omega}}_{\mathbf{1}^{--}}}{\mathbf{M}^{\mathbf{\Omega}}_{\mathbf{1}^{--}\mathbf{0}^{++}}}\right)^2, \tag{2.69}$$

is not negligible. The first factor in curved brackets is a factor of a few, while the second factor in curved brackets may be large, especially at large n_v. Decays to electrons and muons will be reconstructable as a resonance, so despite the uncertain branching fractions this decay mode is worthy of careful consideration.

Decay of the 1^{--} state to the 1^{+-} v-glueball can only proceed with the emission of at least two SM gauge bosons. Although such decays are suppressed, the details of the calculation for $1^{--}\to 1^{+-}+gg$ are presented in the Appendix.

2.3.3 Decays of the remaining states

We may infer without detailed calculation that the likely decays of the other v-glueballs in the C-odd sector are radiative. Three-body decays to two gauge bosons plus another C-odd v-glueball are quite suppressed by phase space, because the mass splittings in the C-odd sector are never large. Even the splitting of the 0^{+-} state from the 1^{+-} state is only 1.1 $m_{0^{++}}$. By contrast, two-body radiative decays into the C-even sector have significantly larger phase space. (In the appendix A.1, we confirm this for decays of the 1^{--} state.) Meanwhile, no operator appearing in the effective action at dimension $D=8$ permits the 0^{+-}, $2^{\pm-}$, or $3^{\pm-}$ states to

annihilate directly to standard model particles. Therefore, we should expect that *all* of these states decay radiatively, emitting typically a photon or more rarely (if kinematically allowed) a Z, to a v-glueball of opposite C. Their lifetimes will be of order or slightly shorter than that of the 1^{-+}, due to enhanced phase space and additional decay channels.

The 3^{++} state is more complicated. No operator allows it to annihilate directly to standard model gauge bosons, so it will decay either by a two-body radiative transition to the C-odd sector or by a three-body decay to two gauge bosons plus a C-even v-glueball. For this state, in contrast to the C-odd states, the mass splittings tend to suppress the radiative decay and enhance the three-body decays. With many contributing decay channels and unknown form factors, it seems impossible to estimate which type of decay is dominant. Indeed simple estimates suggest they are of the same order, with large uncertainties. Qualitatively, if the colored X particles are very heavy and χ_s is very small, radiative decays will probably dominate, while tight degeneracies within the X multiplet(s) could suppress χ and reverse the situation. But quantitative prediction seems impossible.

2.4 Conclusions

Let us first summarize our results and their immediate implications.

- We have seen that annihilation decays dominate those states that can be created by dimension $d = 4$ operators (the $0^{\pm+}$ and $2^{\pm+}$). Their branching fractions are dominated by decays to gg, with decays to $\gamma\gamma$ having a branching fraction of $\sim 0.4\%$, assuming the X fields form complete $SU(5)$ multiplets of equal mass. If the colored X particles are much heavier than the uncolored ones, then decays to electroweak bosons can dominate.

- Most other states decay by radiatively emitting a photon, or (at a rate that is at most $\tan^2\theta_W$ compared to photon emission) a Z boson.

- The 1^{--} is a special case; it typically prefers to decay radiatively but has a non-negligible annihilation decay to an off-shell γ or Z.

- The 3^{++} is also special; three-body decays to gluons plus a C-even v-glueball could be of the same order or even dominate over radiative decays to the C-odd sector.

- In all, we expect the final states from v-glueball production to be rich in jets and stray photons, with occasional photon pairs, leptons and some missing energy from neutrinos. The two-photon resonances from the annihilation decays of C-even v-glueballs are likely to

be the discovery signatures, along with the $\gamma\gamma\gamma$ and γgg resonances from cascade decays of C-odd v-glueballs.

- Depending on the parameters, the lifetime of any given state can vary over many orders of magnitude. But for any fixed choice of parameters, lifetimes of the v-glueballs vary over at least three or four orders of magnitude, the details depending on unknown v-glueball matrix elements and mass ratios, as well as the X mass spectrum. Displaced vertices can potentially serve as a discovery channel.

- There are several opportunities for discovery of this signal in displaced vertices. One option arises from gg decays in events triggered by photons, another from W^+W^- decays triggered by the muon or electron in a leptonic W decay, and a third from photons that arrive late or (if converted) point away from the primary vertex.

Our results are robust, but some cautionary and clarifying remarks are in order. Clearly, numerical application of our formulas is currently subject to considerable uncertainties, due especially to the many unknown matrix elements that arise, and due also to the unknown spectrum for gauge groups other than $SU(3)$. Of course these uncertainties are largely reducible through additional lattice gauge theory computations, should a discovery of a sector of this type be made. However, there are other potential subtleties to keep in mind. If the X fields and the v-glueball states have comparable masses, then mixing between these states cannot be neglected. This could lead to additional physical effects that we have not considered. We also remind the reader that we have worked at leading non-vanishing order and that higher-order corrections are not negligible when precise predictions are required.

A more qualitative uncertainty, and an interesting opportunity, arises from the gauge group. For $SU(n)$, $n > 2$, it is anticipated that the glueball spectrum is similar to that of $SU(3)$, as calculated by [24]. However the $SU(2)$ spectrum, and more generally that of any $Sp(2n_v)$ or $SO(2n_v + 1)$ gauge group, has no C-odd sector. The operators $\Omega^{(i)}_{\mu\nu}$ do not exist, as they are built from the d^{abc} symbol absent from such groups, and the corresponding C-odd states are also absent.

For $SO(2n_v)$ the situation is more subtle. The first cases are $SO(4)$, which is not simple and has two sets of $SU(2)$ v-glueballs, and $SO(6)$, which is the same as $SU(4)$. The $d = 6$ $\Omega^{(i)}_{\mu\nu}$ operators are present for $SO(6)$, but for general $SO(2n_v)$ the $\Omega^{(i)}_{\mu\nu}$ operators become Pfaffian operators of dimension $2n_v$, built from a single epsilon symbol and n_v field strengths. As suggested by [46] and as verified by [24], there is a correlation in the QCD spectrum and in the glueball spectrum between the dimension of an operator and the mass of the lightest

corresponding state. For this reason we expect that for a pure $SO(2n_v)$ gauge theory with $n_v > 3$, the C-odd states are heavier than in figure 2.1 relative to the C-even states. Their production rate is likely to be quite suppressed as a result, but are still interesting, since several are likely to be unable to decay to other v-glueballs alone, and will be metastable. Certainly the lightest C-odd state (probably still the 1^{+-}) cannot decay to two or more C-even v-glueballs, so it will likely decay by radiating a photon or Z. Moreover, the degeneracy of the light C-odd states seen in $SU(3)$ may well persist more generally, making these states potentially unable to decay to two v-glueballs in a C-odd final state, such as $1^{+-} + 0^{++}$. All of these states will decay therefore to the C-even sector by radiating a photon (or Z), except the 1^{--} that may again decay to standard model fermions. The larger phase space for $n_v > 3$ means the lifetimes may be much shorter than those of the C-even states, a fact which could be phenomenologically important if Λ_v and Λ_v/M are so small that the C-even states are unobservably long-lived.

Thus study of the spectrum of the v-glueballs may provide some information on the gauge group. Combined with some partial information about the X production rate and the branching fractions of $X\bar{X}$ annihilations, it may well be possible to identify the gauge group precisely.

Finally, we have assumed here that the v-glueballs are the low-energy degrees of freedom of an asymptotically weakly-coupled gauge theory. The AdS/CFT correspondence [69, 70] allows us to learn what one might observe if the theory has a large 't Hooft coupling in the ultraviolet. In particular, the low-lying glueballs of such a theory can be described as modes of a string theory on a 10-dimensional space compactified to 5 dimensions. Such a theory [71–73] will have light scalars, pseudoscalars, tensors, etc., but will not have any light 2^{-+} state. Apparently the mass of this state may serve as a crude probe of the size of the ultraviolet 't Hooft coupling, as long as its mass is not so high as to render the state unstable to decay to lighter glueballs.

Chapter 3

Pure-glue hidden valleys through the Higgs portal

Based on [20], in this chapter we shall our extend earlier results on hidden valleys to include couplings of the messenger fields to the standard model Higgs sector, with the aim of obtaining an acceptable phenomenology for even lower v-glueball masses.

The v-glueballs are non-interacting with the SM particles, except for higher dimension operators in the effective Lagrangian induced by the heavy mediators X_r. In this work, we will focus on the possibility of operators between the v-sector and the Higgs sector (also referred to as the Higgs portal),

$$\frac{1}{M^{D-4}}\,\mathcal{O}_s^{D-d}(H^\dagger, H)\,\mathcal{O}_v^{(d)} \tag{3.1}$$

where H is the standard model Higgs doublet; M is a heavy mass scale, associated with the masses of the heavy mediator fields. Here we have split the dimension-D operator into a Standard-Model part $\mathcal{O}_s^{(D-d)}$ of dimension $D-d$ and a hidden-valley part $\mathcal{O}_v^{(d)}$ of dimension d. The $\mathcal{O}_v^{(d)}$ are constructed from gauge invariant combinations of v-gluon fields such as tr $\mathcal{F}^2$ or tr $\mathcal{F}^3$, while the $\mathcal{O}_s^{(D-d)}$ involve gauge invariant operators built out of the Higgs field, such as $H^\dagger H$ or $H^\dagger D_\mu H$. We will see that the lowest order term is given by the dimension-six operators of the form $H^\dagger H$ tr $\mathcal{F}^2$. With some exceptions to be discussed below, most of the v-glueballs in figure 2.1 can decay via the Higgs portal interaction (3.1), with a strong dependence of the lifetimes on the confinement scale Λ_v and the mass scale M.

Loops of the heavy particles also induce dimension-eight effective interactions coupling the v-gluons to the standard model gauge bosons, either of the form tr F_i^2 tr $\mathcal{F}^2$ or F_1 tr $\mathcal{F}^3$ where F_i ($\mathcal{F}$) is the field strength tensor for standard model (hidden-valley) gauge bosons. The field strength tensors are contracted according to different irreducible representations of the Lorentz group. A detailed study of the phenomenology of these operators in the context of hidden valleys was carried out in [19]. In this case the v-glueball widths are dominated by decays into SM gauge-boson pairs, or radiative decays to another v-glueball and a photon (or to a lesser extent a Z boson), leading to jet and photon rich final states.

In this chapter, we will first extend the results of [19] on v-glueball decays in pure-Yang-Mills

theory to allow for higher dimension interactions of the form (3.1). We will need to compute the effective Lagrangian coupling the v-gluons to the Higgs sector. Then we will use it to find formulas for the decay widths of the states in the spectrum shown in figure 2.1. Specifically, we will find that the 0^{++} state can decay via the Higgs portal to standard model particles with branching ratios which are determined by the couplings of the standard model Higgs boson. Other states can decay to a lighter state by emission of a Higgs boson. For v-glueball states which can decay either through dimension-eight operators or through the emission of a Higgs boson the situation is rather involved, with the relative branching ratios depending on the various parameters and the unknown v-glueball matrix elements.

Our primary motivation here is in the case where the lifetimes are short enough that at least a few v-glueball decays can be observed at the LHC detectors. This typically requires the lifetimes of the hidden particles to be shorter than a few micro-seconds, if the production cross-section is substantial. The key point in our scenario is that with different operators describing the decays, often competing with each other, we typically find a large spread in the lifetimes of the v-glueballs, even after all the parameters have been fixed. Then there is no necessity to adjust any parameter to obtain short lifetimes.

Incidentally, our results are also relevant for studies of dark matter, either in the case of self-interacting dark matter [39], where the v-glueballs would be the dark matter candidates, or indirectly, in a recent attempt to study scenarios of dark matter with novel signatures [40, 41].

This chapter is organized as follows. In section 2, we introduce our model and describe the effective interactions coupling the two sectors. We also classify the matrix elements. Section 3 presents our computation of the decay modes. Section 4 is devoted to a summary of the different experimental constraints on the parameters of the model. Then in section 5 we present our numerical estimates for the branching ratios. Possible generalizations of the model are described in section 6. Finally, we conclude in section 7 with a brief summary of our results and some comments. Additional computations appear in the appendix.

3.1 The model and the effective action

We first set up our framework and conventions. The generic scenario of hidden valleys with a pure-gauge hidden sector can be characterized as follows [6, 19],

- The SM is extended by the addition of an extra $SU(n_v)$ gauge group, with a mass scale scale m_0 in the $1 - 1000$ GeV range. We will refer to this sector as the hidden valley, or briefly the v-sector. There are no light flavours in the v-sector, so after confinement the

lightest states in the spectrum are bound states of v-gluons, or v-glueballs.

- There are heavy vector-like particles X_r ("mediators") that couple the v-sector very weakly to the visible sector at low energies. For definiteness, we will take the X_r to transform as a fundamental representation of $SU(n_v)$ and in complete $SU(5)$ representations of the standard model. We label the fields and their masses as shown in table 3.1. Also, for convenience, we define dimensionless parameters $\rho_r = m_r/M$ where M is an arbitrarily chosen mass scale, usually taken as the mass of the lightest X_r particle[1].

Field	$SU(3)$	$SU(2)$	$U(1)$	$SU(n_v)$	Mass
$X_{\bar{d}}$	**3**	**1**	$\frac{1}{3}$	$\mathbf{n_v}$	$m_{\bar{d}}$
X_ℓ	**1**	**2**	$-\frac{1}{2}$	$\mathbf{n_v}$	m_ℓ
$X_{\bar{u}}$	$\overline{\mathbf{3}}$	**1**	$-\frac{2}{3}$	$\mathbf{n_v}$	$m_{\bar{u}}$
X_q	**3**	**2**	$\frac{1}{6}$	$\mathbf{n_v}$	m_q
X_e	**1**	**1**	**1**	$\mathbf{n_v}$	m_e

Table 3.1: The new fermions X_r that couple the hidden valley sector to the SM sector.

In addition, we assume that the mediators X_r can get part of their mass from electroweak symmetry breaking through Yukawa-like interactions. For concreteness, we consider the following Lagrangian (in four-component Dirac notation),

$$\mathcal{L}_{mass} = \sum_{r=\bar{d},l,\bar{u},q,\bar{e}} m_r \bar{X}_r X_r + \left(y_l \bar{X}_l H X_{\bar{e}} + y_u \bar{X}_q \tilde{H} X_u + y_d \bar{X}_q H X_d + h.c. \right) \tag{3.1}$$

where $\tilde{H} = \epsilon \cdot H^\dagger$. For the moment, we will restrict ourselves to the case in which the Yukawa couplings conserve both C and P independently. In general one or more of the Yukawa couplings could be CP-violating. This CP violation can contribute new terms to the effective action and can induce additional v-glueball decays, as will be discussed in section 6.

There are several constraints on the couplings y_r and the mass scale M from precision electroweak measurements. These constraints will be discussed in some detail in section 4. We require that $y_r \lesssim 1$ and $M \gtrsim 250$ GeV in order to avoid potentially dangerous corrections to precision electroweak bounds. A high mass scale is in any case necessary to avoid current experimental bounds from collider searches for extra particles.

We are concerned with the low-energy effective theory of the model described above. The effective interaction that couples the v-gluons and v-glueballs to the SM particles is induced

[1] In this work, we normalize hypercharge as $Y = Q - T_3$, where T_3 is the third component of weak isospin.

through a loop of X particles. The coupling between the Higgs sector and the v-sector to non-vanishing leading order in $1/M$ at low energies arises from a diagram with four external lines, as depicted in figure 3.1a. This gives rise to the dimension-six operator

$$\mathcal{L}^{(6)} = \frac{\alpha_v\, y^2}{3\pi\, M^2}\, H^\dagger H \,\mathrm{tr}\, \mathcal{F}_{\mu\nu}\mathcal{F}^{\mu\nu} \tag{3.2}$$

where α_v is the $SU(n_v)$ coupling, $\mathcal{F}_{\mu\nu}$ is the v-gluon field strength tensor[2]. The coefficient y depends on the mass ratios of the heavy particles from table 3.1 and their couplings to the Higgs field. It is given by

$$y^2 \equiv \frac{y_l^2}{\rho_l \rho_e} + \frac{3y_d^2}{\rho_q \rho_{\bar{d}}} + \frac{3y_u^2}{\rho_q \rho_{\bar{u}}}. \tag{3.3}$$

The computation of (3.2) is presented in appendix A.2. Note that (3.2)-(3.3) are strictly valid in the $\beta_r \equiv y_r^2 v_H^2/2M^2 \ll 1$ limit; otherwise, the corrections to these equations can be readily obtained by the substitutions $\rho_r \rho_{r'} \to \rho_r \rho_{r'} - \beta_r$ in (3.3). Once the Higgs gets an expectation value, the following interaction terms are induced between the v-sector and the physical standard model Higgs boson (h),

$$\mathcal{L}^{(6)} = \frac{\alpha_v\, y^2}{3\pi M^2}\, v_H\, h \,\mathrm{tr}\, \mathcal{F}_{\mu\nu}\mathcal{F}^{\mu\nu} + \frac{\alpha_v\, y^2}{3\pi M^2}\, \frac{h^2}{2} \,\mathrm{tr}\, \mathcal{F}_{\mu\nu}\mathcal{F}^{\mu\nu} \tag{3.4}$$

where $v_H = 246$ GeV is the Higgs vacuum expectation value[3].

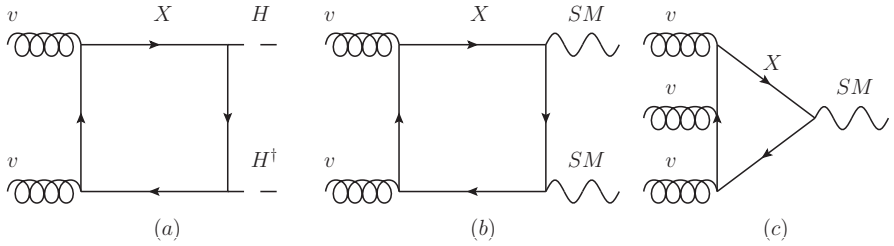

Figure 3.1: Diagrams contributing to the effective action

While dimension-six operators are only suppressed by two powers of the mass scale M, further suppression can arise if the operators are suppressed by small coupling y. This requires us to consider effective operators of dimension higher than six as well.

The next operators have $D = 8$, and they describe the coupling of the two v-gluons to two SM gauge bosons (figure 3.1b), either gluons (g), weak bosons (W and Z) or photons (γ), as well

[2]Here we represent the v-gluon fields as $\mathcal{F}_{\mu\nu} = \mathcal{F}^a_{\mu\nu} T^a$, where T^a denote the generators of the $SU(n_v)$ algebra with a common normalization $\mathrm{tr}\, T^a T^b = \frac{1}{2}\delta^{ab}$.

[3]In (3.4), we have not included a term which is proportional to the v-gluon kinetic term. This term can be removed by redefining the v-gluon coupling.

as the fusion of three v-gluons into a γ or Z (figure 3.1c). Within the SM, effective two gluon - two photon, four gluon, and three gluon - photon vertices can be found in [42], [43] and [44] respectively. They were also extensively discussed in the previous chapter. The pure-gauge effective Lagrangian linking the SM sector with the v-sector is given in (2.9).

We will not consider operators of dimension 8 containing both gauge-boson fields and the Higgs field, as well as dimension-ten or higher operators, since their effects are suppressed by extra powers of M and/or y.

The interactions in the effective action then allow the v-glueballs that cannot decay within the v-sector to decay to final states with SM particles and at most one v-glueball. This is similar to the weak decays of hadrons, such as $\pi^+ \to l\nu$, $n \to p\nu_e e^-$, and so forth, where the Fermi effective interaction allows otherwise stable hadrons to decay into leptons. To compute these decays, we will only need the following factorized matrix elements[4]:

$$\langle SM|\mathcal{O}_s^{(D-d)}|0\rangle\langle 0|\mathcal{O}_v^{(d)}|\Theta_\kappa\rangle \ , \tag{3.5}$$

$$\langle SM|\mathcal{O}_s^{(D-d)}|0\rangle\langle \Theta_{\kappa'}|\mathcal{O}_v^{(d)}|\Theta_\kappa\rangle. \tag{3.6}$$

Here d is the mass dimension of the operator in the v-sector, $\langle SM|$ schematically represents a state built from Standard Model particles, and $|\Theta_\kappa\rangle$ and $|\Theta_{\kappa'}\rangle$ refer to v-glueball states with quantum numbers κ, which include spin J, parity P and charge-conjugation C. The SM part $\langle SM|\mathcal{O}_s^{(D-d)}|0\rangle$ can be evaluated by the usual perturbative methods of quantum field theory, but a computation of the hidden-sector matrix elements $\langle 0|\mathcal{O}_v^{(d)}|\Theta_\kappa\rangle$ and $\langle \Theta_{\kappa'}|\mathcal{O}_v^{(d)}|\Theta_\kappa\rangle$ requires the use of non-perturbative methods.

3.1.1 Matrix elements

We wish to classify the non-vanishing v-sector matrix elements of the scalar operator $S \equiv$ tr $\mathcal{F}_{\mu\nu}\mathcal{F}^{\mu\nu}$ in (3.2). As we saw, the matrix elements relevant to v-glueball transitions are given by $\langle 0|S|\Theta_\kappa\rangle$ and $\langle \Theta_{\kappa'}|S|\Theta_\kappa\rangle$, where Θ_κ and $\Theta_{\kappa'}$ refer to v-glueball states with given quantum numbers.

It is convenient to write the most general possible matrix elements in terms of a few Lorentz invariant amplitudes or form factors. The decomposition of S into irreducible representations of the Lorentz group contains only the 0^{++} quantum numbers [46]. This allows the 0^{++} state to decay directly to standard model particles. For the annihilation matrix element of the 0^{++}

[4] As mentioned in the introduction, decays with no SM particles in the final state are forbidden because of kinematics and/or conserved quantum numbers.

v-glueball, we will write

$$\langle 0|S|0^{++}\rangle \equiv \mathbf{F}^{\mathbf{S}}_{\mathbf{0^+}} \tag{3.7}$$

where $\mathbf{F}^{\mathbf{S}}_{\mathbf{0^+}}$ is the 0^{++} decay constant.

Likewise, we can consider the transition matrix elements of the operator S between a spin J state with momentum p and a spin J' state with momentum q. For the moment we make no assumptions about the parity or charge conjugation quantum numbers of the states. Of course, if we impose parity some of the transitions may be forbidden. The matrix elements can be compactly written as

$$\langle J'|S|J\rangle \equiv \sum_i \mathcal{M}^{(i)}_{JJ'}\, \mathbf{M}^{\mathbf{S(i)}}_{\mathbf{JJ'}} \tag{3.8}$$

where now $\mathbf{M}^{\mathbf{S(i)}}_{\mathbf{JJ'}}$ is the transition matrix, which depends on the transferred momentum, and $\mathcal{M}^{(i)}_{JJ'}$ is determined by the Lorentz representations of $|J\rangle$ and $|J'\rangle$. In Appendix C we have listed $\mathcal{M}^{(i)}_{JJ'}$ for the simplest cases considered later in this work.

The main uncertainties in the study of decays of the v-glueballs stem from the evaluation of the transition matrix elements $\mathbf{M}^{\mathbf{S(i)}}_{\mathbf{JJ'}}$ which at present are unknown. Many of these could be in principle be determined by additional lattice computations. In spite of these uncertainties, we will still be able to obtain many interesting and robust results.

3.2 Decay rates

An interesting feature of the model described above is that it has a spectrum of v-glueballs which can interact very weakly with the particles in the standard model through effective operators of different mass dimensions. The dimension-six operator, as we see below, permits the v-glueballs to decay directly into standard model particles (the 0^{++}) or radiatively by emitting a Higgs boson (the 2^{++}, 2^{-+}, 3^{++}, 3^{+-}, 2^{+-}, 0^{+-}, 1^{--}, 2^{--}, 3^{--}). On the other hand, dimension-eight operators contribute with additional decay modes. As shown in [19], these include direct annihilations into SM gauge-boson pairs (the 0^{++}, 2^{++}, 0^{-+} and 2^{-+}) or C-changing radiative transitions with emission of a photon or a Z boson (all others).

In this section, we will compute the decay rates for most of the v-glueballs in figure 2.1. We will first present our results for the v-glueball decays induced by dimension-six operators given in (3.2). Then we will make a quick review of the results of [19] for dimension-eight operators that are relevant for our work.

3.2.1 V-glueball decays by dimension-six operators

We begin with the 0^{++} v-glueball, which can be created by the operator S. The dimension-six coupling leads to $0^{++} \to \zeta\zeta$ annihilations, where ζ denote any of the final states of the Higgs boson. Above the threshold for Higgs boson pair production, the $0^{++} \to hh$ decay can also proceed with a sizeable rate. Other decay modes induced by dimension-six couplings include processes of the form $\Theta_\kappa \to \Theta_{\kappa'} h$, where Θ_κ, $\Theta_{\kappa'}$ denote two v-glueballs with given quantum numbers. As an example of a Higgs-radiative decay, we will present the computation of the $2^{++} \to 0^{++}h$ decay with some detail. Then we will consider the general case $\Theta_\kappa \to \Theta_{\kappa'} h$ for v-glueballs with arbitrary quantum numbers. In the end, we make some comments on the 0^{-+} and 1^{+-} v-glueballs, which are the only ones that are not permitted to decay via dimension-six operators.

Annihilation of the 0^{++} state

The scalar state can be created or destroyed by the S operator. Then, the effective interaction (3.2) allows the decay of the 0^{++} state via s-channel Higgs-boson exchange $0^{++} \to h^* \to \zeta\zeta$, where ζ collectively denotes a standard model particle. According to (3.2), the amplitude for this decay reads

$$\frac{y^2\,\alpha_v}{3\pi M^2}\,\langle \zeta\zeta | m_f \bar{f} f + m_Z^2 Z_\mu Z^\mu + 2 m_W^2 W_\mu^+ W^{\mu -} |\, 0\rangle\, \frac{1}{m_H^2 - m_0^2}\,\langle 0|S|0^{++}\rangle \tag{3.1}$$

where $\alpha_v = g_v^2/(4\pi)$ and m_H is the Higgs mass. The width of the decay is given by

$$\Gamma_{0^{++}\to\zeta\zeta} = \left(\frac{y^2\, v_H\, \alpha_v\, \mathbf{F^S_{0^+}}}{3\pi M^2 (m_H^2 - m_0^2)}\right)^2 \Gamma^{SM}_{h\to\zeta\zeta}(m^2_{0^+}) \tag{3.2}$$

where $\mathbf{F^S_{0^+}} \equiv \langle 0|S|0^{++}\rangle$ is the 0^{++} decay constant. Here $\Gamma^{SM}_{h\to\zeta\zeta}(m^2_{0^+})$ is the width for the decay $h \to \zeta\zeta$ for a standard model Higgs boson with a mass m_{0^+}. Then, formula (3.2) implies that the branching ratios of the 0^{++} are those of the SM Higgs boson in the range of mass of interest. Expressions for the branching ratios and full width of the Higgs boson can be found in the literature, for masses ranging from a few MeV up to 1 TeV (for a review, see [45]).

Although these are standard model tree-level results, we should also remark that the range of validity of (3.2) is beyond the simple perturbative QCD domain. For masses below $2-3$ GeV, the 0^{++} v-glueball can decay into a pair of hadrons via its interaction with two gluons through a top-quark loop or its interaction with quarks. The hadronization of these quarks and gluons is a rather complex and non-perturbative process. However, the branching ratios are still given by (3.2), with ζ now running over the possible hadrons in the final states, such as π, K, and so forth.

If $m_{0^+} > 2m_h$, the decay channel $0^{++} \to hh$ opens up and the partial width is given by

$$\Gamma_{0^+\to hh} = \frac{1}{32\pi m_{0^+}} \left(\frac{y^2\,\alpha_v\,\mathbf{F}^{\mathbf{S}}_{\mathbf{0^+}}}{3\pi\,M^2}\right)^2 \left(1+\frac{3m_H^2}{(m_{0^+}^2-m_H^2)}\right)^2 \left[g(m_H^2,m_H^2;m_{0^+}^2)\right]^{1/2} \tag{3.3}$$

where $g(x,y;z) \equiv (1-x/z-y/z)^2 - 4xy/z^2$. The off-shell decays $0^{++} \to h^*h$ and $0^+ \to h^*h^*$ are also possible in the intermediate mass range. However, these channels receive an extra suppression from the smaller available phase space, so it is reasonable to expect they will have little effect on the full 0^{++} width.

As m_{0^+} becomes larger than $2m_t$ and $2m_H$, we have the following approximate relationship among the dominant decay rates

$$\Gamma_{W^+W^-} : \Gamma_{ZZ} : \Gamma_{hh} : \Gamma_{t\bar{t}} = 2:1:1:3\,x_t\,\sqrt{1-x_t} \tag{3.4}$$

where $x_t = 4m_t^2/m_{0^+}^2$.

An example of Higgs-radiative decays: the $2^{++} \to 0^{++}h$ case

As an illustration of the computation of the decay rates for transitions with the emission of Higgs boson, let us first consider in some detail the decay of the 2^{++} v-glueball. Contrarily to the 0^{++}, direct annihilation of the 2^{++} v-glueball into Higgs bosons would require an operator in the effective action of dimension $D = 8$, and is hence negligible. Instead, for $m_{2^+} - m_{0^+} > m_H$, the S operator induces the $2^{++} \to 0^{++}h$ decay. In a parton-model picture, one may imagine this process as being caused by the radiative emission of a Higgs boson through $g_v \to g_v h$, with one spectator v-gluon going to the final state. The amplitude of this two-body decay is given by

$$\frac{y^2\,\alpha_v}{3\pi M^2}\langle h|h|0\rangle\langle 0^{++}|S|2^{++}\rangle = \frac{y^2}{3\pi M^2}\,\mathbf{M}^{\mathbf{S}}_{\mathbf{0^+2^+}}\,\epsilon_{\mu\nu}q^\mu q^\nu \tag{3.5}$$

where q^μ is the momentum of the 0^{++} and $\epsilon_{\mu\nu}$ the polarization of 2^{++}. Here $\mathbf{M}^S_{0^+2^+}$ denotes the transition matrix element defined by $\mathbf{M}^S_{0^+2^+}\epsilon_{\mu\nu}q^\mu q^\nu = \langle 0^{++}|S|2^{++}\rangle$; for simplicity we have assumed it is independent of the transferred momentum. The corresponding width of the decay reads

$$\Gamma = \frac{y^4\,\alpha_v^2}{480\pi(3\pi)^2M^4} m_{2^+}^3 \left[g(m_{0^+}^2,m_H^2;m_{2^+}^2)\right]^{5/2} (\mathbf{M}^{\mathbf{S}}_{\mathbf{0^+2^+}})^2. \tag{3.6}$$

If the 2^{++} is not heavy enough, $m_{2^+} - m_{0^+} < m_H$, it can decay to the 0^{++} and SM particles through the emission of an off-shell Higgs. The corresponding amplitude for the three-body decay $2^{++} \to 0^{++}\zeta\zeta$ is

$$\frac{y^2\alpha_v}{3\pi M^2}\,\langle\zeta\zeta|m_f\bar{f}f + m_Z^2 Z_\mu Z^\mu + 2m_W^2 W_\mu^+ W^{\mu-}|\,0\rangle\,\frac{1}{k^2-m_H^2+i\Gamma_h^{SM}m_H}\,\langle 0^{++}|S|2^{++}\rangle \tag{3.7}$$

where k^2 is the transferred momentum. The width is given by

$$\Gamma_{2^{++}\to 0^{++}\zeta\zeta} = \frac{m_{2^+}^3 (\mathbf{M}^{\mathbf{S}}_{\mathbf{0^+2^+}})^2}{160\pi^2}\left(\frac{y^2\,\alpha_v v_H}{3\pi M^2}\right)^2 \int dm_{12}^2 \frac{\left[g(m_{0^+}^2, m_{12}^2; m_{2^+}^2)\right]^{5/2}\Gamma^{SM}_{h\to\zeta\zeta}(m_{12})}{(m_{12}^2 - m_H^2)^2 + (\Gamma_h^{SM})^2\, m_H^2} \tag{3.8}$$

where the limits of integration are set by available phase space.

Higgs-radiative decays. General case $J \to J'h$

We now consider the 2-body decays $\Theta_J \to \Theta_{J'}\, h$, in which Θ_J, $\Theta_{J'}$ are v-glueballs with spin J, J' respectively. For the moment, we make no reference to the parity of the v-glueballs and proceed generally. Parity conservation will force some of the matrix elements to be zero. Making use of the general formulas for the matrix elements (A.24)-(A.31), we arrive at the decay rate

$$\Gamma^{(i)}_{J\to J'h}(m_H^2) = \frac{y^4\, v_h^2\, \alpha_v^2}{16\pi(3\pi)^2 M^4\, m_J\,(2J+1)} |\mathbf{M}^{\mathbf{S}}_{\mathbf{J},\mathbf{J'}}|^2\, \Gamma^{(i)}_{JJ'}\ \left[g(m_{J'}^2, m_H^2; m_J^2)\right]^{1/2} \tag{3.9}$$

where i runs over the various form factors. The coefficients $\Gamma^{(i)}_{JJ'}$ are dimensionless functions of the masses and depend on the angular momentum transfer associated with each transition. They are summarized in table 3.2.

i	1	2	3	4	5
$\Gamma^{(i)}_{32}$	$\frac{x}{15}(4x^2+28x+35)$	$\frac{4x^3}{15}(x+2)$	$\frac{4x^5}{15}$	$\frac{2x^2}{15}(2x+7)$	$\frac{4x^4}{15}$
$\Gamma^{(i)}_{31}$	$\frac{2x^2}{15}(3x+7)$	$\frac{2x^4}{5}$	$\frac{8x^3}{15}$	-	-
$\Gamma^{(i)}_{30}$	$\frac{2x^3}{5}$	-	-	-	-
$\Gamma^{(i)}_{22}$	$\frac{1}{9}(4x^2+30x+45)$	$\frac{x^2}{18}(8x+17)$	$\frac{4x^4}{9}$	$\frac{x}{2}(x+5)$	$\frac{x^3}{2}$
$\Gamma^{(i)}_{21}$	$\frac{x}{3}(2x+5)$	$\frac{2x^3}{3}$	x^2	-	-
$\Gamma^{(i)}_{20}$	$\frac{2x^2}{3}$	-	-	-	-
$\Gamma^{(i)}_{11}$	$x+3$	x^2	$2x$	-	-
$\Gamma^{(i)}_{10}$	x	-	-	-	-

Table 3.2: The coefficients $\Gamma^{(i)}_{JJ'}$ arise from the average of the squared matrix elements. We denote $x = \frac{m_J^2}{4m_{J'}^2} g(m_{J'}^2, m_H^2; m_J^2)$. The dashes denote those cases where form factors are absent.

Below the threshold for Higgs boson production, the decay rate for the 3-body decay $\Theta_J \to \Theta_{J'}\,\zeta\zeta$ reads,

$$\Gamma_{J\to J'\zeta\zeta} = \frac{1}{\pi}\int dm_{12}^2 m_{12} \Gamma^{(i)}_{J\to J'h}(m_{12}) \frac{1}{\Delta(m_{12}^2, m_H^2)} \Gamma^{SM}_{h\to\zeta\zeta}(m_{12}). \tag{3.10}$$

where $\Delta(m_{12}^2, m_H^2) = (m_{12}^2 - m_H^2)^2 + m_H^2(\Gamma_h^{SM})^2$. The integration automatically includes the case where the radiated Higgs boson can be close to onshell.

Some of the transitions may be parity-forbidden (e.g. $0^{-+} \to 1^{+-}h$). However, it is a straightforward exercise to check that for each v-glueball Θ_κ in figure 2.1 , there exists at least one other v-glueball $\Theta_{\kappa'}$ such that the transition $\Theta_\kappa \to \Theta_{\kappa'}h$ is allowed, with a rate which is given by (3.9)-(3.10). The only exceptions are the 0^{+-} and 1^{+-} v-glueballs that we discuss next.

Decays of the pseudoscalar and pseudovector

The only states that are not allowed to decay via dimension-six operators are the 1^{+-} and the 0^{-+} v-glueballs.

Since the 1^{+-} state is the lightest state in the C-odd sector, it necessarily has to decay to a v-glueball of opposite C. One possibility is that the 1^{+-} decays by radiatively emitting a Higgs boson (e.g. $1^{+-} \to 0^{-+}h$). However, this decay mode would violate C and, hence, is forbidden.

A second way to induce decays of the 1^{+-} v-glueball would be via its coupling to the hypercharge current $H^\dagger D_\mu H$. In this case, there are three v-sector operators that can be contracted with $H^\dagger D_\mu H$, namely,

$$\text{tr } \mathcal{F}_{\alpha\beta} D_\mu \mathcal{F}^{\alpha\beta}, \quad \text{tr } \mathcal{F}^{\alpha\beta} D_\beta \mathcal{F}_{\alpha\mu}, \quad \text{tr } \mathcal{F}_{\mu\beta} D_\alpha \mathcal{F}^{\alpha\beta}. \tag{3.11}$$

However, one can see that these operators cannot induce C-changing transitions. First, notice that classically $\text{tr } \mathcal{F}_{\alpha\beta} D_\mu \mathcal{F}^{\alpha\beta} = \frac{1}{2}\partial_\mu \text{tr } \mathcal{F}_{\alpha\beta}\mathcal{F}^{\alpha\beta}$. As explained in [46], this implies that the transitions induced by the first operator in (3.11) are not new. They are just the same ones created by the operator S. Likewise, using equations of motion and conservation of the energy-momentum tensor, the second operator in (3.11) can be related to a total derivative of the operator S. Finally, equations of motion also imply that the last operator in (3.11) vanishes identically. Therefore, up to operators of total mass dimension six, the 1^{+-} state is stable. In the next subsection, we shall see that dimension-eight operators can induce photon-radiative decays of the 1^{+-} v-glueball to C-even v-glueballs.

On the other hand, C-invariance by itself would allow the Higgs-radiative transition $0^{-+} \to 0^{++}h$. However, this decay could not conserve both angular momentum and parity P: since the initial state is 0^-, angular momentum conservation requires the orbital angular momentum of the 0^+ and h final state to be $L = 0$, which in turn requires total parity $P = +1$, rather than $P = -1$ as demanded by parity conservation. This decay mode is thus forbidden. This is analogous to the way that the η meson strong interaction mode $\eta \to \pi\pi$ is forbidden in the SM. A similar argument shows that the three-body decay $0^{-+} \to 0^{++}hh$ is not permitted. In this case, the corresponding $\eta \to \pi\pi\pi$ decay is allowed in the SM because, contrary to the 0^{++} and

h, the pions have intrinsic parity -1. As we will see in section 6, this line of argument alters if we relax our assumptions and allow for P-violating couplings.

3.2.2 V-glueball decays by dimension-eight operators

The operators in the effective action (2.9) induce decays for all of the v-glueball states in figure 2.1. The lightest states in the C-even sector (the 0^{++}, 2^{++}, 0^{-+} and 2^{-+}) can directly decay to pairs of standard model gauge bosons (gg, $\gamma\gamma$, ZZ, WW or γZ) via the S, P, T and L operators. All other states can decay by radiatively emitting a photon or, to a lesser extent, a Z boson, via the $d = 6$ $D = 8$ operators $\Omega_{\mu\nu}$. Here we briefly summarize our results concerning the computation of the decay rates induced by $D = 8$ operators in chapter 2.

In order to retain simplicity, we will often assume, in the subsequent discussion, the X fields form approximately degenerate multiplets of $SU(5)$, i.e. $\rho_r \approx 1$. When there is a large hierarchy between the colored and the uncolored X particles, $\rho_{\bar{d}} \gg \rho_l = \rho_e$ and $\rho_{\bar{u}} \approx \rho_q \gg \rho_e$, the decay pattern becomes slightly more complicated because the decay channels into $\gamma\gamma$, γZ, ZZ and WW may all play a role and even dominate in some regions of the parameter space. We will make some comments later in this paper on some of the interesting phenomenology that arises in this regime.

For the decay of the 0^{++}, 2^{++}, 0^{-+} and 2^{-+} v-glueballs into gluons we have the following rates,

$$\Gamma(0^+ \to gg) = \frac{\alpha_s^2 \alpha_v^2}{2\pi M^8} \chi_3^2 \left(\frac{1}{60}\right)^2 m_{0^+}^3 (\mathbf{F^S_{0^{++}}})^2. \tag{3.12}$$

$$\Gamma(2^+ \to gg) = \frac{\alpha_s^2 \alpha_v^2}{20\pi M^8} \chi_3^2 m_{2^+}^3 \left[\frac{1}{2}\left(\frac{11}{45}\right)^2 (\mathbf{F^T_{2^{++}}})^2 + \frac{4}{3}\left(\frac{1}{30}\right)^2 (\mathbf{F^L_{2^{++}}})^2\right], \tag{3.13}$$

$$\Gamma(0^- \to gg) = \frac{\alpha_s^2 \alpha_v^2}{2\pi M^8} \chi_3^2 \left(\frac{2}{45}\right)^2 m_{0^-}^3 (\mathbf{F^P_{0^{-+}}})^2 \tag{3.14}$$

$$\Gamma(2^- \to gg) = \frac{\alpha_s^2 \alpha_v^2}{15\pi M^8} {\chi_3}^2 m_{2^-}^3 \left(\frac{1}{30}\right)^2 (\mathbf{F^L_{2^{-+}}})^2 \tag{3.15}$$

where $\alpha_s = g_3^2/(4\pi)$ is the QCD coupling constant and the coefficient χ_3 is given in table 2.6. Of great interest is the branching fraction into two photons,

$$\frac{\Gamma(\Theta \to \gamma\gamma)}{\Gamma(\Theta \to gg)} = \frac{1}{2}\frac{\alpha^2}{\alpha_s^2}\frac{\chi_\gamma^2}{\chi_3^2} \tag{3.16}$$

for $\Theta = 0^{++}, 2^{++}, 0^{-+}, 2^{-+}$. Here α is the fine structure constant and $\chi_\gamma \equiv \chi_1 + \chi_2/2$, where χ_1 and χ_2 are shown in table 2.6. The expressions for the branching fractions into electroweak bosons are omitted for the sake of brevity but can be found in [19]. Some comments on the weak boson decay modes will be given in section 5.

In the C-odd sector, all the v-glueballs decay radiatively with the emission of a photon to the lightest v-glueballs in the C-even sector. Direct annihilations into three SM gauge bosons are suppressed since they would be induced by dimension-twelve operators. One can also show that three-body decays are suppressed due to the small phase space that is available for these decays [19].

The lightest states in the C-odd sector are the pseudovector 1^{+-} and the vector 1^{--}. The width of the decay $1^{+-} \to 0^{++} + \gamma$ is given by

$$\Gamma_{1^+ \to 0^+ + \gamma} = \frac{\alpha \alpha_v^3}{24 \pi M^8} \chi^2 \frac{(m_{1^+}^2 - m_{0^+}^2)^3}{m_{1^+}^3} (\mathbf{M^{\Omega}_{1^{+-}0^{++}}})^2. \tag{3.17}$$

A similar expression holds for the decay $1^{--} \to 0^{++} + \gamma$

$$\Gamma_{1^- \to 0^+ + \gamma} = \frac{\alpha \alpha_v^3}{24 \pi M^8} \chi^2 \frac{(m_{1^-}^2 - m_{0^+}^2)^3}{m_{1^-}^3} (\mathbf{M^{\Omega}_{1^{--}0^{++}}})^2. \tag{3.18}$$

For the 1^{--} state, annihilation to SM fermions via an off-shell γ or Z is also possible, with branching ratio

$$\frac{\Gamma_{1^- \to \gamma^*/Z^* \to f \bar{f}}}{\Gamma_{1^- \to 0^+ + \gamma}} = \frac{16 \pi \alpha}{\cos^4 \theta_W} (Y_L^2 + Y_R^2) \left(\frac{m_{1^-}^2}{m_{1^-}^2 - m_{0^+}^2} \right)^3 \left(\frac{\mathbf{F^{\Omega}_{1^{--}}}}{\mathbf{M^{\Omega}_{1^{--}0^{++}}}} \right)^2. \tag{3.19}$$

Here Y_L and Y_R are left and right hypercharge of the emitted fermions. Decay to electrons and muons will be reconstructable as a resonance, so despite its uncertain branching fractions, this decay mode is mode is worthy of careful consideration.

One can also generalize formulas (3.17) and (3.18) to include the radiative decays of the heavier C-odd v-glueballs. Easy computations show that

$$\Gamma_{J \to 0^{++} \gamma} = \frac{\alpha \, \alpha_v^3 \, \chi^2}{4 \pi \, M^8} \frac{(J+1) \, (J!)^2}{2^J \, J \, (2J)! \, (2J+1)} \frac{(m_J^2 - m_{0^+}^2)^{2J+1}}{m_J^{2J+1} m_{0^+}^{2J-2}} (\mathbf{M^{\Omega}_{J0^{++}}})^2 \tag{3.20}$$

$$\begin{aligned} \Gamma_{J \to 2^{++} \gamma} \; = \; & \frac{\alpha \alpha_v^3}{48 \pi \, M^8} \chi^2 \frac{(m_J^2 - m_{2^+}^2)^{2J+1}}{m_J^{2J+3} m_{2^+}^{2J}} \frac{2^{J-7} (J!)^2}{3 \, J \, (2J)! \, (2J+1)} \\ & \left(2(71J + 65) m_J^2 m_{2^{++}}^2 + 3(5J+3) m_J^4 + 3(5J+3) m_{2^{++}}^J \right) (\mathbf{M^{\Omega}_{J2^{++}}})^2. \end{aligned} \tag{3.21}$$

with similar expressions for the modes $J \to 0^{-+}\gamma$ and $J \to 2^{-+}\gamma$.

3.2.3 Summary of decays

In table 3.3 we summarize the final states for the most important decay channels of the v-glueballs in figure 2.1 for $D = 6$ and $D = 8$ operators. We therefore see the presence of operators of different mass dimensions opens a plethora of decay modes, which is particularly interesting from the phenomenological point of view, but complex to analyze. It is the purpose of the next two sections to disentangle the effects from $D = 6$ and $D = 8$ operators, and extract the most frequent decay modes.

State	$D = 6$ operators	$D = 8$ operators
0^{++}	bb, W^+W^-, ZZ, hh	gg, WW, ZZ, $Z\gamma$, $\gamma\gamma$
$2^{\pm+}$	$0^{\pm+}h(h^*)$	gg, WW, ZZ, $Z\gamma$, $\gamma\gamma$
0^{-+}	-	gg, WW, ZZ, $Z\gamma$, $\gamma\gamma$
3^{++}	$0^{-+}h$, $2^{\pm+}h(h^*)$	$0^{-+}gg$ $2^{++}gg$, $1^{+-}\gamma$
1^{+-}	-	$0^{\pm+}\gamma$, $2^{-+}\gamma$
1^{--}	$1^{+-}h(h^*)$	$0^{\pm+}\gamma$, $2^{\pm+}\gamma$, ff
0^{+-}, 2^{+-}, 3^{+-} 2^{--}, 3^{--}	$J^{P-}h(h^*)$	$0^{\pm+}\gamma$, $2^{\pm+}\gamma$

Table 3.3: Possible final states of the various v-glueballs in figure 2.1 generated by $D = 6$ and $D = 8$ operators. Note the absence of Higgs-mediated decay modes for the 0^{-+} and 1^{+-} v-glueballs. Here J^{P-} denotes a C-odd v-glueball state.

3.3 Constraints on new physics

In this section, we discuss direct experimental constraints on the operators used in this paper from Tevatron searches for new physics, as well as potential limits from precision electroweak measurements.

3.3.1 Electroweak oblique corrections

If new heavy particles exist, they can manifest in the standard model in terms of corrections to the gauge-boson self-energies. When the new physics scale is much larger than M_Z, this effect can be described by just three parameters (S, T, U) at the one-loop level [58, 59] [5]:

$$S = 16\pi \frac{d}{dq^2} \left[\Pi_{33}(q^2) - \Pi_{3Q}(q^2)\right] |_{q^2=0}, \tag{3.1}$$

$$T = \frac{4\pi}{s^2 M_W^2} \left[\Pi_{11}(0) - \Pi_{33}(0)\right], \tag{3.2}$$

$$U = 16\pi \frac{d}{dq^2} \left[\Pi_{11}(q^2) - \Pi_{33}(q^2)\right] |_{q^2=0}, \tag{3.3}$$

where M_W is the mass of the W, and $s^2 \equiv \sin^2\theta_W$. The subscripts 1 and 3 refer to the weak $SU(2)$ currents, while Q denotes the electromagnetic current. In practise, only the S and T parameters are relevant for our work because the U parameter is suppressed by an extra factor of the heavy fermion masses. These parameters are a measure of the size of electroweak breaking, which is parametrized by the breaking scale yv_H. On the other hand, they must be suppressed

[5] The reader should not confuse these S and T which are both vacuum polarization functions with the operators S and T in (2.9)

by the mass scale M in the limit $M \to \infty$. Therefore even if one introduces heavy fermions with extremely large couplings, their contributions to the S, T and U parameters can become small at least in the limit $M \gg y v_H$. This leaves ample available parameter space within which extra vector-like fermions are in agreement with all experimental constraints.

In this section, we analyze how current limits on S and T from precision electroweak fits can be used to obtain constraints on the mass splittings of heavy fermions. To calculate S and T, we use exact one-loop expressions for the gauge-bosons self-energies which are valid for all values of the new vector-like fermion masses.

Our scenario contains three vector-like fermion fields, one doublet and two singlets of $SU(2)_L$, transforming under the fundamental representation of $SU(n_v)$,

$$\psi_q = \begin{pmatrix} Q^U \\ Q^D \end{pmatrix} \qquad \psi_u = U \qquad \psi_d = D \tag{3.4}$$

with hypercharge Y, $Y + 1/2$ and $Y - 1/2$, respectively. We will make our computations using the above quark-like fermions. With a simple modification, our results can be readily applied to the case in which the fermions have lepton quantum numbers.

The full fermionic Lagrangian is given by

$$\mathcal{L} = \bar{\psi}_q(D_\mu\gamma^\mu + m_q)\psi_q + \bar{\psi}_u(D_\mu\gamma^\mu + m_u)\psi_u + \bar{\psi}_d(D_\mu\gamma^\mu + m_d)\psi_d + \\ + (y_u\bar{\psi}_q H\psi_u + y_d\bar{\psi}_q H\psi_d + h.c.) \tag{3.5}$$

where m_q, m_u and m_d are Dirac masses. For simplicity we have assumed that the mass matrix is symmetric and real, but complex masses may be present as well. Finally, the covariant derivative is

$$D_\mu = \partial_\mu - igT_aW_\mu^a - ig'YB_\mu. \tag{3.6}$$

When the Higgs acquires an expectation value $\langle H\rangle = \begin{pmatrix} 0 \\ v \end{pmatrix}$, off-diagonal mass terms are induced for ψ_q, ψ_u and ψ_d

$$M_u = \begin{pmatrix} m_q & y_u\, v \\ y_u\, v & m_u \end{pmatrix} \qquad M_d = \begin{pmatrix} m_q & y_d\, v \\ y_d\, v & m_d \end{pmatrix} \tag{3.7}$$

The mass matrix M is diagonalized by

$$\begin{pmatrix} \psi_1 \\ \psi_2 \end{pmatrix} = \begin{pmatrix} c_1 & s_1 \\ -s_1 & c_1 \end{pmatrix} \begin{pmatrix} Q^u \\ \psi_u \end{pmatrix} \quad \begin{pmatrix} \psi_3 \\ \psi_4 \end{pmatrix} = \begin{pmatrix} c_2 & s_2 \\ -s_2 & c_2 \end{pmatrix} \begin{pmatrix} Q^d \\ \psi_d \end{pmatrix} \tag{3.8}$$

where $c_1 = \cos\phi_1,\ s_1 = \sin\phi_1,\ c_2 = \cos\phi_2,\ s_2 = \sin\phi_2$ with

$$\tan 2\phi_1 = \frac{2y_u v}{m_q - m_u} \qquad \tan 2\phi_2 = \frac{2y_d v}{m_q - m_d}. \tag{3.9}$$

The corresponding eigenvalues are given by

$$m_{1,2} = \frac{1}{2}\left(m_q + m_u \pm \sqrt{(m_q - m_u)^2 + 4y_u^2}\right) \tag{3.10}$$

$$m_{3,4} = \frac{1}{2}\left(m_q + m_d \pm \sqrt{(m_q - m_d)^2 + 4y_d^2}\right) \tag{3.11}$$

with the following inverse relations,

$$\begin{aligned} m_q &= c_1^2\, m_1 + s_1^2\, m_2 = c_2^2\, m_3 + s_2^2\, m_4 \\ m_u &= s_1^2\, m_1 + c_1^2\, m_2 \\ m_d &= s_2^2\, m_3 + c_2^2\, m_4 \\ 2\, y_u\, v &= (m_1 - m_2)\, \sin 2\phi_1 \\ 2\, y_d\, v &= (m_3 - m_4)\, \sin 2\phi_2. \end{aligned} \tag{3.12}$$

These expressions now permit the evaluation of the S and T parameters as follows,

$$\begin{aligned} S = \frac{n_v\, N_c}{3\pi}\Big\{ &-\frac{c_1^2}{2}(Y + \frac{s_1^2}{2})\log m_1^2 - \frac{s_1^2}{2}(Y + \frac{c_1^2}{2})\log m_2^2 + \frac{c_2^2}{2}(Y - \frac{s_2^2}{2})\log m_3^2 + \\ &+ \frac{s_2^2}{2}(Y - \frac{c_2^2}{2})\log m_4^2 + \frac{3c_1^2 s_1^2}{8}\Pi^{'}(0, m_1, m_2) + \frac{3c_2^2 s_2^2}{8}\Pi^{'}(0, m_3, m_4)\Big\} \end{aligned} \tag{3.13}$$

$$\begin{aligned} T = \frac{n_v\, N_c}{8\pi s^2 M_W^2}\big\{ &c_1^2 c_2^2 \Pi(0, m_1, m_3) + c_1^2 s_2^2 \Pi(0, m_1, m_4) + s_1^2 s_2^2 \Pi(0, m_2, m_4) + \\ &+ s_1^2 c_2^2 \Pi(0, m_2, m_3) - c_1^2 s_1^2 \Pi(0, m_1, m_2) - c_2^2 s_2^2 \Pi(0, m_3, m_4)\big\} \end{aligned} \tag{3.14}$$

where the functions $\Pi(0, m_1, m_2)$ and $\Pi'(0, m_1, m_2)$ are given by

$$\begin{aligned} \Pi\,(0, m_1, m_2) = \frac{1}{m_1^2 - m_2^2}\big(&-m_1^4 + 4m_1^3 m_2 + 4m_1^3(m_1 - 2m_2)\log m_1 - 4m_1 m_2^3 + \\ &+ 4m_2^3(2m_1 - m_2)\log m_2 + m_2^4\big) \end{aligned} \tag{3.15}$$

$$\begin{aligned} \Pi^{'}\,(0, m_1, m_2) = \frac{2}{9(m_1^2 - m_2^2)^3}\big(&-12m_1^3(m_1^3 - 3m_1 m_2^2 + 3m_2^3)\log m_1 + \\ &+ 12m_2^3(3m_1^3 - 3m_1^2 m_2 + m_2^3)\log m_2 + \\ &+ (m_1^2 - m_2^2)(2m_1^4 + 9m_1^3 m_2 - 16m_1^2 m_2^2 + 9m_1 m_2^3 + 2m_2^4)\big)\,. \end{aligned} \tag{3.16}$$

In this context, the S and T parameters are a measure of the deviation of the heavy particles from the pure Dirac mass case. When the couplings y_r are turned off, the custodial $SU(2)_c$ and

isospin $SU(2)_L$ symmetries are restored, and both S and T vanish. To see this in more detail, we can expand the S and T parameters in powers of $(m_1-m_2)/(m_1+m_2)$, $(m_3-m_4)/(m_3+m_4)$. If $m_q = m_u = m_d = M \gg y_u v, y_d v$ we obtain,

$$S = \frac{N_c\, n_v\, v^2\, \left[(11+20Y)y_u^2 + (11-20Y)y_d^2\right]}{30\pi M^2} \tag{3.17}$$

$$T = \frac{N_c\, n_v\, v^4\, (y_u^2 - y_d^2)^2}{40\pi\, s_W^2\, M_W^2\, M^2}. \tag{3.18}$$

where $s_W = \sin\theta_W$ and M_W is the mass of the W boson. Then we see that $S, T \to 0$ when $y_u, y_d \to 0$, i.e., $m_2 \to m_1$ and $m_4 \to m_3$. The corresponding formulas for the lepton-like fermion case can be obtained by substituting $y_u \to 0$, $y_d \to y_l$, $N_c \to 1$ in equations (3.17) and (3.18).

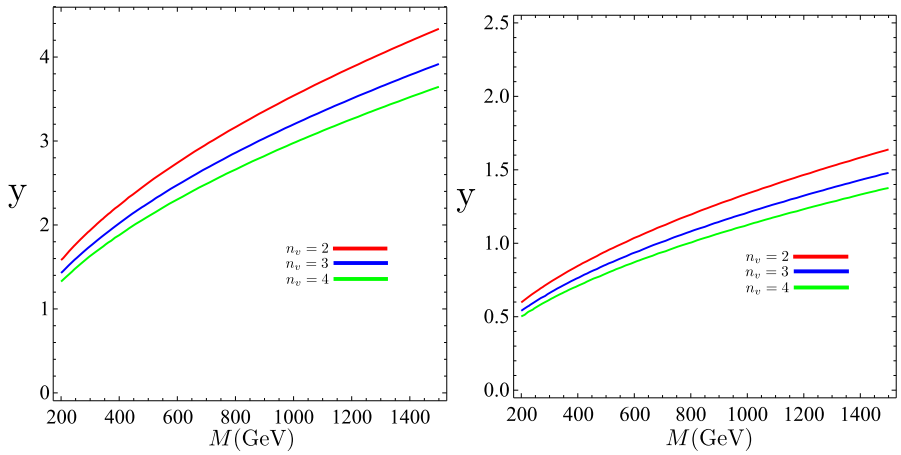

Figure 3.2: The bounds at 95% CL on the (M, y) parameters from constraints on the oblique parameters (S, T) for $n_v = 2, 3, 4$ and two different regimes: $\rho_r \approx 1\,(y = \sqrt{7}y_l)$ (Left panel), and $\rho_{\bar{d}} = \rho_{\bar{u}} = \rho_q \gg \rho_l = \rho_e \approx 1 (y = y_l)$ (Right panel). The upper-left region is excluded in these plots.

Fits of the combined electroweak data provide constraints on the S and T parameters and have been obtained in many places. Here we use the results from the PDG fits. The standard model is defined by $(S, T) = (0, 0)$ with $m_t = 170.9$ GeV and $m_H = 115$ GeV. The best fit to data is (without fixing $U = 0$)

$$S = -0.10 \pm 0.10 \tag{3.19}$$

$$T = -0.08 \pm 0.11. \tag{3.20}$$

These equations then imply the bounds $S \leq 0.10$ and $T \leq 0.13$ at 95% CL. From the experimental data, we can readily find the constraints on the parameters of the model. For example, for lepton-like fermions, if we take $Y = -1/2$ and $m_1 = 1$ TeV, then $S \sim 0.01 y_l^2 n_v$ and $T \sim 0.08 y_l^4 n_v$. Notice that the small value of S leads to only mild constraints on y_l and n_v. By constrast, the parameter T provides the most stringent bounds.

There is, however, one important effect that can mitigate the contribution to T. From (3.18), we see that electroweak corrections to the T parameter are insensitive along the $y_u = y_d$ direction in the parameter space, where the isospin symmetry is restored. In this case, the only constraints on the y_u and y_d contributions to y are given by the S parameter, which, as we have just seen, are less stringent.

In figure 3.2 we show the bounds on y at the 95% C.L. from the X particles in table 3.1 as a function of the mass scale M and for $n_v = 2, 3, 4$. For illustration, we have considered $y_u = y_d = y_l$ and two different regimes: the degenerate case, $\rho_r \approx 1$, (Left panel) and the non-degenerate case, $\rho_{\bar{d}} = \rho_{\bar{u}} = \rho_q \gg \rho_l = \rho_e \approx 1$, (Right panel). In this case, one has $y = \sqrt{7} y_l$ and $y = y_l$ for the degenerate and non-degenerate cases, respectively, (cf. (3.3)). Since y_u and y_d are unconstrained by T along the $y_u = y_d$ line, and the limits from S are less severe, the only bound we can obtain on y comes from the most stringent bound on y_l due to the T parameter. We then see that typical values $M \simeq 1, 1.5$ TeV and $y \simeq 1$ are permitted for $n_v = 2$. For larger values of n_v, the allowed split between the mass eigenstates is smaller, but still large enough that a coupling $y \simeq 0.5$ is not unreasonable.

To summarize, we conclude that for a sufficiently large range of the parameters the fit to electroweak observables is in agreement with the existence of extra vector-like fermions. This parameter space is characterized by

$$\begin{aligned} \rho_r \approx 1 : \;\; & y \lesssim 1.2 - 1.6 \\ \rho_{\bar{d}} = \rho_{\bar{u}} = \rho_q \gg \rho_l = \rho_e : \;\; & y \lesssim 0.6 - 1.2 \end{aligned} \tag{3.21}$$

together with the current direct search limits

$$\begin{aligned} M_l, M_{\bar{e}} &\gtrsim 200 \text{ GeV} \\ M_q, M_{\bar{u}}, M_{\bar{d}} &\gtrsim 250 \text{ GeV}. \end{aligned} \tag{3.22}$$

3.4 Numerical analysis

An interesting feature of the pure-glue hidden valley is that the v-glueballs can have many decay modes, depending on their quantum numbers and on the values of the various parameters. To give a general survey of decays is beyond the scope of this work, since a more detailed treatment would have to incorporate precise values of the matrix elements which at present are unknown. However, a few examples are useful to illustrate the main qualitative features of v-glueball decays.

3.4.1 Decay patterns of v-glueballs

The relevant parameter space consists of the mass scale M, the 0^{++} mass m_0, the coupling y and the Higgs mass m_H. Here we present our results in terms of m_0 which is more transparent than the confining scale Λ_v, since m_0 is the relevant parameter for LHC studies. To simplify the discussion in the SM, it is convenient to assume that the Higgs boson is SM-like and fix its mass to be $m_H = 120$ ("low mass" range) or $m_H = 200$ GeV ("high mass" range). Moreover, since the branching ratios depend on M and y only through the combination yM, our problem is reduced to a two-dimensional parameter space described by yM and m_0.

For our estimates below, we will use the lattice results [25] [6]

$$4\pi\alpha_v \mathbf{F^S_{0^{++}}} = 3.06 m_0^3, \quad \mathbf{F^T_{2^{++}}} = 0.03 m_0^3\,(n_v/3), \quad 4\pi\alpha_v \mathbf{F^P_{0^{-+}}} = 0.83 m_0^3. \tag{3.1}$$

We also need estimates of the other v-glueball decay constants and transition matrix elements, which at this point are unknown. A reasonable educated guess is that they are of order $\mathbf{F^T_{2^{++}}}$, which is the only known decay constant that is largely independent of the size of the v-glueballs. We can also guess $\mathbf{M^{\Omega}_{1^{--}0^{++}}} \sim 1/\mathbf{F^S_{0^{++}}}$, as it would be true for pion emission. In the following, we will therefore assume

$$\mathbf{F^L_{2^{\pm+}}} = \frac{n_v}{3}\mathbf{M^{S(i)}_{2^{++}0^{++}}} m_0 \simeq \mathbf{F^T_{2^{++}}}, \qquad \mathbf{M^{S(i)}_{1^{--}1^{+-}}} m_{1^{+-}} = \sqrt{\frac{n_v}{3}}\mathbf{M^{\Omega}_{1^{--}0^{++}}} \simeq \frac{n_v}{3} m_0^6/\mathbf{F^S_{0^{++}}}. \tag{3.2}$$

Later in this section, we will comment on how large deviations from this guess might affect our estimates.

Using the decay rates expressed in section 3, we identify $\Gamma^{(6)}$ and $\Gamma^{(8)}$ as the summed contributions to the decay rates from dimension-six and dimension-eight operators, respectively. The corresponding branching ratios are denoted by $BR^{(6)}$ and $BR^{(8)}$, satisfying $BR^{(6)}+BR^{(8)} = 1$. To illustrate the dependence of the branching fractions on yM and m_0, we present in figures 3.3 and 3.4 contours of constant $BR^{(6)}$ in the m_0 vs yM plane for various choices of v-glueball states and $m_H = 120$ GeV, 200 GeV. In figure 3.3, we see that the values of $BR^{(6)}_{0^{++}}$ are large over most of the parameter space plane, except at very low yM. By contrast, the values of $BR^{(6)}_{2^{++}}$ are small, except for a small region at large yM. The most interesting decay pattern is found in the 1^{--} v-glueball. We see that $BR^{(8)}_{1^{--}}$ typically dominates when $m_{1^{--}} - m_{1^{+-}} < m_H$

[6] Here the coupling constant $4\pi\alpha_v$ is included alongside $\mathbf{F^S_{0^{++}}}$ and $\mathbf{F^P_{0^{-+}}}$ to make them renormalization invariant so that there is no question at which point $4\pi\alpha_v$ is normalized. On the contrary, $\mathbf{F^T_{2^{++}}}$ is renormalization invariant as is, since it is the matrix element of the energy-momentum tensor which is known to be scale invariant. Also, since the values reported in [25] are not expressed in a continuum renormalization scheme, we have converted $g^2\mathbf{F^T_{2^{++}}}$ to $\mathbf{F^T_{2^{++}}}$ using the value of the lattice parameter $\beta = 6/g^2 = 3.2$ as an approximation to the continuum limit.

and the emitted Higgs boson is off-shell, whereas $BR^{(6)}_{1^{--}}$ dominates when $m_{1^{--}} - m_{1^{+-}} > m_H$ and the emitted Higgs boson is on-shell. An analogous behaviour is found for $m_H = 200$ GeV, as demonstrated in figure 3.4.

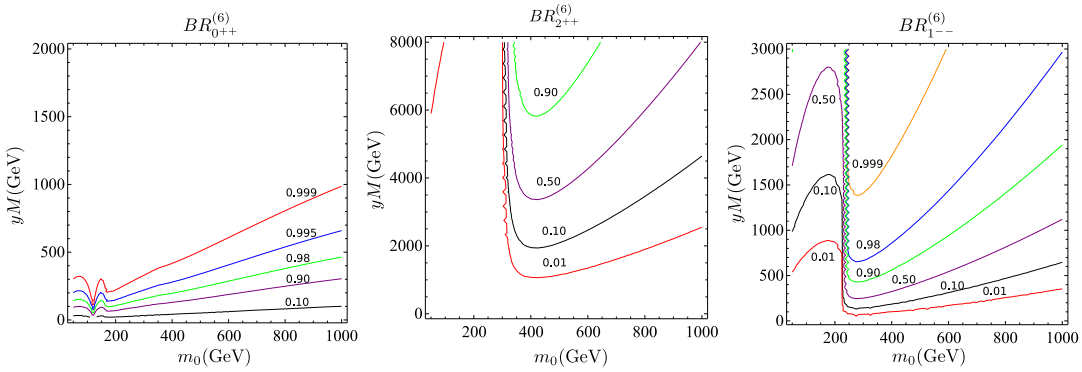

Figure 3.3: Curves of constant branching ratio $BR^{(6)}$ in the parameter space (m_0, yM) for various representative states and $m_H = 120$ GeV. Left: 0^{++}, Center: 2^{++}, Right: 1^{--}.

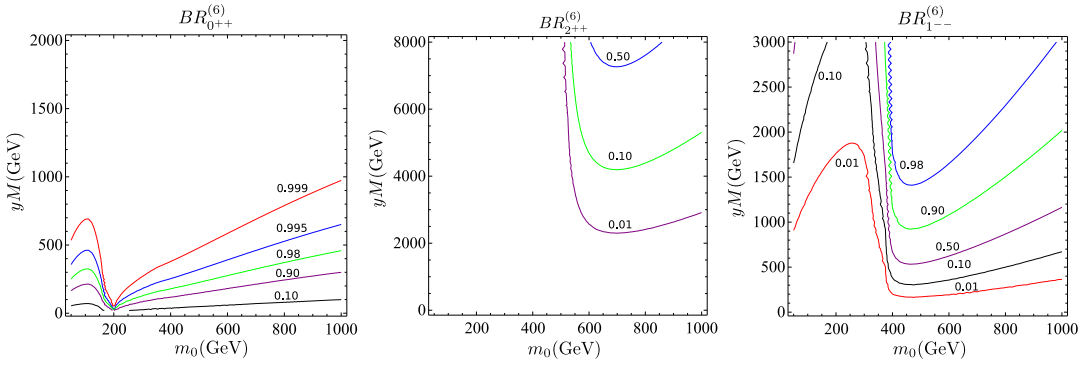

Figure 3.4: Same as figure 3.3 for $m_H = 200$ GeV.

The values of yM determine to a large extent the decay pattern of v-glueballs with three distinctive energy regions: (i) $yM \ll 1$ TeV, (ii) $yM \gg 1$ TeV and (iii) $yM \approx 1$ TeV. Recall that these ranges of parameters are further constrained by existing experimental limits, as described in section 4. As will be discussed below, the common feature of all these different regimes is the great diversity of decay modes and lifetimes, even for a given choice of parameters.

(i) $yM \ll 1$ TeV. For sufficiently small yM, the contribution of the dimension-six operators can be effectively disregarded and, hence, the dimension-eight operators have the largest effects on v-glueball decays. As shown in [19], annihilation decays dominate the 0^{++}, 2^{++}, 0^{-+} and 2^{-+} v-glueballs. Their branching ratios are dominated by decays to gg, with decays to $\gamma\gamma$ having a branching fraction of $\sim 0.4\%$, assuming the X fields form complete $SU(5)$ multiplets of equal

mass. If the colored particles are much heavier than the uncolored particles, then decays to electroweak bosons and photons can dominate. Most other states decay by radiatively emitting a photon, or a Z boson. In addition, the 1^{--} state can also decay to standard model fermions via an off-shell γ or Z. The 3^{++} state is special in that its three-body decay mode $3^{++} \to 0^{++}gg$ could be of the same rate as the radiative $3^{++} \to 1^{+-}\gamma$ decay. The clearest signatures for this regime are likely to be the two-photon resonances from the prompt annihilation decays of C-even v-glueballs. In addition, for part of the parameter space, the v-glueballs are rather long-lived particles, so that they produced displaced vertices in the detectors, which can be an experimentally challenging, but certainly important signature.

(ii) $yM \gg 1$ TeV. In this case, the Higgs couplings to v-glueballs dominate over all other couplings. As a result, the decay pattern is relatively simple. In the $PC = ++$ sector, we find that the 0^{++} v-glueball annihilates directly into pairs of standard model particles via $0^{++} \to h^*$, with the same final states and branching fractions of a Higgs boson with mass m_0. For $m_0 > 2m_h$, the mode $0^{++} \to hh$ opens up, in addition to $0^{++} \to h^*$, contributing $20 - 25\%$ to the total width with the decays into weak boson and top quark pairs accounting for the remaining $75 - 80\%$. The 2^{++} v-glueball decays predominantly to the lighter 0^{++} by radiatively emitting a Higgs boson. In the $PC = -+$ sector the lightest states are the 0^{-+} and 2^{-+} v-glueballs. The 2^{-+} v-glueball decays in a similar way to the 2^{++}, with the rate dominated by $2^{-+} \to 0^{-+}h$. Although the 2^{-+} v-glueball is heavier than the 0^{++}, the $2^{-+} \to 0^{++}h$ decay is not allowed, due to parity and conserved angular momentum. The 0^{-+} v-glueball is a special case. Without explicit breaking of parity, the 0^{-+} v-glueball decays slowly into gg via dimension-eight operators.

Turning to the $PC = +-$ sector, we find that most of the states can decay by emission of a Higgs boson, through processes of the form $\Theta_\kappa \to \Theta_{\kappa'}h$, where Θ_κ, $\Theta_{\kappa'}$ denote two v-glueballs with given quantum numbers. Since C-changing transitions are not allowed by the S operator, the v-glueballs in that sector typically undergo a cascade decay, radiating a Higgs boson at each step, which ends at the lightest 1^{+-} state. The v-glueballs in the $PC = --$ sector decay in a similar manner, with the lightest 1^{--} v-glueball decaying to the 1^{+-} v-glueball with the emission of a Higgs boson. Since the 1^{+-} v-glueball is not permitted to decay via dimension-six operators, its dominant decay modes are photon-radiative transitions to C-even v-glueballs, as in (i).

We should note that this theoretical regime may be difficult to access in practice. For the 2^{++} v-glueball (and hence the 2^{-+}), this requires $yM \gtrsim 10$ TeV (see figures 3.3 and 3.4). As

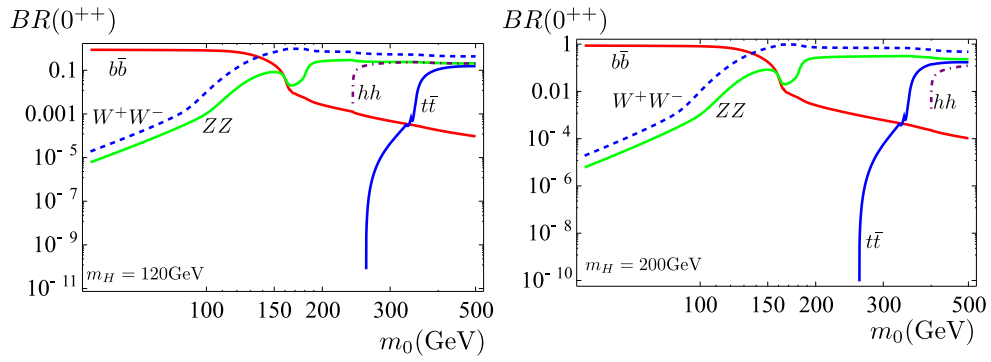

Figure 3.5: The branching ratios of the 0^{++} v-glueball as a function of m_0 for $yM \sim 1$ TeV. Left Panel: $m_H = 120$ GeV. Right Panel: $m_H = 200$ GeV. For clarity, only the main decay modes are shown.

shown in (3.21), the heavy mediators can at most have Yukawa couplings $y \sim 1$ in order to avoid potentially dangerous electroweak corrections. With $M \sim \mathcal{O}(10$ TeV), the rate for production of v-glueballs ($\propto \sigma_{gg\to XX} \ll 1$fb) is rather small, rendering this region of parameter space experimentally inaccessible to the future experiments at the LHC.

(*iii*) $yM \approx 1$ TeV. For Higgs couplings with intermediate strength, the v-glueball decay pattern is more complicated because the couplings to the gauge bosons become important, leading to a interesting interplay between dimension-six and dimension-eight operators. From the point of view of prospective experiments at the LHC, this is also the most interesting regime, due to the diversity of v-glueball decay channels and variability of lifetimes as well.

The 0^{++} v-glueball still decays predominantly to pairs of standard model particles via $0^{++} \to h^*$ or, if kinematically allowed, $0^{++} \to hh$. The branching ratios for the main decay channels of the 0^{++} v-glueball are shown in figure 3.5 for $yM = 1$ TeV in the cases of $m_H = 120$ GeV and $m_H = 200$ GeV.

For the 2^{++} and 2^{-+} v-glueballs, the dominant decay mode is gg. This is because the $2^{\pm+} \to 0^{\pm+}h(h^*)$ decay is phase-space suppressed by a $10^{-8} - 10^{-3}$ factor. For $m_{2^{++}} - m_{0^{++}} > m_H$, the phase space suppression is smaller ~ 0.01, but in this regime the $(m_{2^{++}}/M)^4$ suppression of $D = 8$ operators is inefficient, rendering the $D = 6$ operators subdominant.

The dominant decay modes of the 1^{--} v-glueball are transitions with a Higgs boson in the final state, $1^{--} \to 1^{+-}h$, for $m_{1^{--}} - m_{1^{+-}} > m_H$ or, photon-radiative decays to the lighter v-glueballs in the C-odd sector for $m_{1^{--}} - m_{1^{+-}} < m_H$. The decays of the other v-glueballs in the C-odd sector proceed in a similar fashion. In addition, the decay of the 1^{--} v-glueball into fermion pairs can play a significant role for $m_{1^{--}} - m_{1^{+-}} < m_H$.

Since the 1^{+-} and 0^{-+} v-glueballs cannot decay via their couplings to the Higgs boson, their

dominant decay modes are gg for the 0^{-+} v-glueball and radiative transitions to the C-even states with emission of a photon for the 1^{+-} v-glueball.

The 3^{++} state is more complicated. With many contributing decay channels and unknown form factors, it seems impossible to estimate which decay mode is dominant. Indeed, a simple estimate suggests that the $3^{++} \to 0^{++}gg$, $3^{++} \to 1^{+-}\gamma$ and $3^{++} \to 0^{-+}h$ decays are all of the same order.

Summarizing all three cases, we expect the v-glueball decays to produce any of the kinematically allowed final states of the Higgs boson, such as $b\bar{b}$, $\tau^+\tau^-$, W^+W^-, etc, as well as possible photons, both singly and in pairs, and gluon pairs. If kinematically allowed, multiple production of standard model Higgs bosons from cascade decays can also proceeds with a sizable rate. A typical final visible state would then be of the form $b\bar{b}b\bar{b}$, $WWWWb\bar{b}$, $b\bar{b}\tau^+\tau^-$, $b\bar{b}gg$, $b\bar{b}\gamma\gamma$, and so on.

3.4.2 Lifetimes

Meanwhile, with so many v-glueball states and decay channels, the lifetimes of the v-glueballs can vary over many orders of magnitude. This is already clear from the fact that the lifetimes are very sensitive to both M and m_0. In our approach, the large contributions of the dimension-six operators also suggest a wider spread of the lifetimes than that found when the Higgs couplings are absent, as in [19]. In figure 3.6, we plot the lifetimes of some of the v-glueballs as a function of m_0 for the three representative regimes studied in the last subsection. We see that for $yM \approx 1 - 10$ TeV the various v-glueball states have lifetimes that typically span 5-6 orders of magnitude, for any given choice of the parameters.

An important consequence of the large spread in the lifetimes is that there is a significant probability that one or more of the v-glueballs will often decay a macroscopic distance away from the primary interaction vertex. Only one of these states needs to be both long-lived and frequently produced to provide a strong signature of new physics.

If production rates are substantial, displaced vertices are expected for average decay lengths[7] $c\tau$ of the order $10^{-4} - 100\,\mathrm{m}$, resulting in lifetimes of $10^{-12} - 10^{-6}\,\mathrm{sec}$. Outside this range, the displaced-vertex signature is no longer present, either because the lifetime is much longer than 10^{-6} sec, so that a typical v-glueball produced at the LHC will escape the detectors, or because

[7]Note that the actual v-glueball decay length l in the laboratory frame, distributed according to $P(l) \propto e^{-l/\gamma c\tau}$ with the Lorentz boost factor $\gamma = 1/\sqrt{1-\beta^2}$, may be actually much smaller than the average decay length $c\tau$. So even if $c\tau$ far exceeds the dimensions of the detector, there is still a significant chance that these v-glueballs will be observable, providing the rates are substantial.

the decays are prompt and the v-glueball decay lengths cannot be resolved.

As shown in figure 3.6, displaced vertices could be observed for 10 GeV $\lesssim m_0 \lesssim$ 200 GeV and $0 \lesssim yM \lesssim 1$ TeV or for 10 GeV $\lesssim m_0 \lesssim$ 400 GeV and $yM \gg 1$ TeV. As long as m_0 becomes greater than about 400 GeV, all v-glueball decays will be prompt and the displaced-vertex signature will be absent. In the case $yM \approx 0$ the 1^{+-} and 1^{--} v-glueball lifetimes reach values high enough for displaced vertices for m_0 between 50 GeV and 150 GeV. The 0^{++}, 0^{-+}, 2^{++} and 2^{-+} v-glueballs may also decay with displaced vertices in the very low mass range $m_0 \lesssim 70$ GeV. On the other hand, in the case $yM \approx 10$ TeV the spread in the lifetimes is two or three orders of magnitude larger, so even larger v-glueball masses 150 GeV $< m_0 <$ 400 GeV may allow for displaced vertices. This is the case of the 2^{++} and 2^{-+} v-glueballs, as shown in the middle panel of figure 3.6. Their lifetimes are so long that these v-glueballs may escape the detectors for $m_0 \lesssim 100$ GeV. In the low mass range 50 GeV $< m_0 <$ 200 GeV other v-glueballs such as the 1^{+-} and 1^{--} also have a significant chance to decay with displaces vertices. In this case, the 0^{++} and 2^{++} v-glueballs will remain short-lived over most of the parameter space down to masses of order 50 GeV where displaced vertices may start to occur for these states as well. Finally, the case $yM \approx 1$ TeV shown in the right panel of figure 3.6 is an example of an intermediate situation, with the 0^{++} v-glueball being short-lived, except for very-low masses $m_0 \lesssim 50$ GeV, and at least five states having a chance to decay with displaced vertices in some part of the parameter space: the 1^{+-} and 1^{--} v-glueballs for $m_0 \lesssim 200$ GeV, and the 2^{++}, 2^{-+} and 0^{-+} v-glueballs for 20 GeV $\lesssim m_0 \lesssim 100$ GeV.

From the analysis above it is quite evident that long-lived resonances are a common feature of pure-glue hidden valleys for an ample range of parameters. Nonetheless, detecting long-lived particles presents several experimental challenges. Displaced jets, though they have no standard model background, suffer from substantial detector backgrounds from secondary vertices inside the detector material. On the other hand, displaced leptons are technically easier, and have much less background, but branching ratios to leptons are usually quite small. Displaced photons also present several experimental challenges, since one has to detect not only the position where the photons enter the electromagnetic calorimeter but also their angle of incidence. Thus the issue of detecting displaced vertices is not straightforward, and requires novel analysis strategies.

Interestingly enough, the v-glueball masses can be as low as a few GeV's and at the same time the lifetimes could be short enough that a few v-glueball events could be observed at the LHC. Specifically, let us examine closely the case of the scalar 0^{++} v-glueball. From (3.2) we

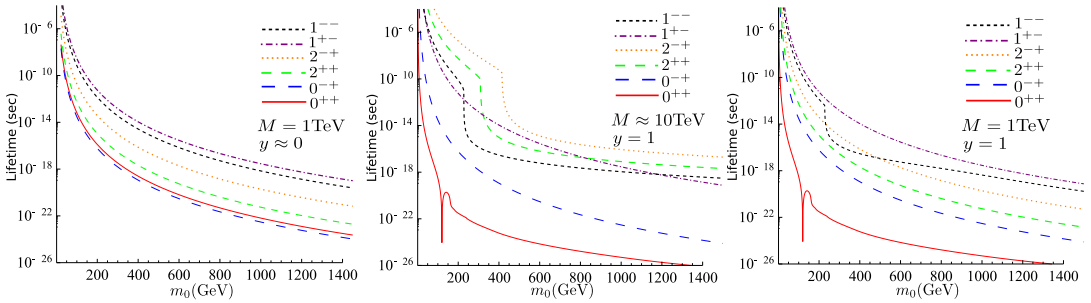

Figure 3.6: Lifetimes of the v-glueballs as a function of the v-glueball mass scale m_0 for three representative regimes: $yM \approx 0$ (Left panel), $yM \approx 10$ TeV (Middle panel), and $yM \approx 1$ TeV (Right panel).

see that for X particles of order 1 TeV the lifetime of the 0^{++} v-glueball is of order

$$c\tau \sim 1\text{cm} \left(\frac{M}{1\text{ TeV}}\right)^4 \left(\frac{20\text{ GeV}}{m_0}\right)^7 \left(\frac{5\text{ GeV}}{m_b}\right)^2 \left(1 - \frac{4m_f^2}{m_0^2}\right)^{-1.5}. \tag{3.3}$$

We see that for $m_0 \gtrsim 10$ GeV the 0^{++} state can decay inside the detector. It is important to remark that even for $c\tau$ well above 10 meters, a significant fraction of the v-glueballs will still decay inside the detector. If detector backgrounds are sufficiently low, and production cross-section is substantial, discovery would also be possible, in principle, for states in the low-mass range 1 GeV $\lesssim m_0 \lesssim$ 10 GeV.

3.4.3 Uncolored X particles

If there is a substantial hierarchy between the colored X particles and the uncolored X particles, the latter may dominate v-glueball decays. Decay rates to a pair of SM gluons in the C-even sector are proportional to the coefficients χ_3^2 (3.12), which would be suppressed. If the particles carrying QCD color are heavier by factors of 2 or more, the hierarchy of decay rates changes, as $\chi_3^2/\chi_\gamma^2 \sim 10^{-2} - 10^{-4}$. In this case, decays to gluons no longer dominate the partial widths $\Gamma^{(8)}$ for the C-even states. Also, the regime for m_0 and yM in which $\Gamma^{(8)}$ dominates over $\Gamma^{(6)}$ is somewhat reduced. Without any detailed computation, we may infer from figures 3.3 and 3.4 that the decays of the 0^{++} v-glueball, with its large branching fraction to off-shell Higgs boson, will not be much affected. For $m_{0^-} < 2m_W$, the dominant decay mode of the 0^{-+} v-glueball is now $\gamma\gamma$ with a branching ratio of 90% with the decays into gg and $Z\gamma$ accounting for the remaining 10%. In the high mass range $m_{0^-} > 2m_W$, the 0^{-+} v-glueball decays dominantly into WW with a branching ratio of $\sim 70\%$ followed by the decays into ZZ, $\gamma\gamma$ and $Z\gamma$ with branching ratios of 20%, 5% and 5%, respectively. Also, the lifetime of the 0^{-+} v-glueball is longer. For the 2^{++} and 2^{-+} v-glueballs, the decays into photon pairs typically dominate

for $m_{2^{\pm+}} - m_{0^{\pm+}} < m_H$, while the Higgs-radiative transitions $2^{\pm+} \to 0^{\pm+}h$ can dominate for $m_{2^{\pm+}} - m_{0^{\pm+}} > m_H$. The decays of the v-glueballs in the C-odd sector are largely unaffected. We will comment further in the conclusions and in our LHC study [60], but suffice it to say that the fact that the annihilation into photon pairs may dominate the lifetimes of some v-glueballs (the 0^{-+}, 2^{++}, 2^{-+}) has important consequences for experimental searches.

3.4.4 Uncertainties in the v-glueball matrix elements

In another respect, we should emphasize that even though our estimates are in general robust, they are subject to significant uncertainties, due especially to the many unknown v-glueball matrix elements. Although lattice computations are at present not available, it is of interest to see what one might expect once lattice computations are incorporated. Of course, the decays of the 0^{++} v-glueball will remain unchanged, since its branching ratios are independent of the decay constant $\mathbf{F^s_{0^+}}$. The same is true for the 1^{+-} and 0^{-+} v-glueballs. On the contrary, the decays of the 2^{++} and 1^{--} v-glueballs depend on ratios of the unknown non-perturbative matrix elements,

$$r_{2^+} = \frac{\mathbf{M^S_{2^{++}0^{++}}} m_0}{\mathbf{F^T_{2^{++}}}} \qquad r_{1^-} = \frac{\mathbf{M^S_{1^{--}1^{+-}}} m_{1^{+-}}}{\mathbf{M^\Omega_{1^{--}0^{++}}}}. \tag{3.4}$$

Since there is no reason for the form factors $\mathbf{M^S_{2^{++}0^{++}}}$ and $\mathbf{M^S_{1^{--}1^{+-}}}$ to be significantly suppressed or enhanced at $k^2 = m_H^2$, the ratios r_{2^+} and r_{1^-} are probably of order $\mathcal{O}(1)$ (actually somewhat smaller[8], especially at large n_v). To illustrate the possible range of impact lattice computations may lead to, we can simply make the rescaling $yM \to yM\sqrt{r_{2^+}}$ and $yM \to yM\sqrt{r_{1^-}}$ in figure 3.3. One can see that when r_{2^+} is varied by a factor of 10 in both directions around $r_{2^+} \sim 1$ for $yM \sim 1$ TeV, the ratio $BR^{(6)}_{2^+}$ changes by around $10 - 20\%$, and the dominant mode of the 2^{++} v-glueball is still gg. A similar conclusion is obtained for the 2^{-+} v-glueball. For the 1^{--} v-glueball, in contrast to the 2^{++} and 2^{-+}, the branching ratios are more uncertain. The reason is that the contributions from $D = 6$ and $D = 8$ operators are comparable in strength, so a small enhancement in one of the matrix elements can lead to a large effect on the branching ratios. For $r_{1^-} \sim 0.1$, the photon-radiative decay gets enhanced very greatly and could dominate the branching ratio in most of the mass range, while $r_{1^-} \sim 10$ tends to enhance the Higgs-radiative decay. Therefore, additional lattice computations would be needed to distinguish between these two modes. Fortunately, it turns out that the impact of precise lattice computations on the phenomenology of the lightest v-glueballs 0^{++}, 2^{++}, 0^{-+} and 2^{-+},

[8] Using standard large-n_v counting rules and taking into account explicit factors of $1/\sqrt{n_v}$ in the coupling constant, one obtains $r_{2^+} \sim \mathcal{O}(1/n_v)$ and $r_{1^-} \sim \mathcal{O}(1/\sqrt{n_v})$; see (3.2).

which, as will be argued in our LHC study, are probably the most copiously produced, is in general very mild.

3.5 Other extensions

In this section, we consider two simple extensions that may alter the phenomenology of v-glueballs in a number of ways, with a special emphasis on the 0^{-+} and 1^{+-} v-glueballs. Firstly, we analyze the two Higgs doublet model (2HDM), which is the simplest extension of the standard model Higgs sector, and secondly, we study the possibility of CP violation in the theory and its implications for v-glueball decays. We will not attempt to systematically compute all the decay rates, but simply point out a few salient features of these extensions.

3.5.1 2HDM

As in the MSSM, we consider the SM with two Higgs doublets H_u and H_d, where H_u only couples to up-type quarks and neutrinos and H_d only couples to down-type quarks and leptons. In this model, there are five physical Higgs bosons: two charged scalars ($H^{\pm}$); two neutral scalars (H and h); and a neutral CP-odd scalar (A). The presence of the CP-odd scalar A is of particular interest. Since the A is CP-odd, a gauge invariant CP-conserving coupling to the v-gluons must be of the form $\epsilon^{\mu\nu\alpha\beta}\mathrm{tr}\ \mathcal{F}_{\mu\nu}\mathcal{F}_{\alpha\beta}A\Phi$, with $\Phi = 1, H, h$. Because of this coupling, new possible decays of the pseudoscalar 0^{-+} state emerge in the 2HDM. These are

$$0^{-+} \quad \to \quad A^* \to \ ff, \tag{3.1}$$

$$0^{-+} \quad \to \quad HA, \tag{3.2}$$

$$0^{-+} \quad \to \quad hA \tag{3.3}$$

$$0^{-+} \quad \to \quad 0^{++}A. \tag{3.4}$$

For all other v-glueballs, there are new contributions to their decays in the 2HDM, but the decay pattern as described in sections 3 and 5 remains basically unchanged. For the 0^{++} v-glueball, the new channels include $0^{++} \to hh, Hh, AA$ as well as the off-shell Higgs decay $0^{++} \to h^*$. For all other states, new decay modes arise from the processes $\Theta_\kappa \to \Theta_{\kappa'}\phi$, where now $\phi = H, h, A$. Recall that in the single-Higgs model, the lowest-dimension operators that can induce decays of the 1^{+-} v-glueball arise at mass dimension eight. A similar conclusion applies to the 1^{+-} v-glueball in the context of the 2HDM. Therefore, while the CP-odd scalar A makes a drastic change on the 0^{-+}, it does not affect the 1^{+-} v-glueball.

To estimate the effect of the CP-odd scalar A on the branching ratios, we will need to find the effective Lagrangian. Using the basic results of section 2, the effective Higgs couplings to v-gluons, induced at one-loop by the X particles, is given by

$$\mathcal{L}^{(6)} = \frac{\alpha_v}{3\pi\, M^2}\left[y_u^2\, H_u^\dagger H_u + y_d^2\, H_d^\dagger H_d\right]\ \mathrm{tr}\ \mathcal{F}_{\mu\nu}\mathcal{F}^{\mu\nu} + \\ + \frac{\alpha_v}{2\pi\, M^2}\left[y_d^2\left(\frac{H_d - H_d^*}{2i}\right)^\dagger\left(\frac{H_d + H_d^*}{2}\right) + y_u^2\left(\frac{H_u - H_u^*}{2i}\right)^\dagger\left(\frac{H_u + H_u^*}{2}\right)\right]\ \mathrm{tr}\ \mathcal{F}_{\mu\nu}\tilde{\mathcal{F}}^{\mu\nu}. \quad (3.5)$$

Here y_u and y_d represent the couplings of the X particles to the Higgs doublets H_u and H_d, respectively. The couplings of the physical Higgs bosons to v-gluon pairs are readily obtained by including the appropriate mixing angle factors

$$\mathcal{L}^{(6)} = \frac{\alpha_v}{6\pi\, M^2}\left(\xi_{HH}H^2 + \xi_{hh}h^2 + \xi_{Hh}Hh + \xi_{AA}A^2\right)\ \mathrm{tr}\ \mathcal{F}_{\mu\nu}\mathcal{F}^{\mu\nu} + \frac{\alpha_v\, v_H}{2\pi\, M^2}\,\xi_A\, A\,\mathrm{tr}\ \mathcal{F}_{\mu\nu}\tilde{\mathcal{F}}^{\mu\nu} \\ + \frac{\alpha_v\, v_H}{3\pi\, M^2}\left(\xi_H H + \xi_h h\right)\ \mathrm{tr}\ \mathcal{F}_{\mu\nu}\mathcal{F}^{\mu\nu} + \frac{\alpha_v}{4\pi\, M^2}\left(\xi_{AH}AH + \xi_{Ah}Ah\right)\ \mathrm{tr}\ \mathcal{F}_{\mu\nu}\tilde{\mathcal{F}}^{\mu\nu} \quad (3.6)$$

where the coeffients ξ_{ij} and ξ_i are given by

$$\xi_{HH} = y_u^2 s_\alpha^2 + y_d^2 c_\alpha^2 \quad \xi_{hh} = y_u^2 c_\alpha^2 + y_d^2 s_\alpha^2 \quad \xi_{Hh} = 2 s_\alpha c_\alpha (y_u^2 - y_d^2)$$

$$\xi_{AH} = y_u^2 s_\alpha c_\beta - y_d^2 c_\alpha s_\beta \quad \xi_{Ah} = y_u^2 c_\alpha c_\beta + y_d^2 s_\alpha s_\beta \quad \xi_{AA} = y_u^2 c_\beta^2 - y_d^2 s_\beta^2$$

$$\xi_H = y_u^2 s_\alpha s_\beta + y_d^2 c_\alpha c_\beta \quad \xi_h = y_u^2 c_\alpha s_\beta - y_d^2 s_\alpha c_\beta \quad \xi_A = s_\beta c_\beta (y_u^2 - y_d^2) \quad (3.7)$$

where α the mixing angle and the ratio of the vacuum expectation values $\tan\beta = v_u/v_d$. The combination $v_d^2 + v_u^2$ is fixed by the electroweak scale $v_H = \sqrt{v_d^2 + v_u^2} = 246$ GeV.

The decay rates can be readily extracted from our general results in section 3 by replacing y^2 with the appropriate couplings in (3.7). For the scalar 0^{++} state, the decay rates for the off-shell Higgs decay $0^{++} \to H^*/h^* \to \zeta\zeta$ can be read from (3.2) through the substitution

$$\frac{y^2}{m_0^2 - m_H^2} \to \frac{\xi_H}{m_0^2 - m_H^2} + \frac{\xi_h}{m_0^2 - m_h^2}, \quad (3.8)$$

while the rate for the two-body decays $0^{++} \to HH,\, hh,\, Hh,\, AA$ is obtained from (3.3) by replacing

$$y^2\left(1 + \frac{3m_Z^2}{2(m_0^2 - m_H^2)}\right) \to \xi_{ij} + \frac{\xi_H g_{Hij}}{m_0^2 - m_H^2} + \frac{\xi_h g_{hij}}{m_0^2 - m_h^2}, \quad (3.9)$$

where $i,j = HH, Hh, hh, AA$ and g_{ijk} are the cubic self-couplings in the 2HDM. Likewise, the width of the decays $\Theta_\kappa \to \Theta'_\kappa \Phi_i$, $\Phi_i = H, h, A$, can be obtained from (3.9) and (3.10) by substituting $y^2 \to \xi_i$. Finally, we summarize the rates for the new decay modes of the 0^{-+} v-glueball (3.1-3.4),

$$\Gamma_{0^{-+}\to f\bar{f}} = \left(\frac{\xi_A\, \tan\beta\, v_H\, F_{0^+}^P}{2\pi M^2(m_A^2 - m_0^2)}\right)^2 \Gamma^{SM}_{h\to f\bar{f}}(m_{0^-}^2) \quad (3.10)$$

$$\Gamma_{0^{-+}\to 0^{++}A} = \frac{1}{16\pi m_{0^-}} \left(\frac{\mathbf{M^P_{0^-0^+}}\xi_A}{2\pi M^2}\right)^2 \left[g(m_H^2, m_A^2; m_{0^-}^2)\right]^{1/2} \tag{3.11}$$

$$\Gamma_{0^{-+}\to AH} = \frac{1}{16\pi m_{0^-}} \left(\frac{F^P_{0^-}}{2\pi M^2}\right)^2 \left(\xi_{AH} + \frac{3\xi_A}{2(m_{0^-}^2 - m_A^2)}\right)^2 \left[g(m_H^2, m_A^2; m_{0^-}^2)\right]^{1/2} \tag{3.12}$$

$$\Gamma_{0^{-+}\to Ah} = \frac{1}{16\pi m_{0^-}} \left(\frac{F^P_{0^-}}{2\pi M^2}\right)^2 \left(\xi_{Ah} + \frac{3m_Z^2\xi_A}{2(m_{0^-}^2 - m_A^2)}\right)^2 \left[g(m_h^2, m_A^2; m_{0^-}^2)\right]^{1/2}. \tag{3.13}$$

The expressions above are clearly very model dependent. First, notice that for $y_u \simeq y_d$, ξ_A is very small, and the decay rate of the 0^{-+} v-glueball is suppressed. On the other hand, for $y_d \simeq 0$, a quick check shows that this rate, whose ratio to the 0^{++} width is (for small masses $m_0 < m_h$)

$$\frac{\Gamma_{0^{-+}}}{\Gamma_{0^{++}}} \simeq 0.5 \left(s_\alpha \frac{m_A^2}{m_H^2} + c_\alpha \frac{m_A^2}{m_h^2}\right)^{-2}, \tag{3.14}$$

is not negligible. This ratio may be anywhere from ~ 0.1 up to about 4 depending on the mixing angle and the masses of the scalars. Unless the 0^{-+} decay rate is unduly suppressed, the lifetimes of the 0^{++} and 0^{-+} v-glueballs are in general within one order of magnitude from each other.

3.5.2 Models of explicit CP violation

It is of interest to see what one might expect once CP-violation effects are incorporated in the theory, in the context of a single-Higgs model. For example, parity-violating interaction terms can be induced in the effective Lagrangian if we assume that the couplings of the heavy particles X_r to the Higgs boson are complex. In this case, a P-odd C-even interaction is generated of the form $H^\dagger H \,\mathrm{tr}\, \mathcal{F}_{\mu\nu}\tilde{\mathcal{F}}^{\mu\nu}$. As in the 2HDM, this interaction drastically changes 0^{-+} decays, since without it, the 0^{-+} v-glueball would decay via dimension-eight operators, suffering an extra suppression. The 0^{-+} v-glueball can then decay via $0^{-+} \to h^*$, producing any of the kinematically-allowed final states of the Higgs boson.

Similarly, one can contemplate interactions that explicitly break C-invariance. Interestingly enough, the lowest-dimension operators of this kind (e.g. $H^\dagger H d_{abe} f_{cde} \mathcal{F}^a_{\mu\nu}\mathcal{F}^b_{\mu\nu}\mathcal{F}^c_{\alpha\beta}\mathcal{F}^d_{\alpha\beta}$) arise at dimension ten and, therefore, their effects are extremely suppressed by extra powers of $1/M$. The dominant decay modes of the 1^{+-} v-glueball are then induced by dimension-eight operators, even if we allow for CP-violation.

In the rest of this section, then, we will focus on P-violating but C-conserving interactions. To estimate the decay widths, let us consider the following Lagrangian, in two-component notation,

$$\mathcal{L}_{mass} = y_d X_q H^\dagger X_d^c + y_d X_q^c H X_d + h.c. \tag{3.15}$$

where y_d is a complex Yukawa coupling. By integrating out the X_q and X_d particles, we obtain the following dimension-six operators[9]:

$$\mathcal{L}^{(6)} = \frac{\alpha_v\,(y^2-\tilde{y}^2)}{3\pi\,M^2}\,H^\dagger H\,\mathrm{tr}\;\mathcal{F}_{\mu\nu}\mathcal{F}^{\mu\nu} + \frac{\alpha_v\,(2\,y\,\tilde{y})}{\pi\,M^2}\,H^\dagger H\,\mathrm{tr}\;\mathcal{F}_{\mu\nu}\tilde{\mathcal{F}}^{\mu\nu}. \tag{3.16}$$

where $y = Re\,y_d$ and $\tilde{y} = Im\,y_d$. Here $\tilde{\mathcal{F}}_{\mu\nu} = (1/2)\epsilon_{\mu\nu\lambda\sigma}\mathcal{F}^{\mu\nu}$ denotes the dual of the field strength tensor. The first term on the right-hand side of (3.16) is the same operator that we had already found in (3.2). The second term of (3.16) is new and violates P. As mentioned above, the P-odd interaction allows the pseudoscalar 0^{-+} state to decay into SM particles via s-channel Higgs-boson exchange $0^{-+} \to h^* \to \zeta\zeta$, where ζ denotes a standard model particle. The width of the decay is given by

$$\Gamma_{0^{-+}\to\zeta\zeta} = \left(\frac{2y\tilde{y}\,v_H\,\alpha_v\,F^P_{0^-}}{\pi M^2(m_H^2-m^2_{0^-})}\right)^2 \Gamma^{SM}_{h\to\zeta\zeta}(m^2_{0^-}) \tag{3.17}$$

where $F^P_{0^-} \equiv \alpha_v\,\langle 0|\mathrm{tr}\;\mathcal{F}_{\mu\nu}\tilde{\mathcal{F}}^{\mu\nu}|0^{++}\rangle$ is the 0^{-+} decay constant. The same operator also induces the decay $0^{-+} \to 0^{++}h$, with partial width

$$\Gamma_{0^{-+}\to 0^{++}h} = \frac{1}{16\pi m_{0^-}}\left(\frac{2y\tilde{y}\,v_H\,\alpha_v\,\mathbf{M^P_{0^-0^+}}}{\pi\,M^2}\right)^2 \left[g(m_H^2, m^2_{0^+}; m^2_{0^-})\right]^{1/2} \tag{3.18}$$

where now $\mathbf{M^P_{0^-0^+}}$ is the transition matrix. This decay is phase-space suppressed for $m_{0^{-+}} - m_{0^{++}} < m_h$, but may be quite significant for $m_{0^{-+}} - m_{0^{++}} > m_h$ when the radiated Higgs boson is onshell. For example, for $m_h \sim 100$ GeV we obtain $BR(0^{-+} \to 0^{++}h) \sim 0.3$.

In the SM, the most stringent limits on the size of the CP violation effects come from experimental limits on the electric dipole moment of the neutron. The same experimental constraints also allow us to place limits on the CP-violating operator in (3.16). To see this, let us recall that the X particles can also carry QCD color. Then, the following dimension-six operators are induced:

$$\mathcal{L}^{(6)} = \frac{\alpha_s\,(y^2-\tilde{y}^2)}{3\pi\,M^2}\,H^\dagger H\,\mathrm{tr}\;G_{\mu\nu}G^{\mu\nu} + \frac{\alpha_s\,(2\,y\,\tilde{y})}{\pi\,M^2}\,H^\dagger H\,\mathrm{tr}\;G_{\mu\nu}\tilde{G}^{\mu\nu}. \tag{3.19}$$

where now $G_{\mu\nu}$ denotes the SM gluon field strength tensor and $\tilde{G}_{\mu\nu}$ its dual. The CP violating term in (3.19) with the Higgs field replaced by its vacuum expectation value contributes to the

---

[9]The effective Lagrangian (3.16) can be evaluated either by following the procedure displayed in appendix A or, equivalently, in the limit of vanishing Higgs momentum by taking derivatives of the v-gluon self-energy and the axial anomaly:

$$\mathcal{L}^{(6)} = H^\dagger H/v_H^2\,(y_d^2\partial^2/\partial y_d^2 + y_d^{*2}\partial^2/\partial y_d^{*2})\,\mathcal{L},$$

where

$$\mathcal{L} = (\alpha_v/6\pi)\ln(\Lambda^2_{UV}/\mathrm{det}M^\dagger M)\,\mathrm{tr}\;\mathcal{F}_{\mu\nu}\mathcal{F}^{\mu\nu} + (\alpha_v/2\pi i)\ln(\mathrm{det}M/\mathrm{det}M^\dagger)\,\mathrm{tr}\;\mathcal{F}_{\mu\nu}\tilde{\mathcal{F}}^{\mu\nu}$$

with $M = \begin{pmatrix} M & y_d v_H \\ y_d v_H & M \end{pmatrix}$.

θ angle. We assume that this contribution to the θ angle is removed by whatever mechanism that solves the strong CP problem in QCD. The next operators in the expansion around the Higgs VeV contain one or two powers of the Higgs field. Their contribution to the electric dipole moment of the neutron can be estimated using Naive Dimensional Analysis [61, 62]. Following the analysis of [63, 64], we estimate the neutron electric dipole moment as

$$d_n = \frac{e}{2\pi f_\pi}\frac{\alpha_s\,(2\,y\,\tilde{y})}{4\pi\,M^2}\,\frac{(2\pi f_\pi)^2}{(4\pi)^2} \sim 10^{-25}\mathrm{e}-\mathrm{cm}\,\times\,\frac{(2y\tilde{y})\,\alpha_s}{8\pi^2}\,\times\,(1\ \mathrm{TeV}/M^2). \tag{3.20}$$

where $2\pi f_\pi \simeq 1190$ MeV is the chiral-symmetry-breaking scale. Combining this result with the current experimental bound on d_n, we derive a limit on $2y\tilde{y}$

$$|2y\tilde{y}| < 10 \times (M/1\ \mathrm{TeV})^2. \tag{3.21}$$

Consequently, values for $|y|$, $|\tilde{y}|$ in the range $0.01-1$ are consistent with the existing experimental limits.

3.6 Conclusions

In this work, we have investigated a particularly challenging hidden valley scenario with a broader class of couplings to SM particles than those considered in [19]. In particular, we have focused on the effect of dimension-six operators by which the hidden sector interacts with the standard model through the Higgs sector.

The resulting v-glueball phenomenology is fairly complex in this scenario, but there are some simple features. In particular, we find the following interesting signatures:

- Decays of the 0^{++} v-glueball through h^*, producing any of the kinematically-allowed Higgs final states such as $b\bar{b}$, $\tau^+\tau^-$, WW, etc.
- Multiple Higgs boson emission, from cascade decays $\Theta_\kappa \to \Theta_{\kappa'}h$, or annihilations $0^{++} \to hh$.
- Due to the diversity of v-glueball states, and the presence of operators of different mass dimension, the lifetimes can vary at least over 5 or 6 orders of magnitude, for any given choice of parameters (see figure 3.6). This has two immediate consequences: (i) Displaced vertices are quite common, which could potentially serve as a discovery channel, and (ii) v-glueballs can be as light as a few GeV's and still be visible.
- For sufficiently small v-glueball masses, a different opportunity arises in the form of non-standard Higgs decays such as $h \to \Theta_\kappa\Theta_{\kappa'}$, with branching ratio to v-glueballs of order $10^{-3} - 10^{-2}$.

In addition, other possible final states include gg, $\gamma\gamma$, and radiative transitions with emission of a photon, all of which are induced by dimension-eight operators [19]. The rare diphoton channel is particularly interesting because, thanks to its moderate QCD background, it may serve as the discovery channel for the v-glueballs at the LHC.

We should nevertheless emphasize that some of our results are subject to significant theoretical and numerical uncertainties. In this respect, it would be interesting to know the spectrum of pure-Yang-Mills theory for gauge groups other than $SU(3)$, as well as the various v-glueball matrix elements that arise. With enough motivation, such as a hint for discovery, these could in principle be determined by additional lattice computations. If the v-sector gauge group is not $SU(n_v)$, some of the v-glueballs may not be present; for instance, for $SO(n_v)$ or $Sp(n_v)$ gauge groups the C-odd sector is absent or heavy. However, as explained in [19], the lightest C-even v-glueballs are expected to be present in any pure-gauge theory, with similar production and decay channels, so at least for them, the basic features of a pure-gauge hidden valley are expected to be retained. We also have not considered higher-order corrections to the decay rates, and they should be taken into account when precise predictions are required.

We have seen that the operators considered in this paper are not heavily constrained by current experimental searches or precision electroweak data, thus leaving ample parameter space to be explored by the next generation of hadron collider experiments. Application of our results for phenomenological studies, particularly as relevant for the LHC, will be carried out in a companion paper [60]. We expect that detection should be feasible, if the mass M of the X particles is small enough to give a reasonable large cross-section, and Λ_v is large enough to ensure the v-glueballs decay inside the detectors. Decays to bottom quarks and gluons often dominate, but they suffer from a huge multijet background. At the Tevatron and at the LHC, the v-glueballs are most likely to be found in searches for diphoton resonances in events with 2 photons plus jets or with 3 or more photons and possibly additional jets, or in searches for displaced decays to jet pairs, W/Z pairs, or photon pairs. A potentially novel signature, which could be currently searched for at the Tevatron, arises in the form of two b-tagged jets plus diphoton events. Contrary to the models of [65–67], the branching ratio to $b\bar{b}\gamma\gamma$ in our model can be $\mathcal{O}(1)$, since the $b\bar{b}$ and $\gamma\gamma$ final states originate in different resonances, leading to a potentially discoverable signal despite the background of $2j + 2\gamma$. Altogether, these signatures provide an interesting opportunity to search for new physics at the Tevatron and at the LHC, which motivates further theoretical and experimental study.

Chapter 4
Phenomenology of quirkonia

The quirk limit has a splendid simplicity, largely devoid of all the complications of relativistic quantum fields, in particular multiparticle production and pair creation. Recall that this theory can be regarded as a certain limit of $SU(n_v)$ gauge theory with heavy quarks such that their masses are much larger than the scale Λ_v where the gauge group $SU(n_v)$ becomes strong. One of the reasons for its simplicity is absence of string breaking. Heavy quirks are confined by a flux tube with energy per length unit of order Λ_v^2. Hence the v-color field contained in the flux tube is too feeble to create a quirk-antiquirk pair: that would require an energy of order $\sim 2M$ localized in a small region of radius $\sim M$ i.e. an energy density $\sim M^2 \gg \Lambda_v^2$. This mechanism is indeed exponentially suppressed.

Furthermore, for sufficiently heavy quirks, one might hope that the characteristic time scale associated with the motion of the constituents quirks inside the quirk mesons is much larger than the time scale associated with the motion of the fast surrounding v-gluons [51]. In this case the adiabatic approximation applies and the effect of the v-gluons can be represented by an average instantaneous interaction potential $V(\mathbf{r})$ between the heavy quirk sources. Moreover, the bound state problem will become non-relativistic, and in the leading order in β the dynamics will be controlled by the Schödinger equation,

$$-\frac{\hbar^2}{2\mu}\nabla^2\Psi(\mathbf{r}) + [V(\mathbf{r}) - E]\,\Psi(\mathbf{r}) = 0, \tag{4.1}$$

where $\mu = m_1 m_2/(m_1 + m_2)$ is the reduced mass of the system formed by the quirks with masses m_1 and m_2, $\mathbf{r}$ is the distance between the quirks, $V(\mathbf{r})$ is the interaction potential, E is the energy eigenvalue, and $\Psi(\mathbf{r})$ is the wave function.

In this work, we assume the quirk mass is in the phenomenologically interesting range 200 GeV $\lesssim M_X \lesssim$ 1 TeV that is not excluded by existing experiments but may be probed at the LHC. The emphasis is on models in which the confining scale in the hidden valley sector, Λ_v, is higher than about 5 GeV, where the v-glueballs produced in quirk annihilation and/or relaxation may decay inside the detectors. Also, for simplicity, we will first consider the case of colored quirks, which are expected to have a larger production cross section than the uncolored

ones unless the mass of the colored quirks is of order 3 times larger than that of the uncolored ones. Then we will comment on the uncolored quirk case.

In this model, quirks can be copiously produced at the LHC via normal QCD interactions. The subsequent evolution of the quirk-antiquirk pair is not familiar so we review it here [47–49]. It is easiest to first view the evolution in the center of mass frame. In that frame the quirks simply oscillate back and forth between their classical turning points. The amplitude of the oscillation can be approximately estimated as E/σ, where E is the energy given to the quirk pair by the collision and σ is the string tension, or energy per unit length of the string, and is about $\sim \Lambda_v^2$. Eventually the oscillations will be damped. In the case of a high confinement scale, two mechanisms are in principle responsible for energy lost. The first is emission of v-glueballs. These can be modeled as bits of closed flux tube, with mass of order a few Λ_v and size $\sim \Lambda_v^{-1}$. Because v-glueballs have a non-perturbative, extended structure their coupling constant to quirks is uncertain. But there is not much reason to expect it to be extremely small, except perhaps the poor overlap between the wave functions of the initial and final quirk states and the fact that v-glueball emission is suppressed by powers of $1/n_v$.

A second mechanism is emission of perturbative gluons. This mechanism appears to be highly important, as it can effectively work to suppress quirk annihilation at high orbital angular momentum waves. Other damping mechanisms may also be present, e.g. non-perturbative hadron emission or radiative transitions with emission of a photon. But it is almost sure that the oscillations will be highly underdamped.

When the quirk and antiquirk come near to rest they will annihilate. The annihilation can be into SM gauge bosons and/or fermion pairs, but also into v-gluons, which at long distance become two or more v-glueballs. The annihilation rate can be estimated using factorization, as in the quarkonium system, where the decay rate is factored into a short-distance part that is related to the annihilation rate of the heavy quirk and antiquirk, and a long-distance factor containing all the nonperturbative effects of $SU(n_v)$ gauge theory. The short-distance factor is calculated in terms of the running coupling constant $\alpha_v(M)$ of $SU(n_v)$, evaluated at the scale of the heavy quirk mass M, while the long-distance factor is expressed in terms of the nonrelativistic quirk meson wavefunction, or its derivatives, evaluated at the origin.

In this work, we focus on some of the key issues outlined above. Our results extend a previous study on quirk phenomenology [49] to our current interest in high confinement scale quirks, $\Lambda_v \gg 1$ GeV. We will consider only one generation of vector-like quirks. Extension to multiple quirk generations is straightforward. First, we need to find formulas for production of colored quirks. We also show that the majority of quirks are produced with kinetic energy

of order M or less. In this regime, the typical separation of the quirk and antiquirk is shorter than Λ_{QCD}^{-1} and therefore nonperturbative QCD effects will in general be unimportant.

Second, we want to solve for the spectrum of quirkonium bound states, particularly to examine mass splittings in different regimes. We will proceed by numerically solving the Schrödinger equation in a appropriately chosen nonrelativistic potential. As part of this process we prove that in general the mass splittings between color octet and color singlet states can be significantly large so that one needs to keep track of quirk color states in detail. [1]

In addition to the production and spectrum calculations, we set up detailed formulas for decay properties of the color-singlet and color-octet quirkonium states. The computation of the rates for gluon radiation and quirk annihilation is relatively simple and can be carried out by following closely the corresponding results for charmonium/bottomium systems. However, the energy loss due to v-glueball emissions is harder to estimate and we will content ourselves by giving some general qualitative arguments.

The organization of the present work is as follows. In the next section, we present the cross-sections for open production of quirks and use them to find the corresponding formulas for production of quirkonium bound states. In section 3, we review the nonrelativistic potential model and its application to the quirkonia spectrum. In section 4, we present the results on the radiative transitions and annihilations of quirkonium and discuss the decay patterns. Conclusions are made in section 5.

4.1 The problem of quirkonium production

The total cross-section $\sigma_{X\bar{X}}$ for production of quirkonium states can be estimated using the operator product expansion, as in the QCD rate for $e^+e^- \to$ hadrons, where the rate is well-estimated by treating the quarks as free, plus a small α_s correction, where α_s is evaluated at the center-of-mass energy $\sqrt{s}$ [76]. We can thus consider the production of quirkonium as proceeding in two steps. The first step is the production of a $X\bar{X}$ pair, and the second step is the binding of the $X\bar{X}$ pair into a quirkonium state. Any Feynman diagram for the production of a quirk pair must involve virtual particles that are off their mass shells by amounts on the order of M or larger. The part of the amplitude in which all internal lines are off-shell by such amounts is called the short-distance part, and it is calculable by using perturbation theory in $\alpha_v(M)$. The parts of the amplitude in which the X and $\bar{X}$ lines are off-shell by amounts much

[1] This is in contrast to the case of very small Λ_v studied in [49] where the bound states are very closely spaced in the spectrum and the QCD color of colored quirks is uncorrelated, so averaging over quirk colors is a good approximation.

less than M can be considered part of the amplitude for the formation of the bound state.

The short-distance part of the amplitude describes the production of a $X\bar{X}$ pair with a spatial separation that is of the order of $1/M$ or smaller. This follows from the fact that the short-distance part is insensitive to changes in the relative 3-momentum of the X and $\bar{X}$ that are much less than M. Since $1/M$ is much smaller than the time scale associated with the quirkonium wavefunction, M/Λ_v^2, the $X\bar{X}$ pair is essentially pointlike on that scale. By that time, the original quirks are far away from each other so that a residual interaction cannot significantly alter the transition cross section which was decided at the first quirk stage. Thus, we need only consider the amplitude for a pointlike $X\bar{X}$ pair to bind to form a quirkonium state. This amplitude will necessarily depend on the quirkonium state and on the quantum numbers of the quirk pair.

In the local duality approach [76–79], the cross section for producing any quirkonium bound state is equal to the cross section for producing a free quirk-antiquirk pair in an appropriately chosen energy interval. The physical picture is that the quirkonium resonances introduce large fluctuations of the cross-section as a function of $\sqrt{\hat{s}}$, and these ought to be convolved with the parton distribution functions. But the resonances are closely spaced well above threshold, so averaging over them is a reasonable approximation for an estimate of an overall rate.

The production of $X\bar{X}$ bound states in hadroproduction can then be estimated by the free $X\bar{X}$ cross section integrated from the kinematical lower limit up to proton energy $\sqrt{s}$,

$$\sum_{\Theta_{X\bar{X}}} \sigma(pp \to \Theta_{X\bar{X}} + \mathcal{X}) \simeq \int_{2M}^{\sqrt{s}} \frac{d\sigma}{d\hat{s}}(pp \to X\bar{X}; s; \hat{s}), \tag{4.2}$$

where the sum on the LHS of (4.2) is over all possible quirkonium resonances in the energy interval $2M \cdots \sqrt{s}$. Here s denotes the squared beam energy. The differential cross section for heavy quirk pair production can be read off the corresponding differential cross section for heavy quark production.

Hadroproduction of open colored quirks in leading perturbative QCD proceeds via quark-antiquark annihilation and gluon-gluon fusion in lowest order [78]. In the former case, a highly virtual gluon is produced, which materializes into a $X\bar{X}$ pair. The $X\bar{X}$ state is thus produced exclusively in the color-octet state. The cross section is given by:

$$\hat{\sigma}_{q\bar{q}\to X\bar{X}}(\hat{s}) = \frac{2}{9}\frac{4\pi\, n_v\, \alpha_s^2}{3\hat{s}}\left(1 + \frac{1}{2}z\right)\beta. \tag{4.3}$$

Here we have defined $z = 4M^2/\hat{s}$, $\beta = \sqrt{1-z}$. The subprocess $g + g \to X + \bar{X}$ is similar to $\gamma\gamma \to e^+e^-$ but contains in addition the fusion of two incident gluons into a virtual gluon,

which then decays into a $X\bar{X}$ state

$$\hat{\sigma}_{gg\to X\bar{X}}(\hat{s}) = \frac{\pi\, n_v\, \alpha_s^2}{3\hat{s}} \left[(1 + z + \frac{1}{16}z^2) \ln \frac{1+\beta}{1-\beta} - \beta \left(\frac{7}{4} + \frac{31}{16} z \right) \right]. \tag{4.4}$$

Hence, gg gives a mixture of color-singlets and color octets.

The cross section for free $X\bar{X}$ production is

$$\frac{d\sigma}{d\hat{s}}(AB \to X\bar{X}; s; \hat{s}) = \frac{1}{s} \int_\tau^1 \frac{dx}{x} H^{AB}(x, \frac{\tau}{x}; \hat{s}), \tag{4.5}$$

where $\tau = \hat{s}/s$. We have introduced the function

$$H^{AB}(x_A, x_B; \hat{s}) = g^A(x_A, \mu^2) g^B(x_B, \mu^2) \hat{\sigma}(gg \to X\bar{X}; \hat{s}) + \sum_q \left\{ q^A(x_A, \mu^2) \bar{q}^B(x_B, \mu^2) + \bar{q}^A(x_A, \mu^2) q^B(x_B, \mu^2) \right\} \hat{\sigma}(qq \to X\bar{X}; \hat{s}) \tag{4.6}$$

where the sum is over light quark flavors relevant to $X\bar{X}$ production. The mass scale μ is of the order of the heavy quirk mass.

In figures 4.1-4.3 we present the LO $X\bar{X}$ differential cross sections at $\sqrt{s} = 14$ TeV as a function of $\sqrt{\hat{s}}$ for different quirk masses $M = 250, 500, 1000$ GeV and $\mu^2 = M^2$. Notice that the cross sections are proportional to n_v.

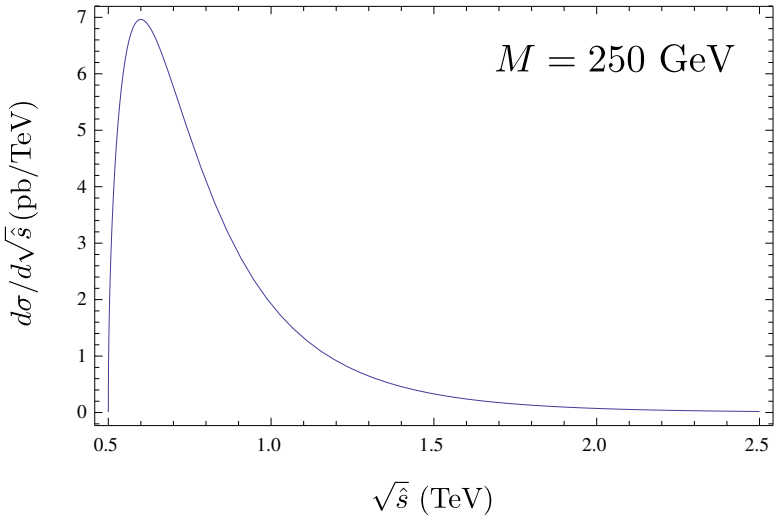

Figure 4.1: The differential cross-section for colored quirk pair production at the LHC ($\sqrt{s} = 14$ TeV) for $M = 250$ GeV.

With the above formulas (4.2) and (4.5) we present in figure 4.4 the total cross section for colored quirk production at the LHC at leading order in perturbation theory. The production rates are significant at to several TeV even though the quirks are heavy.

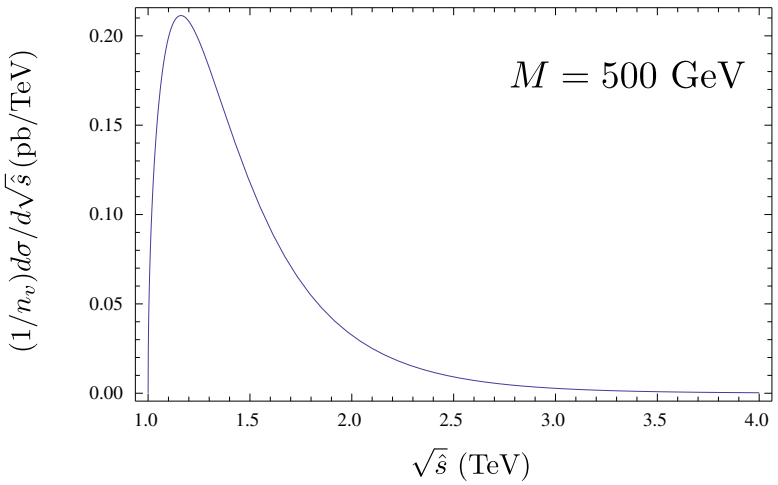

Figure 4.2: The differential cross-section for colored quirk pair production at the LHC ($\sqrt{s} = 14$ TeV) for $M = 500$ GeV.

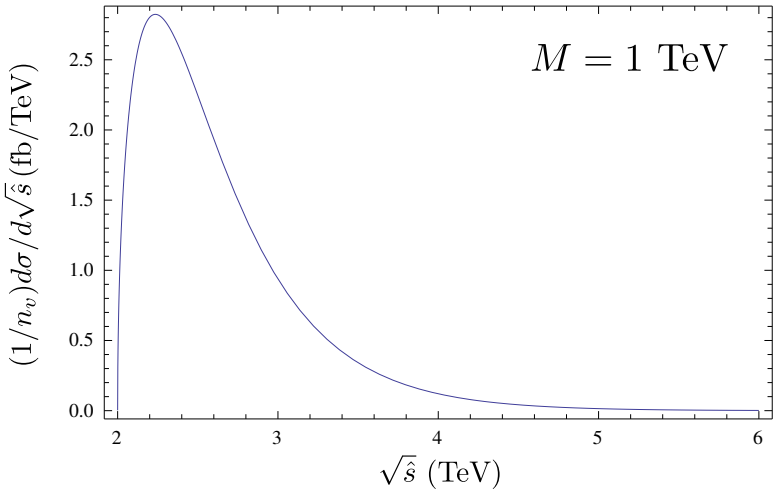

Figure 4.3: The differential cross-section for colored quirk pair production at the LHC ($\sqrt{s} = 14$ TeV) for 1000 GeV.

4.2 Non-relativistic potential model

It is an experimental and theoretical fact that for heavy-quark bound states ("quarkonia") the orbital splittings are smaller than the quark mass M [51,80,81]. This suggests that all the other dynamical scales of these systems are smaller than M. Consistently with this fact, the quark velocity v in these systems is believed to be a small quantity, $v \ll 1$. Therefore, a non-relativistic (NR) picture holds. The nonrelativistic approach has been successfully used for describing the physics of heavy quarkonia since the discovery of the J/ψ meson and we expect it to provide reasonable guidance to the dynamics of heavy quirk-antiquirk systems as well.

There are many possible states of a heavy quirk-antiquirk system. For any given quirkonium state, the Fock state consists of a v-color-singlet quirk pair in a definite angular-momentum

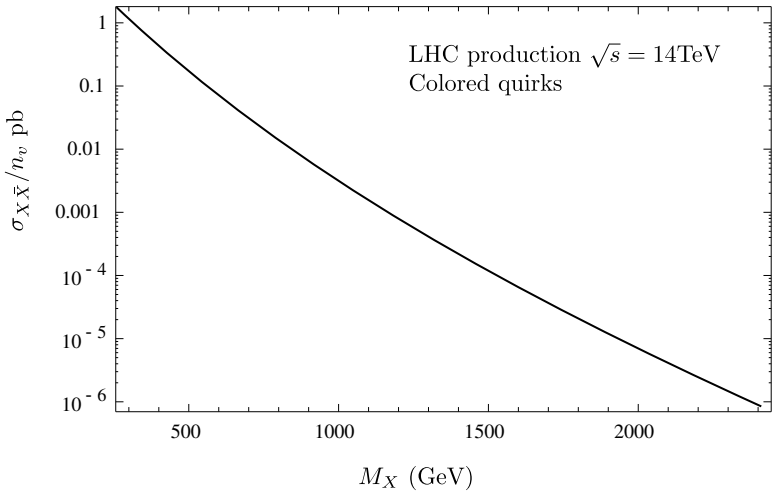

Figure 4.4: Quirk production cross section at the LHC ($\sqrt{s} = 14$ TeV) as a function of the quirk mass.

state. We denote the two possible QCD color states of a quirk pair by **1** for color-singlet and **8** for color-octet. In the nonrelativistic approximation, the states of quirkonium can be cataloged according to the standard spectroscopic notation $n^{2s+1}L_J$, where n denotes the radial excitations and L denotes the orbital angular momenta S, P, D, $\cdots$ for $L = 0, 1, 2, \cdots$ respectively. Each constituent quirk has spin $\frac{1}{2}$, and so the total spin quantum number can be either $S = 0$ or 1. J is the quantum number of the total momentum, a vector sum of the spin and orbital momenta. An alternative notation used to denote the quirkonium states is J^{PC} , where P is the space parity and C is the charge conjugation parity. For a quirk-antiquirk system these can be expressed as $P = (-1)^{L+1}$ and $C = (-1)^{L+S}$, respectively. In table 4.1 we have collected the quantum numbers of the lightest quirkonium states in the spectrum.

State	J^{PC}	$^{2S+1}L_J$
$\eta_{\mathbf{1}}$, $\eta_{\mathbf{8}}$	0^{-+}	$^1S_0$
$\psi_{\mathbf{1}}$, $\psi_{\mathbf{8}}$	1^{--}	$^3S_1$
$h_{\mathbf{1}}$, $h_{\mathbf{8}}$	1^{+-}	$^1P_1$
$\chi_{J,\mathbf{1}}$, $\chi_{J,\mathbf{8}}$	J^{++}	^3P_J

Table 4.1: The quantum numbers of the low lying states in the spectrum.

A complete treatment of the spectrum of quirkonium in non-relativistic effective field theory (NREFT) is beyond the scope of this work. We will discuss briefly when the nonrelativistic potential model is expected to work. The validity of the potential model rests upon the existence of a hierarchy of energy scales, $M \gg Mv \gg Mv^2$ in nonrelativistic systems with mass M and velocity v [81]. This hierarchy allows for the construction of a sequence of effective field theories: nonrelativistic (NREFT) and potential NREFT (pNREFT). First, the transition is

from the effective field theory with relativistic quirks to NRQCD with the quirks (and larger momenta $\sim M$) integrated out. The theory describes dynamics of heavy quirk-antiquirk pairs at energy scales in the center-of-mass frame much smaller than their masses. A higher degree of simplification can be achieved by exploiting $Mv \gg Mv^2$ and building the so-called potential-NREFT (or pNREFT), where degrees of freedom of $\sim Mv$ are integrated out. In this way, an analytical calculation of the spectrum becomes possible.

As in QCD, the choice of the potential is not unique, in view of the absence of a consistent theory at all distances. However, it is restricted by theoretical arguments concerning the properties of the interaction between quirks at different distances. The shape of the potential is determined by asymptotic freedom at very short distances and by quirk confinement at very long quirk separations. In the first case, the potential can be computed accurately in $SU(n_v)$ perturbation theory, and in the lowest order it is dominated by single v-gluon exchange between the static quirks. At distances of roughly $1/\Lambda_v$, α_v increases significantly and one-gluon-exchange is no longer a good approximation. In long distances one calculates the potential in a model which is assumed to be a good approximation to pure-Yang-Mills theory, usually in quenched lattice QCD but also in string or flux tube models. A popular suggestion is that at long distances the potential should behave as a linearly growing function of the quirk separation. Qualitatively this linear behavior can be seen as arising from the chromoelectric lines of force that bunch together into a flux tube which leads to a distance independent force or the potential. Thus, in the case of interest the v-color potential has the following asymptotic limits:

$$r \gg \frac{1}{\Lambda_v} \quad : \qquad V_v(r) = \sigma\, r \tag{4.7}$$

$$r \ll \frac{1}{\Lambda_v} \quad : \qquad V_v(r) = -C\,\frac{\alpha_v(r)}{r} \tag{4.8}$$

where σ is the string tension, $\alpha_v(r)$ is the $SU(n_v)$ running coupling constant. The color factor C is obtained by evaluating the product of $SU(n_v)$ generators. Labeling the particles 1 and 2, this product is $-T_1^a T_2^a = \frac{1}{2}((T_1^a)^2) + (T_2^a)^2) - (T_1^a + T_2^a)^2)$, which leads to

$$C = \frac{1}{2}\left(C_1 + C_2 - C_{(12)}\right), \tag{4.9}$$

where C_1 and C_2 are the quadratic Casimirs for the two particles and $C_{(12)}$ that for the bound state. For the case of a quirk-antiquirk pair, the v-color decomposition

$$\mathbf{n_v} \otimes \bar{\mathbf{n}}_\mathbf{v} = \mathbf{1} \oplus (\mathbf{n_v^2 - 1}) \tag{4.10}$$

shows that quirkonium can be a v-color singlet or a v-color adjoint. Then

$$C_\mathbf{1} = C_F = \frac{n_v^2 - 1}{2n_v} \qquad\qquad C_{\rm Adj} = C_F - \frac{C_A}{2} = -\frac{1}{2n_v}. \tag{4.11}$$

Thus the v-color Coulomb force is always attractive in the v-color singlet channel.

One can then use a smooth interpolating function for the transition region, smoothly join the non-perturbative potential to the perturbative one or simply add the perturbative and nonperturbative contributions.

In our numerical study, we have considered the following potential-model choices.

(1) Cornell potential [84]. This is the simplest possibility of a quirk potential satisfying the asymptotic limits above. The potential is simply given by the sum of (4.7) and (4.8) with $\alpha_v(r) = \alpha_v = \text{const}$,

$$V(r) = -\frac{4}{3}\frac{\alpha_v}{r} + \sigma r. \tag{4.12}$$

(2) Richardson potential [85]. A different possibility which incorporates the two concepts of asymptotic freedom and linear confinement in a unified manner is the Richardson potential. In this case the potential is constructed by Fourier transforming a smartly chosen, ad-hoc expression for the potential in momentum space

$$V(\mathbf{q^2}) = -\frac{4}{3}\frac{1}{\mathbf{q}^2}\frac{4\pi/11}{\ln\left(1+\mathbf{q}^2/\Lambda_v^2\right)}. \tag{4.13}$$

The potential grows linearly at long distances and has the short-range behavior to one-loop order in perturbation theory,

$$V(\mathbf{q}^2) = -\frac{4}{3}\frac{16\pi^2\alpha_v(\mathbf{q}^2)}{\mathbf{q}^2}, \tag{4.14}$$

where

$$\alpha_v(\mathbf{q}^2) \sim \frac{4\pi/11}{\ln\left(\mathbf{q}^2/\Lambda_v^2\right)} \qquad \mathbf{q}^2 \to \infty. \tag{4.15}$$

Upon performing the Fourier transform of (4.13) Richardson showed that the potential $V(r)$ can be written in the form

$$V(r) = \frac{8\pi}{33}\Lambda_v\left(\Lambda_v r - \frac{f(\Lambda_v r)}{\Lambda_v r}\right), \tag{4.16}$$

where

$$f(t) = \frac{4}{\pi}\int_0^\infty dq \frac{\sin(qt)}{q}\left[\frac{1}{\ln(1+q^2)} - \frac{1}{q^2}\right]. \tag{4.17}$$

The potential (4.16) has the nice feature that its behavior is determined by a single parameter, the scale Λ_v. The value of Λ_v is conveniently chosen to reproduce the large-distance string tension, i.e. $\sigma = 8\pi\Lambda_v^2/33$.

(3) Wisconsin potential [86]. In order to be able to relate the short-distance behavior of the potential to the parameter $\Lambda_v^{\bar{M}S}$, perturbative corrections up to two loops have to be

included [82]. As an alternative we have adopted the potential proposed in [86] which incorporates the asymptotic behavior predicted by the two-loop calculation, with $\Lambda_{\bar{M}S}$ not directly tied to the string tension,

$$V_v(r) = \sigma r - \frac{4}{3}\frac{1}{r}\frac{4\pi}{b_0 f(r)}\left\{1 + \frac{c}{f(r)} - \frac{b_1 \ln f(r)}{b_0^2 f(r)}\right\} \tag{4.18}$$

where

$$f(r) = \ln\left\{(r\Lambda_v)^{-2} + b\right\} \qquad b_0 = 11 - \frac{2}{3}n_f \tag{4.19}$$

$$b_1 = 102 - \frac{38}{3}n_f \qquad c = \frac{1}{360}\left(31 - \frac{10}{3} + 2\gamma_E\right). \tag{4.20}$$

Here n_f denotes the number of effective flavors; $n_f = 0$ in the hidden sector, and $n_f = 3, 4, 5$ in QCD. The parameter b is introduced to regularize the potential at large distances r. The potential (4.18) grows linearly at long distances and has a short-range asymptotic behavior to two-loop in perturbation theory.

One should be aware of what is being neglected in calculations within the naive potential model. Relativistic and quantum effects such as spin dependence and pair creation, as well as mixing between among states induced by coupling to decay channels, are ignored in the present discussion. Also, as is, the potential model has little to say on the important question of how v-gluonic degrees of freedom may affect the computation of the spectrum.

The size of the relativistic corrections can be estimated by computing the average relative velocity v of quirks in a specific state [87]. At long distances, the potential behaves approximately linearly, $V(r) \sim \sigma r$. In such a potential the expectation value of the kinetic energy $\langle T\rangle = \langle \frac{r}{2}\frac{dV}{dr}\rangle$ is just $\langle T\rangle = \langle V/2\rangle = E/3$ with $\sigma = m_0^2/3.7^2$. Since $\langle T\rangle = 2\dot{(}1/2)Mv^2$, one has $v^2 \simeq 1/3$ for quirk pairs with kinetic energy $E \sim M/4$, where the majority of the states are produced. Thus a nonrelativistic description for highly excited quirkonium states is quite crude, whereas it is substantially better for the states produced near threshold.

In writing the $X\bar{X}$ interaction for colored quirks we must also keep track of the color state c of the quirk pair. The $SU(3)_C$ color potentials in momentum space take the form,

$$V_s(q) = -\frac{4}{3}g^2\frac{1}{q^2}, \qquad V_o(q) = \frac{g^2}{6}\frac{1}{q^2} = -\frac{1}{8}V_s(q), \tag{4.21}$$

governing interactions between colored quirks in color-singlet and color-octet states, respectively. The force in the singlet channel is attractive while that in the octet channel is repulsive and smaller in size.

We shall use the two-loop expression for α_s,

$$\alpha_s(Q^2) = \frac{4\pi}{\beta_0 \log\left[Q^2/\Lambda_{\bar{M}S}\right]^2}\left\{1 - \frac{2\beta_1}{\beta_0^2}\frac{\log\left[\log\left[Q^2/\Lambda^2_{\bar{M}S}\right]\right]}{\log\left[Q^2/\Lambda^2_{\bar{M}S}\right]}\right\}, \tag{4.22}$$

with $\beta_0 = 11 - \frac{2}{3}n_f$, $\beta_1 = 51 - \frac{19}{3}n_f$ and $\Lambda_{\bar{M}S} \simeq 250$ GeV.

We distinguish a priori three regimes in r:

1. For large r the interaction is negligible and the QCD color of colored quirks (which is irrelevant to their motion) is uncorrelated so, to a good approximation, we can average over quirk colors.

2. For intermediate r one must keep track of the color state in detail, and propagate the quirks according to the potential appropriate to their color state. This the regime of non-perturbative QCD transitions, such as pion emission.

3. For small r the large gap between color singlet and octet might induce a large transition rate due to gluon radiation, which changes the color state of the quirks.

The boundaries of these regions must be determined by explicit computation.

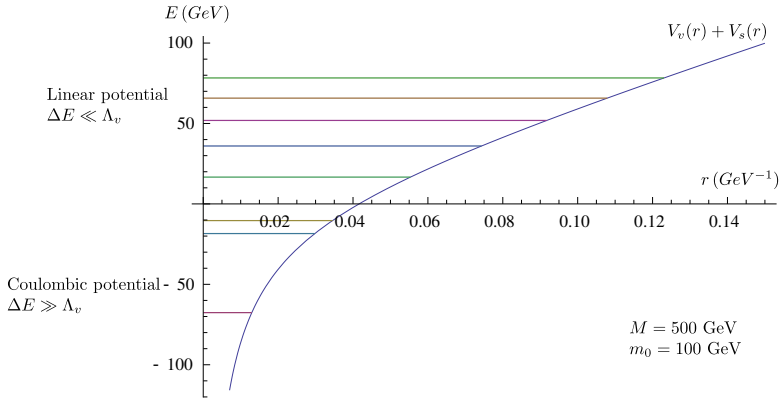

Figure 4.5: Spectrum of the system consisting of two heavy quirks. In the case shown, horizontal lines correspond to the binding energies of a color-singlet bound state of quirkonium.

The energy spectrum of the system of two heavy quirks therefore looks as shown schematically in figure 4.5. The low-lying states are Coulombic, with energy splittings of order $\alpha_v^2 M \gg \Lambda_v \sim m_0/7$, while the states near the continuum threshold are dominated by the linear term. Spin-dependent interactions are suppressed by $1/M$, so spin excitations are small and we do not expect them to play an important role in the process we are considering. The energy splitting between highly-excited states scale as $\sim n^{-1/3}$, where n denotes the radial quantum excitation number. Hence, as n goes to infinity, the highly excited states become closely spaced.

4.3 Decay modes of heavy quirkonia

In this section, we present formulas for the decay widths of color-singlet and color-octet states of heavy quirkonia.

If the quirks are colored, the quirkonium states have many possible ways to decay. To a great extent, the decays of quirkonium fall naturally into three main classes: hard annihilations, SM radiative decays and radiative decays by the v-color strong interaction ("v-glueball radiative decays").

(a) Hard annihilations: The quirk and antiquirk pair annihilates into v-gluons, which at long distance become two or more v-glueballs, or into SM gluons and quarks, which fragment into two or more jets. Note that color-octet quirkonium states cannot annihilate into v-glueballs alone.

(b) SM radiative decays: The quirk and antiquirk pair undergo a cascade decay with emission of a perturbative gluon or two soft gluons which materialize into hadrons (mostly pions and kaons). In the transitions with single-gluon emission a color singlet state is promoted to a color octet state. Electromagnetic cascade transitions with emission of a photon are possible for electrically-charged quirks, but these will be typically suppressed with respect to the hadronic decays.

(c) v-glueball radiative decays: Non-perturbative v-color transitions $\Psi_{\rm I} \to \Psi_{\rm J} + \Theta_\kappa$ are an example of this kind. Here, $\Psi_{\rm I}$, $\Psi_{\rm J}$ and Θ_κ stand for the initial state quirkonium, final state quirkonium and emitted v-glueball, respectively.

Some comments are in order. First, we should note that the decays are constrained by conserved quantum numbers. For instance, it is impossible for a color-singlet quirkonium state with $J^{PC} = 1^{--}$ to decay through a single gluon as the particle is colorless but a gluon carries color. Decays to two SM gluons are also forbidden by C conservation.

Also, as explained in the introduction to this chapter, the coupling of quirkonium to v-glueballs is due to non-perturbative v-color effects and is subject to significant uncertainties. Therefore, in this work we will consider two extreme scenarios: one where there is no suppression of v-glueball production, and one where nonperturbative v-color interactions are effectively absent. In the first case, the quirkonium states can decay quickly down to the ground state by emitting a few v-glueballs if Λ is sufficiently high, or lot of v-glueballs for low Λ. In the second case, the main mechanisms of energy loss are soft-gluon emission or perturbative-gluon emission, depending on the spacing of the excited quirkonium states.

4.3.1 Annihilation decays

In this section we present the decay widths of all color-singlet and color-octet quirkonium states to two-body final states within the hidden valley or the standard model.

The fact that the decay rate factors into a short-distance and a long-distance part was already explained in the introduction. The first is related to the probability that quirk and antiquirk pair annihilate when they are near each other. Since the mass M of the quirks is large the annihilation takes place in a small region of size $\sim 1/M$ and is described by the small coupling constant of strong or v-color interactions. Therefore, one can use perturbation theory to compute the corresponding matrix elements. This is analogous to the way annihilation decays of charmonium are calculated in QCD. In fact, the calculations of the short-distance part in QCD, QED or Pure-Yang-Mills theory are very similar. The reason is that we are considering decays with the minimum number of particles in the final states. Besides, the details of strong or v-strong interactions take place at a much longer time scale, so they should not affect the total annihilation rates. The only difference between photonic, gluonic or v-gluonic annihilation amplitudes reduces to a simple multiplicative color or v-color factor and to the difference of the coupling constants. We will elaborate these factors in detail below.

The evaluation of the long-distance part of the annihilation rate is slightly more subtle. It was shown in [49] that one needs to distinguish between two different cases: $\lambda \gg M^{-1}$ and $\lambda \ll M^{-1}$, where λ is the de Broglie wavelength of the quirks

$$\lambda = \frac{2\pi\hbar}{\sqrt{2\mu E}}. \tag{4.23}$$

where $K = E - 2\mu$ is the kinetic energy, $\mu = M/2$ is the invariant mass of the reduced system. For $\lambda \ll M^{-1}$, one obtains that in a highly excited state the probability to find the quirks near each other is proportional to the fraction of time that the quirks spends in a small region of radius M^{-1}. In the opposite limit $\lambda \gg M^{-1}$ one obtains the familiar result from positronium and quarkonium physics that the S-wave annihilation probability is proportional to the wavefunction at the origin.

It turns out that in the cases considered the majority of the events that produce quirks are such that $\lambda \gg M^{-1}$. Hence inclusive decay widths of quirkonia take the factorized form

$$\Gamma(X\bar{X} \to \text{v-glueballs}) = \left|\frac{d^l}{dr^l} R_{nl}(0)\right|^2 F(\alpha_v), \tag{4.24}$$

and a similar expression for $\Gamma(X\bar{X} \to \text{hadrons})$. In (4.24) $F(\alpha_v)$ comes from the short-distance matrix element.

One cannot expect to compute $R_{nl}(0)$ from perturbative theory in an expansion in α_v. The reason is that the majority of quirkonium states have a mean radius $r_{X\bar{X}} \gg 1/\Lambda_v$, a distance at which nonperturbative effects are important. Thus $R_{nl}(0)$ will be determined in part by the long range part of the potential (4.7), as in the determination of the spectrum. Perturbation theory will only be applicable to quirkonium states whose average radius is smaller than $1/\Lambda_v$, which is predicted for the ground state of $X\bar{X}$ for large quirk masses.

The rate also depends crucially on the angular momentum and spin of the quirk-antiquirk pair. Using the semiclassical formulas for the wave function at the origin (A.46) and (A.47), one can show that

$$\frac{\Gamma_{l\neq 0}}{\Gamma_{l=0}} \sim \frac{1}{l}\left(\frac{\beta}{l}\right)^{l+1}. \tag{4.25}$$

This suppression implies that annihilation is dominated by small l.

We now present our results for the annihilation rates of S-wave quirkonia. As explained above most of the results can be obtained from previous similar calculations for quarkonium decays with appropiate modifications to include color or v-color factors (see for example [42, 49, 88]). Let us start with the case of color-singlet annihilations.

A. Color-singlet quirkonium

1. $\eta_{\mathbf{1}}(S) \to g_v g_v$, gg, $\gamma\gamma$ For the color-singlet $\eta_{\mathbf{1}}(S)$ quirkonium the leading decay mode is $g_v g_v$ with rate:

$$\Gamma(\eta_{\mathbf{1}}(S) \to g_v g_v) = \frac{n_v^2 - 1}{4n_v} N_{\rm c}\, \frac{4\pi\alpha_v^2}{M^2}|\psi(0)|^2 \tag{4.26}$$

where the gauge coupling is to be evaluated at the renormalization scale M. For the v-color coupling, we use

$$\alpha_v(M) = \frac{6\pi}{11 n_v \ln M/\Lambda_v}. \tag{4.27}$$

These v-gluon fields are converted into v-glueballs at long distance, which in turn can decay back to standard model fields as discussed in the previous chapters.

For quirks carrying QCD color, we also have

$$\Gamma(\eta_{\mathbf{1}}(S) \to gg) = \frac{N_c^2 - 1}{4N_c}\, n_v\, \frac{4\pi\alpha_3^2}{M^2}|\psi(0)|^2, \tag{4.28}$$

The QED annihilation processes are

$$\Gamma(\eta_{\mathbf{1}}(S) \to \gamma\gamma) = n_v N_c e_X^4\, \frac{4\pi\alpha^2}{M^2}|\psi(0)|^2, \tag{4.29}$$

where e_X is the electric charge of the quirk and $N_c = 3$ is the number of QCD colors .

We have neglected the contribution from Z boson exchange, which gives a small correction. There are similar expressions for annihilation through a W in the case where the electric charge of the quirks differs by one unit.

2. $\psi_{\mathbf{1}}(S) \to Z^*/\gamma^*,\ g_v g_v g_v, \gamma g_v g_v$

$$\Gamma(\psi_{\mathbf{1}}(S) \to \gamma^* \to f\bar{f}) = \frac{4 n_v N_c N_{Cf} e_X^2 e_f^2}{3} \frac{4\pi\alpha^2}{M^2} |\psi(0)|^2, \tag{4.30}$$

For the color-singlet $\psi_{\mathbf{1}}(S)$ quirkonium the leading decay mode is $g_v g_v g_v$. The width of this decay is

$$\Gamma(\psi_{\mathbf{1}}(S) \to g_v g_v g_v) = \frac{\alpha_v^3}{9\pi} \frac{(n_v^2-1)(n_v^2-4)N_c}{4n_v^2} \frac{4\pi|\psi(0)|^2}{M^2} (\pi^2 - 9). \tag{4.31}$$

$$\Gamma(\psi_{\mathbf{1}}(S) \to \gamma g_v g_v) = \frac{4\alpha_v^2 \alpha\, e_X^2 N_c}{3\pi} \frac{(n_v^2-1)}{n_v} \frac{4\pi|\psi(0)|^2}{M^2} (\pi^2 - 9). \tag{4.32}$$

B. Color-octet quirkonium

We now present the results for S-wave annihilation decays of color-octet quirkonium. In this case, annihilations to v-gluons are forbidden in decays with less than four gauge bosons in the final state.

1. $\eta_{\mathbf{8}}(S) \to gg$.

   For the $\eta_{\mathbf{8}}(S)$ quirkonium, the dominant decay mode is gg with width

$$\Gamma(\eta_{\mathbf{8}}(S) \to gg) = \frac{N_c^2 - 4}{N_c} n_v \frac{4\pi\alpha_3^2}{M^2} |\psi(0)|^2, \tag{4.33}$$

2. $\psi_{\mathbf{8}}(S) \to g^*,\ ggg,\ gg\gamma,\ g\gamma\gamma$.

   Since the $\psi_{\mathbf{8}}(S)$ quirkonium has the same quantum numbers of a gluon, it can decay to SM quarks of either flavor through an off-shell gluon. The width of the decay is given by

$$\Gamma(\psi_{\mathbf{8}}(S) \to f\bar{f}) = \frac{n_v}{4} \frac{4\pi\alpha_3^2}{M^2} |\psi(0)|^2. \tag{4.34}$$

   It is important to observe that the decay involving two on-shell SM gluons, $\psi_{\mathbf{1}}(S) \to gg$, vanishes as a consequences of Yang's theorem which forbids a massive $J = 1$ vector boson from decaying to two massless $J = 1$ bosons [92]. The leading decay modes involving SM gauge bosons are ggg, $gg\gamma$ and $g\gamma\gamma$, and their respective rates read

$$\Gamma(\psi_{\mathbf{8}}(S) \to ggg) = \frac{\alpha_s^3}{9\pi} \frac{(N_c^4 - 4N_c^2 + 12)n_v}{64N_c^2} \frac{4\pi|\psi(0)|^2}{M^2} (\pi^2 - 9) \tag{4.35}$$

$$\Gamma(\psi_{\mathbf{8}}(S) \to gg\gamma) = \frac{\alpha_s^2 \alpha}{9\pi} \frac{(N_c^2-4)n_v}{4N_c^2} \frac{4\pi|\psi(0)|^2}{M^2}(\pi^2-9), \tag{4.36}$$

$$\Gamma(\psi_{\mathbf{8}}(S) \to g\gamma\gamma) = \frac{\alpha_s \alpha^2}{9\pi} \frac{n_v}{4N_c^2} \frac{4\pi|\psi(0)|^2}{M^2}(\pi^2-9). \tag{4.37}$$

4.4 Radiative transitions in quirkonium

Another class of transition rates that can be calculated in the nonrelativistic potential model are the radiative ones. We have seen in the last section that annihilation is dominated at small l. This means that annihilations can be effectively suppressed if there are other interactions that can change the orbital angular momentum of the quirks. Therefore the radiative transitions between quirkonium states which have this property certainly deserve consideration. Interestingly enough, the soft particles emitted during quirk radiation could, in some regimes, potentially serve as the discovery channel for hidden valleys [50].

The multipole expansion in electrodynamics has been widely used for studying radiation processes in which the electromagnetic field is radiated from local sources [42]. If the radius a of a local source is smaller than the wave length λ of the radiated electromagnetic field such that $a/\lambda \sim ak < 1$ (k stands for the momentum of the photon), ak can be a good expansion parameter, i.e., we can expand the electromagnetic field in powers of ak. This is the well-known multipole expansion in QED. The multipole expansion in QED has also been generalized by many authors to describe hadronic transitions in quarkonium systems (See for example [89, 90] for a review).

We now discuss gluon radiative decays in quirkonium systems. We begin with the case $r \ll \Lambda_{QCD}^{-1}$. For sufficiently excited quirks to use the WKB approximation, the typical radius $a = \langle r \rangle$ obtained by using the virial theorem is of order

$$a \simeq \frac{2}{3}\frac{K}{\sigma}, \tag{4.38}$$

where K is the kinetic energy of the quirk pair and σ is the string tension. A similar estimation for the typical energy splitting at binding energies of order $K \sim 0.5M$ gives $\Delta E \sim .25m_0^2/M$. For a gluon emission with gluon energy $k = \Delta E$, $ka \sim 1$. Therefore, this suggests that one can apply the idea of multipole expansion in QCD to calculation of the transitions between quirkonium levels with emission of a gluon[2]. Aside from color factors, the radiative transitions

[2]In classical electrodynamics, the coefficient of the $(ak)^l$ term in the multipole expansion contains an extra factor $\frac{1}{(2l+1)!!}$. Hence the multipole expansion actually works better than what is expected by simply estimating the size of $(ak)^l$.

in quirkonium are similar to those in quarkonium, so many of the formulas presented below will look familiar to the readers with an expertise in quarkonium physics.

The leading terms in the interaction of a nonrelativistic quirkonium with the gluon field that will be important in our further discussion of the realistic processes are the chromoelectric and the chromomagnetic dipoles, $E1$ and $M1$ [90]. The corresponding terms in the Hamiltonian can be written as

$$H_{E1} = -\frac{1}{2}\xi^a \mathbf{r}\cdot\mathbf{E}^a \qquad\qquad H_{M1} = -\frac{1}{2M}\xi^a \boldsymbol{\Delta}\cdot\mathbf{B}^a, \tag{4.39}$$

where $\xi^a = t_1^a - t_2^a$ is the difference of the color generators acting on the quirk and antiquirk (e.g. $t_1^a = \lambda^a/2$ with λ^a being the Gell-Mann matrices), and $\mathbf{r}$ is the vector for relative position of the quirk and the antiquirk. Finally $\mathbf{E}$ and $\mathbf{B}$ are the chromoelectric and chromomagnetic components of the gluon field strength tensor.

From the Hamiltonian (4.39), one can extract selection rules for the radiative transitions. These rules are completely equivalent to the ones found in electric dipole transitions in electrodynamics. The chromoelectric dipole term is odd under space reflection and hence links states with opposite parities. Moreover, it is independent of spin and that means $\Delta S = 0$. On the other hand, the chromomagnetic dipole term is parity even. Therefore, it generates transitions only between spin-singlet ($S = 0$) and spin-triplet ($S = 1$) states of the same parity. Also, unlike electromagnetic transitions, a single H_{E1} or H_{M1} dipole interaction changes a color singlet $X\bar{X}$ state into some color octet $X\bar{X}$ state.

The general formula for the matrix element between an initial state i and a final state f in this approximation reads,

$$\mathcal{M} = -i2\pi\delta(E_f - E_i - \omega)\langle f|H_I|i\rangle \tag{4.40}$$

where ω is the energy of the emitted gluon and $I = E_1, M_1$.

It is easy to also write the total rate. The annihilation decays discussed in the last section depend on the quirkonium wave function at very short $X\bar{X}$ separations. In contrast, the E_1 and M_1 radiative widths involve overlaps of radial wave functions. We consider first electric dipole transitions. One sums over gluon polarizations, integrates over phase space and finds [91]

$$\Gamma(i \xrightarrow{E_1} f + g) = \frac{4\alpha_s}{3}(2J'+1)\mathcal{C}_{if}\mathcal{S}_{if}^E\omega^3|\mathcal{R}_{if}|^2, \tag{4.41}$$

where the gluon energy is $\omega = (M_i^2 - M_f^2)/(2M_i)$; M_i and M_f are the masses of the initial and final states. Here the spin factor $\mathcal{S}_{if}$ is

$$\mathcal{S}_{if}^E = \max(\mathrm{l},\mathrm{l}') \begin{Bmatrix} J & 1 & J' \\ l' & s & l \end{Bmatrix}^2 \tag{4.42}$$

and the color factor $\mathcal{C}_{if}$ is shown in table 4.2. The overlap integral $\mathcal{R}_{if}$ is given by

$$\mathcal{R}_{if} = \frac{3}{\omega}\int drr^2 R_i(r)R_f(r)\left[\frac{\omega r}{2}j_0\left(\frac{\omega r}{2}\right) - j_1\left(\frac{\omega r}{2}\right)\right] \tag{4.43}$$

where $R_i(r)\,(R_f(r))$ is the initial (final) state wave function and $j_n(x)$, $n = 0, 1$ are spherical Bessel functions of the first kind. This expression is valid for quirkonium states of any size. A widely used approximation is the long wave length approximation which consists in taking the limit $\omega \to 0$ in (4.43). In this case the overlap integral simplifies as

$$\mathcal{R}_{if} = \int drr^2 R_i(r)R_f(r)r \tag{4.44}$$

For the typical E_1 transitions one expects $\mathcal{R}_{if}$ very nearly to the average radius of the initial state, because $\omega r \ll 1$ and the initial and final states are sufficiently close to produce a good overlap. On the other hand, E_1 transitions between S and P states with changes in the number of nodes by greater than one are suppressed due to poor overlap between initial and final wave functions. The larger the difference in number of nodes, the greater the suppression.

Transition	$\mathcal{C}_{if}$
singlet-singlet	0
singlet-octet	$(N_c^2-1)/2N_c$
octet-singlet	$1/2N_c$
octet-octet	$2(N_c^2-1)/N_c$

Table 4.2: List of coefficients C_{if} introduced in (4.41).

Magnetic transitions flip the quirk spin. These transitions have $\Delta l = 0$, $\Delta s = \pm 1$. The spin-flip radiative transition between an initial state $n^{2s+1}l_J$, i, and a final state $n'^{2s'+1}l'_J$, f, is:

$$\Gamma(i \xrightarrow{M_1} f + g) = \frac{4\pi\alpha_s}{3M^2}(2J'+1)\mathcal{C}_{if}\mathcal{S}_{if}^M\omega^3|\mathcal{R}_{if}|^2, \tag{4.45}$$

where the overlap integral is given by

$$\mathcal{R}_{if} = \int drr^2 R_i(r)R_f(r)j_0\left(\frac{\omega r}{2}\right). \tag{4.46}$$

Here the spin factor $\mathcal{S}_{if}^M$ is

$$\mathcal{S}_{if}^M = 6(2s+1)(2s'+1)\begin{Bmatrix} J & 1 & J' \\ s' & l & s \end{Bmatrix}^2\begin{Bmatrix} 1 & \frac{1}{2} & \frac{1}{2} \\ \frac{1}{2} & s' & s \end{Bmatrix}^2 \tag{4.47}$$

and the color factor $\mathcal{C}_{if}$ is shown in table 4.2. The M_1 transitions are suppressed by a factor ω/M. Thus, unless forbidden, the E_1 transitions are expected to dominate.

For $r \gg \Lambda_{\rm QCD}^{-1}$, quirks undergo QCD hadronization and therefore we need to consider non-perturbative QCD interactions between the quirks and the QCD brown muck. The brown muck will interact only when the quirks come within a distance of order $\Lambda_{\rm QCD}^{-1}$. It was argued in [49] that these interactions will transfer an energy of order $\Lambda_{\rm QCD}$ and an angular momuntum of order $\Delta l \sim 1$ from the bound state roughly once every crossing time. As a consequence, one light QCD hadron, typically a neutral pion, will be emitted in a single brown muck interaction. If the quirks do not annihilate for a number of crossings, a large number of hadrons $\sim 10^2 - 10^3$ will be emitted with energy $\sim$ GeV each. These new hadrons have been dubbed "hadronic fireballs", and may be the source of a promising discovery signal in the case of very low hidden confining scale [50]. However, in the regime we are considering in this work, these hadronic fireballs are not expected to contribute a significant fraction of the energy loss, as long as $m_0 \gtrsim 50$ GeV.

Before moving on to the discussion of non-perturbative v-color interactions we should consider some concerns. For example, in order for a large amount of energy to be emitted in radiation of perturbative gluons we must ensure that the quirks do not annihilate in a highly excited state. We argue now that this is unlikely.

The probability for annihilation in a single crossing depends strongly on the angular momentum of the bound system and is dominated by low l. From our partial wave analysis in section 4.3.1, we know that the annihilation probability scales like $\sigma_{ann} \propto (\beta/l)^{l+2}$. Given that the angular momentum will grow on average as radiation is emitted, the likelihood of early annihilation is determined by a competition between the annihilation cross section and the radiation rate. Very naively one can expect that radiation would win since the radiation rate is proportional to α_s and the annihilation cross section scales like α_v^2. However to make a clear determination a more careful estimate is required.

Since annihilation rates are dominated by low l we only need to consider S-wave states. The S states $\eta_{\mathbf{1}}(nS)$, $\psi_{\mathbf{1}}(nS)$ can make $E1$ transitions to the P states: $\eta_{\mathbf{1}}(nS) \to h_{\mathbf{8}}((n-1)P)g$, $\psi_{\mathbf{1}}(nS) \to \chi_{J,\mathbf{8}}((n-1)P)g$ (the $M1$ transitions are negligible). Using (4.41) with $J = l = 0, J' = l' = 1$, we can write the width for $\eta_{\mathbf{1}}(nS) \to h_{\mathbf{8}}(P)g$

$$\Gamma = \frac{16}{3}\alpha_s \omega^3 |\mathcal{R}_{SP}|^2, \tag{4.48}$$

where $\mathcal{R}_{SP}$ is the overlap integral between S- and P-wave states. For those states produced near the point where the cross section for quirk pair production peaks, $E \sim M/4$, one has $\omega = \Delta E \sim \pi\sigma/M$. The overlap integral is given by (4.43) and is of the order of the quirkonium radius, $R_{SP} \sim 2E/3\sigma$. The probability for emitting a gluon per period is therefore estimated

as

$$P_{rad} = T\Gamma \simeq \frac{4\pi^3}{27}\alpha_s\beta \sim 2\alpha_s. \tag{4.49}$$

This can be compared with the probability of annihilating at low l's. For example, in the case of the $\eta_{\mathbf{1}}(nS)$ quirkonium annihilation goes dominantly to v-gluons i.e. v-glueballs, with a width given by (4.26). Using (A.33) the width can be rewritten as

$$\Gamma(\eta_{\mathbf{1}}(S)) \to g_v g_v) = \frac{2\alpha_v^2\,\sigma}{M} \tag{4.50}$$

where we have set $n_v = 3$. Following [49], the probability for S-wave annihilation per crossing at high velocities is

$$P_{ann} = 2T\Gamma \sim 4\beta\alpha_v^2 \sim 2\alpha_v^2 \tag{4.51}$$

where β is typically of order $1/2$.

We see that perturbative gluon emissions will typically dominate over hard annihilations for highly excited states. As the states approach the Coulombic regime, annihilation rates are expected to increase. However, the change in angular momentum due to the emission of these gluons (by $\Delta l \sim 10$ on average) will significantly reduce the probability to annihilate. Therefore, we expect that the quirkonium states to radiate most of their kinetic energy before they can pair annihilate into v-gluons or SM particles.

Calculation of color factors

The summation over colors must be done carefully because of the condition that the initial and final states can be in either color singlet or color octet states. We define a basis of color states $|ij\rangle$, where $i, j = 1, 2, 3$ denote the color indices of quirk and antiquirk, respectively. Then the singlet state is given by

$$|1\rangle = \frac{1}{\sqrt{N_c}}\sum_i |ii\rangle. \tag{4.52}$$

while the octet can be written as

$$|8; a\rangle = \sqrt{2}\sum_{ij} T^a_{ij}\,|ij\rangle, \tag{4.53}$$

where the color matrices are normalized in the usual way tr $T^aT^b = \delta_{ab}/2$. When the initial state is a singlet, and the final state and octet, the matrix element contains a color factor

$$\langle 8; a|T^b|1\rangle = \frac{\delta^{ab}}{\sqrt{2N_c}}, \tag{4.54}$$

where the color operator T^a acts on either the quirk or the antiquirk state only. Squaring the matrix element, summing over the final color of the emitted gluon and final octet gives

$$\sum_{ab} |\langle 8; a|T^b|1\rangle|^2 = \frac{N_c^2 - 1}{2N_c}. \tag{4.55}$$

The transitions in which the initial state is an octet can be computed analogously, with the addition that one also needs to average over initial color. This way we obtain the color factors in table 4.2.

4.5 Non-perturbative v-color interactions

Although the spectrum of heavy quirkonium systems can be adequately explained by nonrelativistic potential models, some of their decays concerning nonperturbative v-color interactions are difficult to deal with. Non-perturbative v-color transitions

$$\Psi_{\mathrm{I}} \to \Psi_{\mathrm{J}} + \Theta_{\kappa} \tag{4.56}$$

are an example of this kind. In (4.56), Ψ_{I}, Ψ_{J} and Θ_{κ} stand for the initial state quirkonium, final state quirkonium and emitted v-glueball, respectively. These v-glueball radiative transitions are important decay modes of heavy quirkonia. For instance, if the v-glueball decays into photons, one could use the photon signature to search for these states.

In the absence of light fundamentals, the v-color tube connecting heavy quirks cannot break. Instead, v-glueball formation in a pure Yang-Mills theory occurs heuristically through the crossing of the tube onto itself, a process qualitatively different from fragmentation in QCD (see figure 4.6). In order to make crisp predictions about detection signals coming from quirkonium decay, we therefore need to understand the process of glueball emission in pure Yang-Mills theory. In general this is a subtle problem whose solution is unknown, so for this case we limit ourselves to some qualitative discussion of the dynamics.

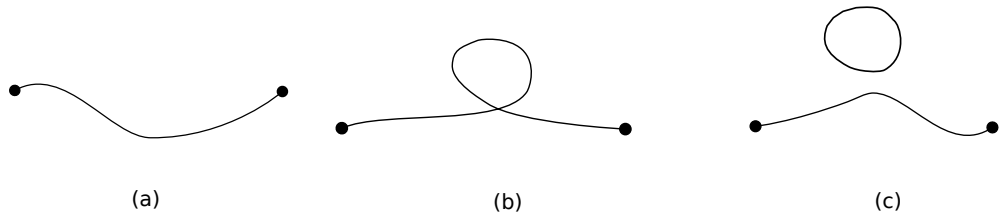

Figure 4.6: A depiction of a v-glueball emission process.

In the semiclassical limit, the momentum which the heavy quirk can exchange with the v-color flux tube is of the order Λ_v and the corresponding uncertainty in the energy of the heavy quirk is of the order Λ_v^2/M_X. No particle in the v-sector spectrum is light enough to be radiated in this energy. When the quirks are close to one another the semiclassical limit breaks down and v-glueball emission is possible.

Non-perturbative interactions of the quirks can convert some of the their kinetic energy into vibrational energy of the flux tube. If enough energy is pumped into the flux tube so as to

excite it to a high vibrational mode, self interactions of the flux tube may result in v-glueball emission (see figure 4.6). It follows that the rate for conversion of quirk kinetic energy into the v-glueball radiation should be proportional to the rate of energy delivered into flux tube vibrations.

We may thus consider the emission of v-glueballs as proceeding in two stages. The first stage is the excitation of vibrational modes of the flux tube by the non-perturbative v-color interactions, and the second stage is the actual radiation of a v-glueball by a vibrational excited flux tube. The rates of these processes are determined by the population of high vibrational levels of quirkonium. The non-perturbative v-color will only take place when the quirks come within a distance of order Λ_v^{-1}. Following [49], the typical energy transfer from the bound state can be estimated from

$$\Delta E \sim F\Delta r \sim \Lambda_v^2 \Lambda_v^{-1} \sim \Lambda_v. \tag{4.57}$$

The probability that the quirks are within a distance Λ_v^{-1} from each other is given by the fraction of time that the quirks are within a distance Λ_v^{-1},

$$\text{Prob}(r_{X\bar{X}} \lesssim \Lambda_v^{-1}) \sim \frac{\Lambda_v^{-1}/\beta}{T} \tag{4.58}$$

where β is the classical quirk velocity at the origin and we have used the fact that the Compton wavelength of the heavy quirk is much smaller than Λ_v^{-1}. If we assume as in [49] that the nonperturbative v-color interactions have a geometrical cross section, we can estimate its rate as

$$\Gamma \sim \frac{1}{T} \sim \frac{\sigma}{M\beta} \tag{4.59}$$

where T is the classical crossing time. Thus, we expect these interactions occur roughly once per classical crossing.

One may naively argue that in the case $\Lambda_v > \Lambda_{QCD}$ v-glueball emission is likely to dominate over radiation of perturbative gluons because of the strong coupling in the v-sector. However, emission of a v-glueball may be suppressed. First, we know from figure 2.1 that the mass of the lightest v-glueball is about 3.6 times heavier than the square root of the string tension. Therefore we can expect that there is some suppression for v-glueball emission, depending on how many transitions are needed to transfer an energy of order m_0 to the flux tube. Furthermore, in the large n_v limit, the v-glueball emission should be suppressed by a factor $\mathcal{O}(1/n_v^2)$, giving an order of magnitude suppression for $n_v = 3$. Combining this with (4.59) and including a phase space factor, we may obtain an upper bound for the rate for v-glueball emission as

$$\Gamma \lesssim \frac{1}{n_v^2}\frac{\sigma}{M\beta} \times \text{ Phase space} \tag{4.60}$$

Nonetheless, one should keep in mind the possibility that the actual rates for radiation of v-glueballs may differ substantially from the estimate (4.60).

4.6 Fragmentation Probabilities

While it is possible to work out quirkonium and v-glueball branching fractions for a given mediation model with the help of lattice data for $N = 3$, it is considerably more difficult to arrive at the full spectrum of visible standard model particles produced in a single quirkonium annihilation. The final state of visible standard model particles depends on the number and spectra of glueballs initially produced in the quirkonium decay. In order to make crisp predictions about indirect detection signals coming from quirkonium decay, we therefore need to understand the process of fragmentation in pure Yang-Mills theory. Unfortunately, this is a situation where neither phenomenological examples from QCD nor data from the lattice can be of help. In the absence of light fundamentals, the color tube connecting hard partons cannot break. Glueball formation in a pure Yang-Mills theory occurs heuristically through the crossing of the tube onto itself, a process qualitatively different from fragmentation in QCD.

One simple approach to estimating the relative abundances of different glueball species is a thermal model. In such a model, the ratio and yield of the multiplicity of glueballs is given by the partition function $\mathcal{Z}$. In a grand-canonical ensemble of glueballs of species i the partition function with chemical potential μ is given by

$$\mathcal{Z} \propto \sum_N \prod_i (2J_i + 1)\, m_i^{3/2}\, e^{-(n_i m_i - \mu n_i)/T} \tag{4.61}$$

where m_i, J_i and n_i are the mass, spin and multiplicity of a glueball of species i, respectively. The temperature T of the spectrum would be taken to be Λ_v. Unlike QCD, where this temperature is comparable to the masses of the pions, the corresponding temperature is much lower than the masses of the glueballs in pure Yang-Mills theories, so that if this is true, the excited v-glueballs are rarely produced. We may guess that, as in QCD, the effective temperature in hadronization models is comparable to the deconfinement phase transition, which is of order 180 MeV in QCD, about 1/10 the QCD glueball mass, but which is significantly higher, about 1/5 - 1/6 m_0 [], for a pure Yang-Mills theory. In particular, accounting for the fact that the spin-two states have a spin-multiplicity of 5, we would have production of the 0^{++} state at 50–60%, and of the 2^{++} state at around 30%, with 2–4% each for the 0^{-+}, 2^{-+} and 1^{+-} states. All other states would be produced at lower rates.

Nevertheless, we should keep in mind that the statistical quasi-thermal model is unlikely to be accurate. Formation of hadrons in QCD occurs through the local snapping of a flux tube

by light-quark pair production, a local effect on its world sheet. Formation of v-glueballs in a Yang-Mills theory occurs through the crossing of a flux tube onto itself, a non-local effect on the worldsheet that involves color rearrangement. The excitation of the flux tube created in the X-onium annihilation may therefore influence the production of v-glueballs, and greatly enhance the rate for the production of heavier v-glueball states, including ones which are unstable and decay immediately to multiple stable v-glueballs. In this scenario, the probability of producing the heavier stable v-glueballs, and perhaps the total number of v-glueballs per X-onium annihilation, could be much larger than estimated in the quasi-thermal model.

Strictly speaking, these estimates should be thought as a priori estimates for the relative abundances of v-glueballs in a given quirkonium annihilation. In general, the actual fragmentation probabilities will be further constrained by conservation of quantum numbers and/or kinematics and may be significantly different from the predictions obtained by naive application of the fragmentation thermal model. For example, because of conservation of charge conjugation the vector $\psi_{\mathbf{1}}$ can only annihilate to final states containing an odd number of C-odd v-glueballs. Also, the pseudoscalar $\eta_{\mathbf{1}}$ cannot annihilate to final states containing only two 0^{++} v-glueballs, because of parity and angular momentum conservation.

4.7 Numerical analysis

From the above discussion it is clear that the characteristic collider signatures of quirkonium are determined both by the final states that the quirks can annihilate into and by the nature of the energy loss during quirk de-excitation to the ground state. In what follows we calculate numerically the quirkonium spectrum, and evaluate the branching ratios for radiative transitions of quirkonium and for pair annihilation into various final states. To give a general survey of decays is beyond the scope of this work, since a more detailed treatment would have to incorporate precise values of the non-perturbative matrix elements for v-glueball emission which at present are unknown. However, a few examples are useful to illustrate the main qualitative features of quirkonium decay pattern.

4.7.1 Quirkonium spectrum

This section is concerned with the energy of a single quirk-antiquirk pair moving in a central potential and obeying nonrelativistic quantum mechanics. The main result is the evaluation of the energy eigenvalues. The Schrödinger equation is numerically integrated using the generalized Runge-Kutta algorithm described in [75].

In order to conduct an analysis of the phenomenology, we first need to have some information about the various scales in the model. The scale, $\Lambda_{\rm QCD}$, where $SU(3)_C$ gauge coupling blows up is around 250 MeV. The remaining parameter space consists of the mass scale M and the 0^{++} mass m_0. Here we present our results in terms of m_0 which is more transparent than the confining scale Λ_v, since m_0 is the relevant parameter for LHC studies. To simplify the discussion in the v-sector, it is convenient to assume that the 0^{++} mass is in the phenomenologically interesting range 25 GeV $\lesssim m_0 \lesssim$ 500 GeV where v-glueballs may decay visibly. Moreover, since the branching ratios depend on M and m_0 only through the combination M/m_0, our problem is reduced to a two-dimensional parameter space described by M and $\xi \equiv M/m_0$.

The mass scale M sets the value of the total production rate and defines the energy region where the majority of the quirks are produced. On the other hand, our focus here is on the main qualitative features of the quirkonium spectrum and decay pattern, which to a great extent are controlled by the single parameter ξ. Therefore it is convenient in this first attempt to fix the quirk mass and choose three representative values of M, 250 GeV, 500 GeV and 1000 GeV.

This scenario implies that three different regimes need to be distinguished: (i): Coulombic regime, $\bar{r}_{X\bar{X}} \ll \Lambda_v^{-1}$; (ii) intermediate linear regime, $\bar{r}_{X\bar{X}} \gg \Lambda_v^{-1}$ and $\bar{r}_{X\bar{X}} \ll \Lambda_{\rm QCD}^{-1}$; and (iii) and nonperturbative QCD linear regime, $\bar{r}_{X\bar{X}} \gg \Lambda_v^{-1}$ and $\bar{r}_{X\bar{X}} \gg \Lambda_{\rm QCD}^{-1}$ (We will not consider the regime for which $\bar{r}_{X\bar{X}} \ll \Lambda_v^{-1}$ and $r_{X\bar{X}} \gg \Lambda_{\rm QCD}^{-1}$, because our focus here is on the case $\Lambda_v \gg \Lambda_{QCD}$ where the v-glueballs can decay visibly). As explained above, there is a qualitative difference between (ii) and (iii): for $\bar{r}_{X\bar{X}} \ll \Lambda_{\rm QCD}^{-1}$, emitted $SU(3)_C$ gluons will be perturbative and will change the spin of the state by one unit. In this case, the width of the decay is proportional to α_s, and the transition can occur at any moment during the quirk oscillation. This implies that the quirkonium states can make a transition down to a lower excited state with $\Delta E \gg \Lambda_{\rm QCD}$. In contrast, for $\bar{r}_{X\bar{X}} \ll \Lambda_{\rm QCD}^{-1}$, non-perturbative QCD interactions are only efficient in damping the quirk oscillation only when the quirk separation is of the order or less than Λ_{QCD}^{-1}. This results in an energy of order Λ_{QCD} emitted in the form of light QCD hadrons about once during every crossing time.

The spectrum of quirkonium binding energies is amenable to an analytical description for both Coulombic and linear regimes, $\bar{r}_{X\bar{X}} \ll \Lambda_v$ and $\bar{r}_{X\bar{X}} \gg \Lambda_v$. Results for these regimes give good qualitative insight also for the crossover region of intermediate coupling constants $\alpha_v \sim 1$, where an analytical description becomes more cumbersome.

Now we want to argue that in the case of interest the Coulombic regime is in general unimportant. We plot numerical results for the quirkonium binding energies E_{nl} as a function of m_0 for three different values of the quirk mass, $M = 250, 500, 1000$ GeV. For simplicity,

only the S-wave $l = 0$ energies are shown. As shown in the figure 4.7 for very low m_0 many excited states tend to gather around the crossover region where Coulombic and linear potential are approximately of the same strength ($E \simeq 0$). However, in the energy interval of interest 50 GeV $\lesssim m_0 \lesssim$ 500 GeV there are only $\mathcal{O}(1)$ states in the Coulombic region.

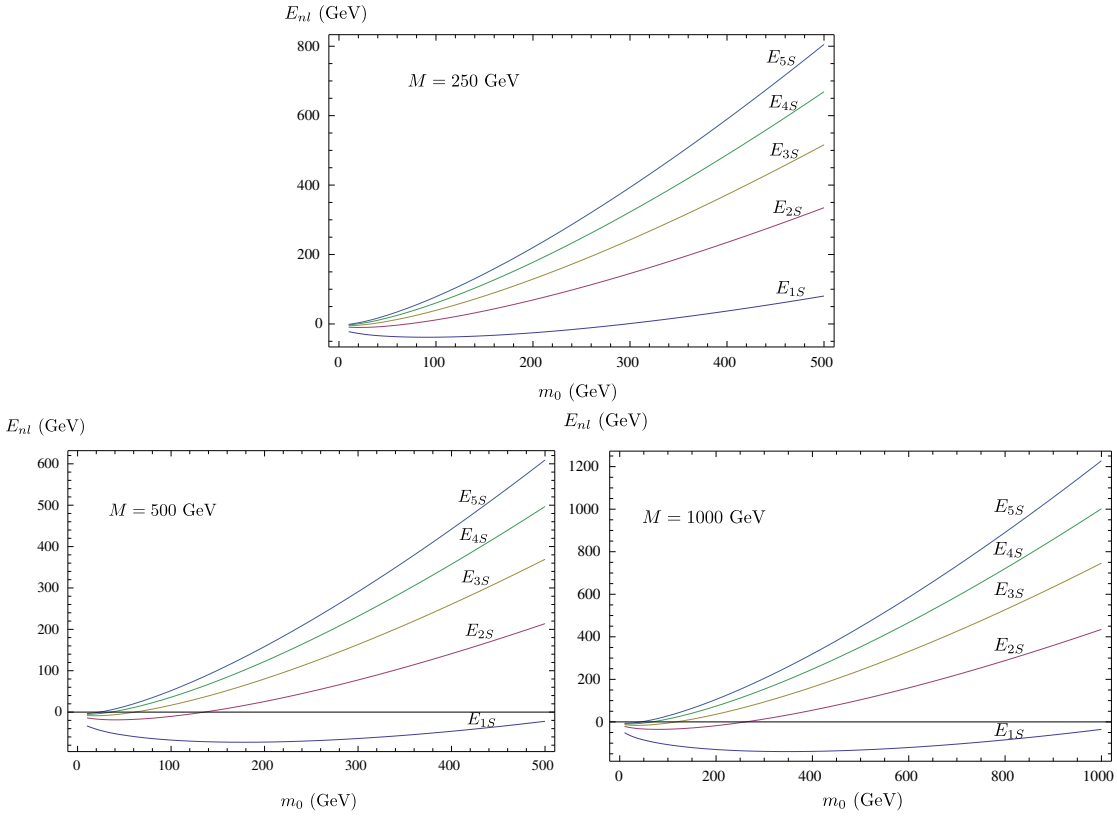

Figure 4.7: The binding energies of low-lying, S-wave color-singlet states in a quirkonium system as a function of the v-glueball mass m_0 for different values of M. For very small m_0, the levels gather around the crossover region between the linear and Coulombic parts of the nonrelativistic potential. However, as long as m_0 becomes larger than about 100 GeV only a few states remain in the Coulombic regime.

This result agrees to a very good approximation with a quasi-analytical result for the number of bound states in the Coulomb region. To see this, let us recall that the average radius of the bound states in a Coulomb potential is given by

$$\bar{r}_n = n^2 \, r_B \tag{4.62}$$

where $r_B = (\mu\alpha)^{-1}$ is the Bohr radius,n is principal quantum number; $\mu = M/2$ is the reduced mass of the quirk-antiquirk and α is the gauge coupling constant. From the Cornell potential (4.12) we can estimate the cross-over point as $r^2 \simeq \alpha/\sigma$. It follows that the number of states in the Coulombic region is approximately given by

$$n^2_{\text{Coulomb}} \sim 1.85 \, \alpha^{3/2} \, \frac{M}{m_0} \sim \frac{M}{m_0}, \tag{4.63}$$

where we have used $m_0 = 3.7\sqrt{\sigma}$ and $\alpha \simeq (4/3)(\alpha_s + \alpha_v) \approx 0.8$. Therefore, we arrive at the same conclusion as above that about one or two color-singlet states are in the Coulomb region in the range of parameter of interest.

Next, we show that regime (*iii*) only accounts for a relatively small fraction of the total cross section. In order to demonstrate this, we integrate (4.5) over the mass range corresponding to $\bar{r}_{X\bar{X}} > \Lambda_{\rm QCD}^{-1}$, namely $\sqrt{\hat{s}} - 2M > 1.5\,\sigma\,\Lambda_{\rm QCD}^{-1}$, where in the last inequality we have used (A.37) with $E = \sqrt{\hat{s}} - 2M$. The numerical results are shown in figure 4.8 as a function of m_0 for $M = 250, 500, 1000$ GeV. We see that for very low v-glueball masses the majority of the states will be produced in the non-perturbative QCD regime. This is indeed the regime considered by the authors of [49]. However, for the interval 100 GeV $< m_0 <$ 500 GeV, the states produced in regime (*iii*) only contribute less than about 20% to the total cross section.

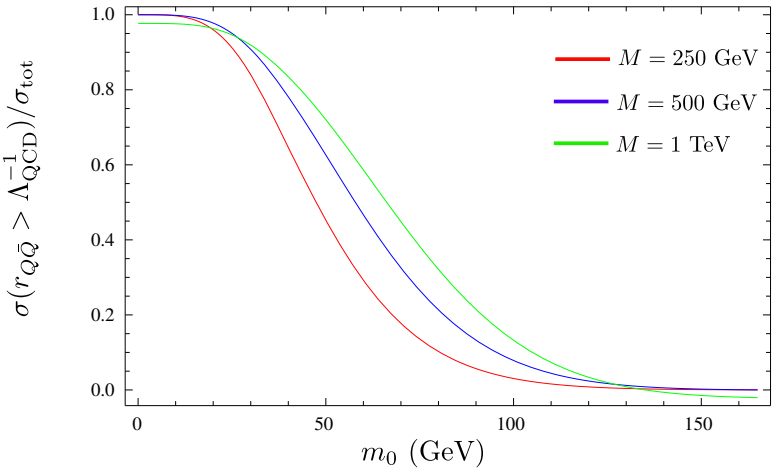

Figure 4.8: The fraction of bound states produced in the non-perturbative QCD regime as a function of m_0 for $M = 250, 500, 100$ GeV.

The results above allow us to restrict attention to regime (*ii*). In this case, crucial simplifications occur due to the fact that QCD interactions of the quirks are perturbative. This is because $r_{X\bar{X}} < \Lambda_{\rm QCD}^{-1}$ and the energy transfer ΔE associated with QCD processes involving quirks and $SU(3)_C$ gluons is greater than $\Lambda_{\rm QCD}$. Indeed, the mass splitting between quirkonium states for transitions with single gluon emission are such that $\Delta E \gg \Lambda_{\rm QCD}$ in the parameter range of interest. This is illustrated in figure 4.9 which shows contour lines of constant ΔE in the M-m_0 plane. In figure 4.9, ΔE is evaluated at the boundary between regime (*ii*) and (*iii*), i.e. for highly excited states such that $\bar{r}_{X\bar{X}} = \Lambda_{\rm QCD}^{-1}$. We see that for very small m_0, ΔE may be smaller than $\Lambda_{\rm QCD}$. However, as long as $m_0 \gtrsim 50$ GeV the energy splitting between two consecutive states becomes larger than $\Lambda_{\rm QCD}$, and QCD interactions, i.e. gluon emission are perturbative.

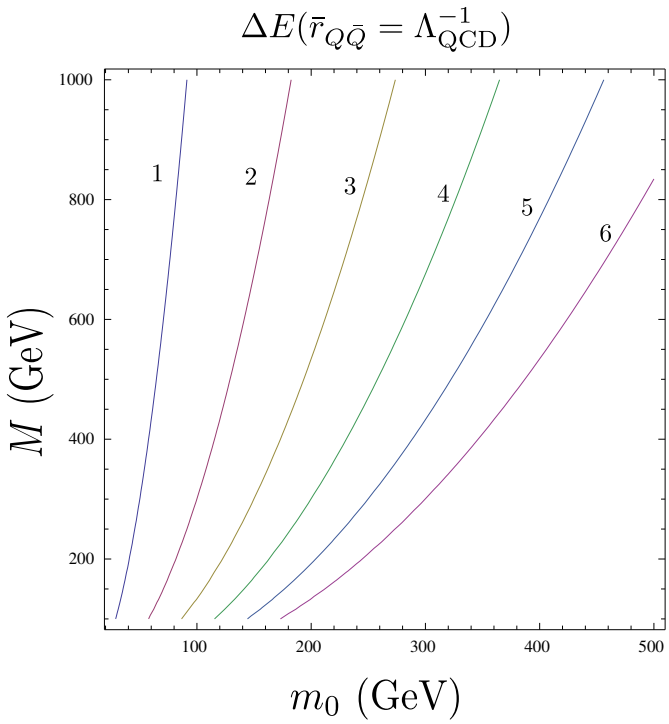

Figure 4.9: The energy splitting for highly excited states such that $\bar{r}_{X\bar{X}} = \Lambda_{\rm QCD}^{-1}$ as a function of M and m_0. The contour lines correspond to $\Delta E = 1, 2, 3, 4, 5$ and 6 GeV.

We are interested in the majority of the events, which produce quirks that are not close to threshold. The maximum of $\frac{d\sigma_{X\bar{X}}}{d\sqrt{\hat{s}}}$ occurs when the center-of-mass energy is approximately $15 - 25\%$ greater than the threshold value. At this energy, quirks will be produced with semi-relativistic energies $\beta \approx 0.3 - 0.5$ and maximal separation $L_{max} \sim E_{\rm max}/\sigma$, where $E_{\rm max} = \sqrt{\hat{s}} - 2M = M\beta^2$ is the initial kinetic energy in the quirk system upon production. The subsequent quirk evolution depends on the number of resonances that lie in the linear regime up to energies of order $E_{\rm max}$. A simple estimate shows that

$$n^2_{\rm linear} \sim \left(\frac{2}{3\pi}\right)^2 \frac{M}{\sigma^2} E^3_{\rm max}. \tag{4.64}$$

In table 4.3, we have collected estimates of $E_{\rm max}$, $L_{\rm max}$, β^2 and ΔE for different values of M are listed. For comparison, we include estimates for the number of radial excitations of the quirk string for the states in the Coulomb and linear part of the $X\bar{X}$ potential.

As we discussed in the last section, this creates an excited quirkonium that decays radiatively to the ground state and finally annihilates to hard decay products. Whether a significant fraction of E_{max} is lost to perturbative gluons, soft QCD hadrons or v-glueballs will depend on the distribution of quirkonium binding energies, in particular on how many of these levels are in the confining linear region, how many are in the Coulombic region and how closely spaced they are.

M(GeV)	$E_{\max}/m_0$	n^2_{Coulomb}	n_{linear}	β^2	$\Delta E/\sqrt{\sigma}$	$< r >_{\max} \sqrt{\sigma}$
250	0.5ξ	$.8\xi$	$1.03\xi^2$	.5	$1.20\xi^{-1}$	1.23ξ
500	0.4ξ	$.8\xi$	$0.73\xi^2$	.4	$1.34\xi^{-1}$	0.99ξ
1000	0.3ξ	$.8\xi$	$0.48\xi^2$	.3	$1.55\xi^{-1}$	0.74ξ

Table 4.3: Some quantities of interest evaluated around the point where the majority of the quirk pairs are produced at the LHC as a function of the parameter $\xi = M/m_0$ and for different quirk masses.

4.7.2 Decay patterns

Quirkonium phenomenology depends sensitively on the parameter $\xi = M/m_0$. Notice that radiative emission of v-glueballs may only be present providing $E_{\max} > m_0$. Also as long as $L_{\max}$ becomes of the order of or greater than 1 GeV, non-perturbative QCD interactions need to be taken into account. Therefore we can distinguish several very different cases.

1) $\mathbf{0.5 \lesssim \xi \lesssim 2.5}$: In this case, v-glueballs are too heavy to be produced during quirk relaxation. Instead, the quirk-antiquirk pair will lose energy by emitting a few perturbative gluons, eventually (unless kinematically forbidden) annihilating into at most two v-glueballs. Besides, only a few quirkonium resonances will be produced so the decay pattern turns out to be very simple. The simplicity of the spectrum is likely to be spoiled by mixing effects between the heavy v-glueballs and the quirkonia.

2) $\mathbf{\sqrt{M/3.7\Lambda_{QCD}} \lesssim \xi \lesssim 40}$: Here the states are very closely spaced in the spectrum. Upon production, the size of the highly excited quirkonium states will be larger than $\sim \Lambda^{-1}_{QCD}$ so non-perturbative QCD effects will be important. The relaxation process was already described in [49]. A significant fraction of colored quirk pairs will lose most of their kinetic energy because of interactions of the nonperturbative QCD and/or v-color interactions, until the typical radius of the states becomes smaller than about $\Lambda^{-1}_{\text{QCD}}$. Meanwhile, if QCD interactions dominate, an energy of order $.5M$ will be radiated as light QCD hadrons each with energy of order GeV (a hadronic fireball). If, on the contrary, v-color interactions dominate around $\mathcal{O}(10)$ v-glueballs will be radiated. The hard annihilation final states will contain several v-glueballs, but also some occasional SM quarks and gluons.

3) $\mathbf{2.5 \lesssim \xi \lesssim \sqrt{M/3.7\Lambda_{QCD}}}$: In this range, quirk kinetic energy is converted to several perturbative gluons and possibly a few v-glueballs. The quirk-antiquirk pair annihilates into v-glueballs, but also into two SM quarks and gluons.

The boundary of these regions is shown in figure 4.10. The shaded region is excluded by current experimental bounds on the mass of heavy colored particles.

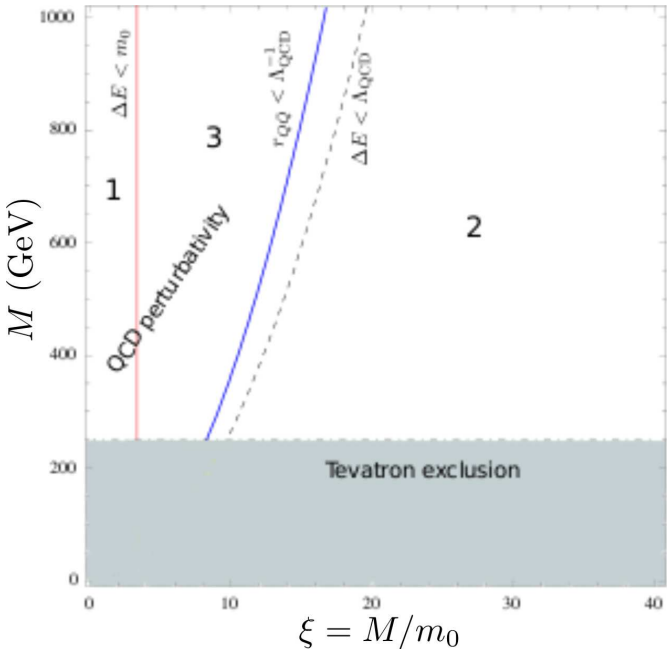

Figure 4.10: The different regimes described in section 4.7.2: 1) Most states will decay via emission of a hard perturbative gluon. Typical energies are insufficient to radiate a glueball. 2) Some moderately hard gluons and a few v-glueballs. 3) Non-perturbative QCD regime. Large number of soft hadrons and possibly many v-glueballs. The shaded region represents the exclusion region.

We present the decay branching ratios of the S-wave quirkonium in figure 4.11 as a function of the S-wave quirkonium binding energy for $M = 500$ GeV and $m_0 = 100$ GeV. For the gluon-radiative decay, we show the summed branching fraction over all the radiative decay modes. We then see that gluon-radiative decays are the dominant decay modes of highly-excited quirkonium states for $M = 500$ GeV and $m_0 = 100$ GeV.

We expect other regions in parameter space to have a similar behavior. This fact may be understood from the following argument. For a linear potential $V(r) = \sigma r$, the gluon-radiative width scales as

$$\Gamma(\eta_{\mathbf{1}}(S) \to h_{\mathbf{8}}(P)g) \sim \frac{m_0^{8/3}}{M^{5/3}}, \tag{4.65}$$

when the quirk and v-glueball masses are changed. The annihilation decay width scales as

$$\Gamma(\eta_{\mathbf{1}}(S) \to g_v g_v) \sim \frac{m_0^{10/3}}{M^{7/3}}. \tag{4.66}$$

We then see that the ratio

$$\frac{\Gamma(\eta_{\mathbf{1}}(S) \to h_{\mathbf{8}}(P)g)}{\Gamma(\eta_{\mathbf{1}}(S) \to g_v g_v)} \sim \left(\frac{M}{m_0}\right)^{2/3} \tag{4.67}$$

does not decrease as M increases. This is a direct verification of our expectations that annihilation decays are not significantly important until the quirkonium state has lost most of its kinetic energy to radiation of gluons. This argument implies the quirkonium states will likely

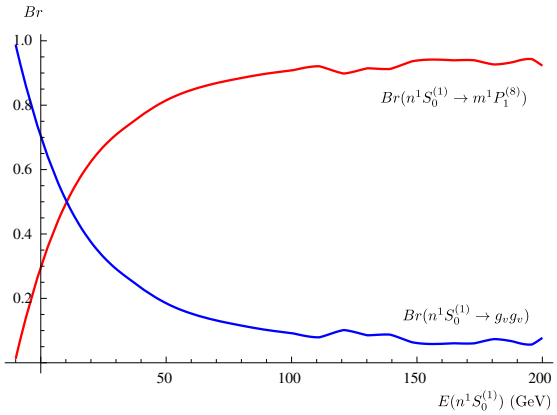

Figure 4.11: Simulated gluon-radiative decays vs. hard annihilations for the S-wave state of quirkonium as a function of the binding energy for $M = 500$ GeV and $m_0 = 100$ GeV. The curves show that gluon-radiative transitions are the dominant modes of highly-excited quirkonium, except for states produced sufficiently close to threshold. Small fluctuations are due to inherent uncertainties in the evaluation of the wave functions for highly excited states with large radial quantum numbers.

decay radiatively to a low lying state before annihilating (see figure 4.12). This is fortunate not only because the soft radiation may provide an interesting signal, but also because the hard annihilation will often occur near the invariant mass of the ground state, easing its identification independently.

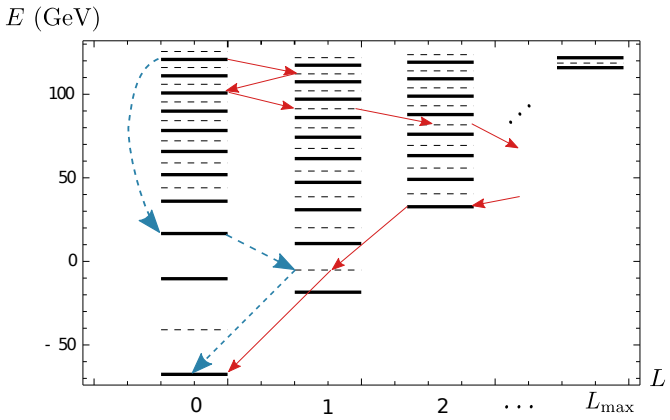

Figure 4.12: A typical cascade of decays in a quirkonium system. Full lines show a particular transition with multiple gluon emission when non-perturbative color interactions are not efficient. Dashed arrows are an example of a cascade decay with v-glueball emission, in which the initial quirkonium state relaxes quickly down to the ground state in a few steps.

Finally, we should discuss the possibility of losing energy by the emission of v-glueballs. In the case we are considering hidden glueballs may decay inside the detectors and therefore lead to an observable signal. In fact, one may naively argue that v-glueball emission is likely to dominate over radiation of perturbative gluons because of the strong coupling in the v-sector. However, as we pointed out in the last section, the probability for such an emission may be suppressed, because of a small hierarchy between the glueball mass and Λ_v. Using (4.59), we

can naively estimate that the rate of energy loss due to v-glueball emission per period as

$$P = 2T\Gamma \sim (2/n_v^2). \tag{4.68}$$

Given the theoretical uncertainties, and the absence of experimental evidence, the latter quantity is rather rough, but it may well be the only semi-quantitative estimates available for some time.

If the rate of v-glueball emission dominates over the radiation of gluons, the decay pattern is simple. This situation is illustrated in figure 4.12 by dashed arrows. The quirk and antiquirk quickly lose their kinetic energy by radiating one or a few v-glueballs, and the orbitals of the bound state shrink to a point where annihilation is very likely. During the last stages in the cascade decay, a few hard gluon jets can be emitted, before the hard annihilation takes place.

The lightest states in the spectrum require a special consideration. As an example, the low-lying spectrum of quirkonia with their transitions for $M = 500$ GeV and $m_0 = 100$ GeV is shown in figure 4.13. The pseudoscalar and vector states, $\eta_{\mathbf{8}}(1S)$ and $\psi_{\mathbf{8}}(1S)$, have the lowest mass within the color octet sector and are stable against decay by $E1$ transition. The only possible decays of these states are the hard annihilations and the $M1$ transitions to the lighter $\eta_{\mathbf{1}}(1S)$ and $\psi_{\mathbf{1}}(1S)$ color singlet states. We present the decay branching ratios of the

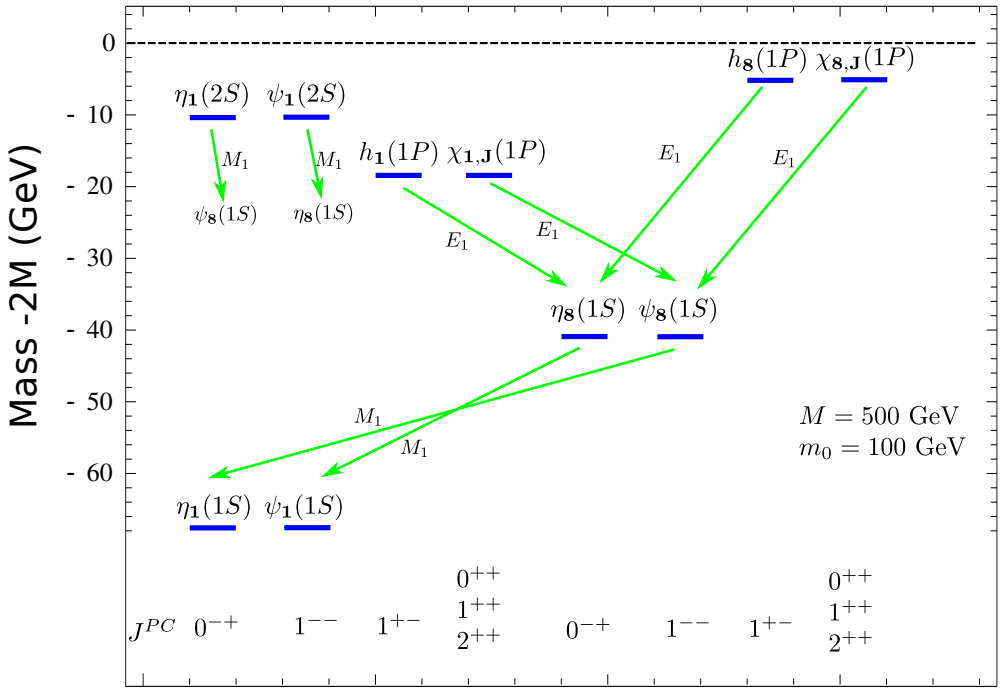

Figure 4.13: The low-lying quirkonium states, with selected transitions, for $M = 500$ GeV and $m_0 = 100$ GeV.

S-wave color-singlet $\eta_{\mathbf{1}}(1S)$ and $\psi_{\mathbf{1}}(1S)$ quirkonium, and the color-octet $\eta_{\mathbf{8}}(1S)$ and $\psi_{\mathbf{8}}(1S)$ in figure 4.14. In these plots we have set $n_v = 3$ and a v-glueball mass $m_0 = 100$ GeV. The

pseudoscalar state, $\eta_{\mathbf{1}}(1S)$, only decays into a pair of gauge bosons, as shown in the top left panel of figure 4.14. The dominant mode for $\eta_{\mathbf{1}}(1S)$ is $g_v g_v$, which is expected to be valid for $m_0 \gtrsim 100$ GeV. In this range it gives a visible decay, from v-glueballs decaying inside the detectors. The second largest mode is gg, followed by $\gamma\gamma$. On the other hand, $g_v g_v g_v$ modes is dominant in the decay of $\psi_{\mathbf{1}}(1S)$, up to quirk masses of order $M \sim 500$ GeV, followed by the decay into fermion-antifermion pairs. The branching fraction into $g_v g_v \gamma$ is small.

We also show the branching fractions of the color-octet states, $\eta_{\mathbf{1}}(1S)$ and $\psi_{\mathbf{1}}(1S)$, in the bottom panels of figure 4.14. The dominant mode for $\eta_{\mathbf{8}}(1S)$ is gg, followed by the M1 $g\psi_{\mathbf{8}}(1S)$ decay mode, which accounts for less than 10% of the total width. The color-octet vector state, $\psi_{\mathbf{8}}(1S)$, decays dominantly into SM quark pairs, via an off-shell gluon. The branching fraction for the M1 mode $\eta_{\mathbf{1}}(1S)g$ is about 15%, and the remaining modes (ggg, $gg\gamma$ and $g\gamma\gamma$) are suppressed by more than 10^{-3}.

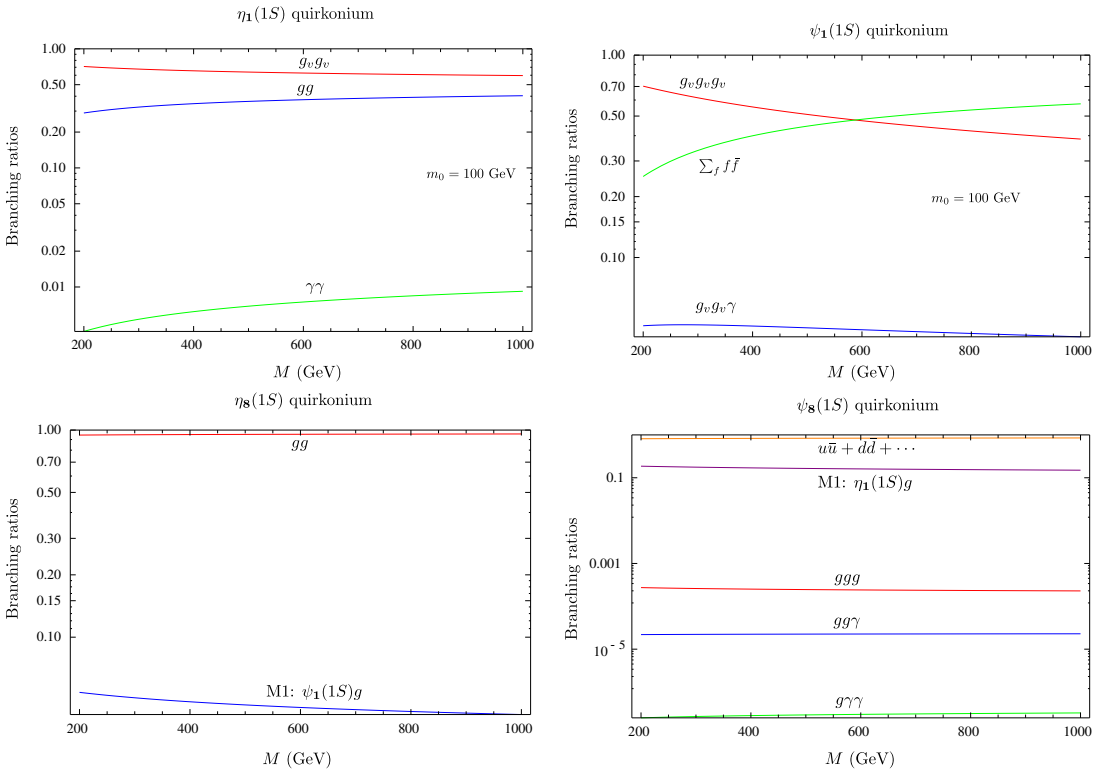

Figure 4.14: The branching fractions of the low lying states in the quikonium spectrum as a function of M for $m_0 = 100$ GeV and $n_v = 3$.

4.8 The case of uncolored quirks

In the class of theories we have studied in this thesis the collider phenomenology crucially depends on whether or not the quirks carry SM color. While up to this point in this chapter we

have focused on hidden valley models where the quirks are indeed charged under SM color, in general this need not be the case. One possibility is that the quirks are only charged under SM $SU(2) \times U(1)_Y$ gauge group, but neutral under $SU(3)_C$ gauge group. The spectrum of states in this theory is similar to that of the colored quirks, but with the crucial difference that the color-octet bound states are absent, and the non-relativistic potential is simply given by the v-color potential e.g. the Richardson potential, without the SM color term.

In addition to the modifications of the spectrum, the uncolored quirks will be produced at the LHC via weak interactions by either a Drell-Yan process or gauge boson fusion. As in the colored quirk case, they will be typically be semi relativistic upon production, with a velocity β^2 of order .5 or so. The radiation emitted during the decay from the highly excited to the ground state is, however, different from that of the colored quirk case. In the case of uncolored quirks the signal will consist of many unclustered soft to hard photons. The hard annihilation products depend on whether the quirkonium bound state are electrically charged. A neutral quirkonium state will typically decay to two hard v-glueballs, which depending on parameters may be long-lived. However, the dominant production of uncolored quirks will be an s-channel $W^{\pm}$ and thus the produced quirkonium is charged under SM electric charge. Its decay products will then always contain a charged particle and leave a visible signal in detectors. An interesting decay channel is $W^{\pm}\gamma$. Because the annihilation is expected to be at or near the ground state, a resonance peak is expected at the invariant mass of $W\gamma$. The details of the search for the hard annihilation of uncolored quirks were discussed in [13] for the case in which Λ_v is close to $\Lambda_{\rm QCD}$.

4.9 Collider searches

When the quirks finally annihilate, they are essentially at rest in their center of mass frame, so the annihilation products appear as a narrow resonance with mass $\sim 2M$. The dominant decay modes of the $\eta_{\mathbf{1}}$ are into v-glueballs, which in turn decay to SM gauge boson pairs. The dominant decay modes of the v-glueballs will be to two jets, which may be a difficult signal due to large backgrounds. The v-glueball decay to photons has a suppressed branching ratio, but offers a cleaner signal that may be easier to look for. The hard annihilation products from v-glueballs will provide the hard primary signal.

In the last section we argued that a significant fraction of the quirks kinetic energy may be lost by radiating soft QCD jets, v-glueballs or a combination thereof. if nonperturbative v-color interactions are inefficient, in most events much of it will appear as low-p_T hadrons or soft jets.

This energy could, in principle, significantly alter the appearance of the events and, importantly for our study, impact the photon isolation cut. If too much of this energy enters the isolation cone around the photon, then it either will reduce the signal substantially or will force the use of a looser isolation criterion. The latter will allow in more fake photons, potentially increasing the backgrounds significantly. The question is then, how serious a problem is this likely to be? Keeping the issue of photon isolation in mind we leave this question for future work.

Conversely, if nonperturbative v-color interactions are efficient, additional v-glueballs might be created either at the production stage (through radiation of hard v-gluons), or in radiation off of quirkonium states (which may be suppressed, since it requires the quirkonium states to make a large jump from a highly-excited state to a much less highly-excited state), Generally, if there are more than three v-glueballs, the rare decays to photons will be more common and easier to observe. However, the events may be more cluttered and the energy of the photons lower, leading potentially to lower detection efficiencies and larger backgrounds from fake photons. While high v-glueball multiplicity is unlikely here, simply due to the kinematics, events with several v-glueballs might be common which may aid to extract a signal from the background.

4.10 Summary

In this chapter, we have discussed various aspects of quirkonium physics. We have shown that the non-relativistic potential model inspired by heavy quarkonium physics allows one to obtain an overall picture of the distribution of binding energies in the quirkonium system. This potential may include both a Coulombic and a linear part for the v-color interactions and also both a Coulombic and a linear part for the QCD color interactions. We dedicated much effort to the regime where the majority of quirkonium states are produced, namely the linear regime of the v-color potential up to energies somewhat below the point where non-perturbative QCD effects set in.

The basic processes which allow excited quirks to deexcite through the bound state are gluon emission in which an $SU(3)_C$ gluon is radiated off between the states with $\Delta E \gg \Lambda_{\rm QCD}$ and v-glueball radiative emission with $\Delta E \gg \Lambda_v$. Gluon-radiative emissions necessarily change the color state of the quirkonium. Assuming $\bar{r}_{X\bar{X}} \gg \Lambda_v^{-1}$, v-glueballs may only be radiated once $\Delta E_{n,1} > m_0$. Because v-glueballs are non-perturbative, extended objects, their coupling to quirks is uncertain. Therefore we consider two different scenarios, one in which v-glueball emissions dominate, and another where v-glueball emissions are effectively absent. In the first case, excited quirkonium decays quickly by big transitions with $\Delta E \gg \Lambda_v$. Once the remaining

splittings are too small for v-glueball emission, then the states usually radiate SM-gluons and relax down to the ground state, where they annihilate. In the second case, $\sim 10 - 100$ gluons are expected to be radiated off the quirkonium states, before the quirk can annihilate, giving a high multiplicity of soft jets.

In both cases, the sensitivity depends strongly on the background and on the theoretical assumptions of the model. It would be interesting to combine all these efforts to invent intelligent strategies for determining the nature of hidden valley sector. The drawback of a model-independent framework is largely compensated by an extremely rich and exotic collider phenomenology.

Chapter 5
Hadron collider searches

In this chapter we will address the question of whether the signatures discussed in the previous chapters are likely to be detectable at the LHC. These questions are subtle because, as discussed in chapter 4, the dynamics of the production process are not calculable either analytically or numerically, and cannot be compared with any known physical process. A full analysis of the signal to background ratios is beyond the scope of the present study and will be considered in a future work. Our aim here is to point out generic signals which may not yet have been fully explored at the Tevatron or in studies for the LHC.

To discover a promptly decaying v-glueball, given the branching fractions computed in chapters 2 and 3, one should clearly make use of its decay to two photons, from which a resonance can be reconstructed. This motivates us to consider signals and backgrounds with 2 photons plus jets.

Late decaying v-glueballs are more complicated, since displaced jet pairs have no physics background but suffer from various detector and triggering issues, and detection of displaced photon pairs are subtle and very dependent upon details of the detector. There is little that a theorist can do to study these backgrounds, so for this case we limit ourselves to some discussion of the signal rates and of the most likely strategies for discovery.

5.1 V-glueball Production

Let us summarize the phenomenological possibilities and reemphasize the main points. Direct resonant production of a single v-glueball, for example through $gg \to \Theta$, is extremely small, suffering an $(m_0/M)^8$ suppression. Instead, production of v-glueballs occurs as a byproduct of the production of quirks, X and $\bar{X}$, as follows (see figure 5.1).

- An $X\bar{X}$ pair is produced in a gg or $q\bar{q}$ collision, possibly along with a hard v-gluon or SM gauge boson.
- The $X\bar{X}$ pair is bound by v-color interactions into a bound state of quirkonium.

- The quirkonium state decays gradually down toward its ground state, eventually annihilating.
- The annihilation is into SM gauge bosons, fermion pairs, or into v-gluons; at long-distance the latter become two or more v-glueballs.

Much of this process is difficult to model. An attempt to address the dynamics of the quirkonium state was made in chapter 4.

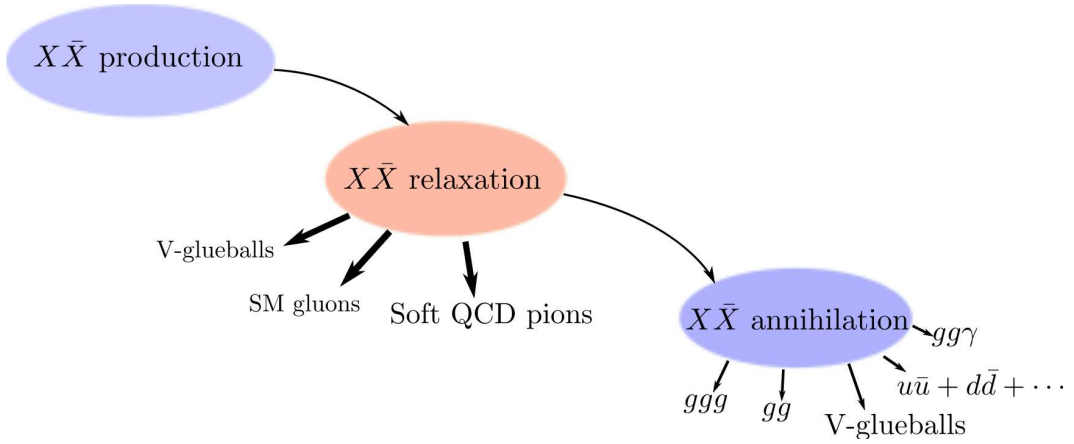

Figure 5.1: Depiction of quirkonium production and decay.

An estimate of the total rate can be obtained, conservatively, by treating the quirks as unaffected by the dynamics of the v-sector. The quirkonium resonances introduce large fluctuations of the cross-section as a function of $\sqrt{\hat{s}}$, and these ought to be convolved with the parton distribution functions. However, as long as the resonances are closely spaced well above threshold, averaging over them is a reasonable approximation for an estimate of an overall rate.

Given the high level of uncertainty in the fraction of excitation energy that is lost to v-glueballs, a full computation of the relaxation process is subtle and beyond the scope of the present work. A more sensible approach would be to consider two phenomenologically different cases: case (i) in which v-glueball emission is highly suppressed and all of the energy is emitted in SM gluons ($\Delta E_{n,n-1} > 1$ GeV), or pions ($\Delta E_{n,n-1} < 1$ GeV), and case (ii) in which most of the energy is lost to v-glueballs until $\Delta E_{n,1} < m_0$ and the rest is lost to relatively hard SM gluons.

5.2 Tevatron results and existing experimental bounds

At the Tevatron, color-singlet quirks could be pair produced through an off-shell photon, Z, or W. If the quirks are colored, their pair production through an off-shell gluon is also possible.

To a great extent, the production rate is only dependent on the gauge couplings of the quirks and so is fixed by their standard model quantum numbers. In the case of colored quirks, the annihilation of neutral quirkonium is most often into v-gluons, which at long-distance become two or more v-glueballs. As explained in section 3, the v-glueballs can then decay via a loop of quirks, producing photons, gluons, bottom quarks, and so forth. As will be seen in section 5, v-glueball decays typically result in an observable signal, providing $\Lambda_v \gtrsim 1$ GeV. For color-singlet quirks that are produced via an off-shell photon or Z, the primary annihilation channel is also to v-glueballs, which can decay back to SM particles. However, the dominant cross-section for production of color-singlet quirks is through an off-shell W boson [13]. The resulting $X^+\bar{X}^0$ bound state is electrically charged and cannot annihilate into v-glueballs alone[1]. Instead, it may annihilate to leptons or quarks via an off-shell W, to $W\gamma$ or WZ, or to Wg_vg_v, that is W plus some v-glueballs. Other contributions to the final states arise from the v-glueballs radiated during the quirkonium relaxation [6, 13, 49]. These might help increase the discovery reach and deserve further investigation which we leave for future work.

The $W\gamma$ process might allow quirkonium to be discovered directly. Events with a photon, lepton and missing energy ($l + \gamma + \not{E}_T$) would reveal a quirkonium resonance in the transverse mass distribution above the $W\gamma$ background. On the other hand, when the v-glueballs decay, they may produce spectacular collider signals, such as $p\bar{p} \to X\bar{X} \to \gamma\gamma\gamma\gamma, \gamma\gamma\tau^+\tau^-$. The 4γ channel, in particular, is very clean, since it is essentially background free, and would reveal the v-glueballs, if the rate is large enough to be detected.

There have not been specific searches for quirks as yet. Present limits are in general very mild because the cross-section for production of quirks at the Tevatron becomes very small once the quirk masses are larger than ~ 250 GeV and because not all the collected data has been analyzed yet. Below we present bounds on the masses of the quirks from CDF searches for new physics in $l + \gamma + \not{E}_T$ events and in searches for anomalous production of two photons and at least one more energetic, isolated and well-identified object (τ lepton or γ). This analysis by no means is exhaustive, but is meant to illustrate potential discovery signals and the bounds that can arise.

Our estimates below are based on the following assumptions. First, we determine the rate for production of quirks through perturbative computations; the cross-section $\sigma_{X\bar{X}}$ is estimated as a function of the mass M_X and for $n_v = 2$, both for the cases of colored and uncolored particles. Second, motivated by a thermal model of fragmentation [40], we have estimated the relative

[1]One can show that the splitting between X^+ and X^0 is so small that X^+ is stable against decay to X^0 on the time scales of interest; for example, see [13].

probability of producing any v-glueball in quirkonium annihilations assuming production of the 0^{++} at $50-60\%$, and that of the 2^{++}, 0^{-+} and 2^{-+} totaling $40-50\%$ in all. Finally, for the purpose of obtaining an approximate bound we assume a 100% efficiency for detecting v-glueballs. The last two assumptions are unlikely to be accurate, as we will discuss more thoroughly in our LHC study, but they are intended to give a rough estimate for the bounds.

(i) $l+\gamma+\not{E}_T$: The CDF collaboration has searched for the anomalous production of events containing a high-transverse momentum charged lepton and photon, accompanied by missing transverse energy [52]. Using 929pb^{-1} of CDF Run II data, these searches exclude X masses below 200 GeV for color-singlet X particles and 250 GeV for colored quirks, under the assumption that the quirkonium has lost most of its energy by radiation of photons and/or v-glueballs and the annihilation takes place at or near the ground state.

(ii) $2\gamma+\gamma$ and $2\gamma+\tau$: The CDF collaboration has also searched for the inclusive production of diphoton events [53]. Using $1155\,\text{pb}^{-1}$ of integrated luminosity, the diphoton plus third photon search places lower limits on the X mass below 200 GeV for color-singlet quirks and $y\sim 0$. The corresponding limit on the X mass for colored quirks turns out to be less severe, roughly below 150 GeV, because, in this case, the branching fraction to photons is $\lesssim 0.35\%$. If quirks couple to the SM Higgs boson additional constraints arise because of the 0^{++} branching ratio to tau leptons $\sim 10\%$. Using $2014\,\text{pb}^{-1}$, the diphoton plus tau search places lower limits on the X mass for $y\sim 1$ below 250 GeV for color-singlet quirks and 175 GeV for colored particles.

Some comments are in order. The mass bounds from potential v-glueball signals are necessarily model dependent. Unfortunately, unlike our computations of the branching ratios, there is no way to make a reliable estimate of the probability for producing any given v-glueball state in quirkonium annihilation, since phenomenological input from QCD is not relevant to the pure-glue case. V-glueballs could be created during the relaxation of quirkonia, and during their annihilation, so events with more than two v-glueballs might be common. Generally, with more than two v-glueballs produced in each quirkonium annihilation, events with multiple photons would be common and easier to observe. However, the events may be more cluttered and the energy of the photons lower, leading potentially to lower detection efficiencies. Since we cannot model this reliably, in the simple analysis of this paper, we will rely on the model independent bounds from the production of quirkonium through s-channel $W^{\pm}$ outlined above.

Moreover, the bounds from the $W+$ photon final state assume that the quirkonium state decays to its ground state before annihilating. However, it has been argued in [49] that the annihilation may often occur at higher energy, before the ground state is reached. With many

quirkonium states annihilating at different energies, the signal in the transverse mass distribution will be diluted. Besides, annihilation to two fermions via an off-shell W or to $W+$ v-glueballs becomes increasingly significant at higher energies. While the branching ratios to $W\gamma/Z$, $f\bar{f}$ and $W+$v-glueballs can be estimated, the wide range of quirkonium states and the uncertain annihilation probability as a function of the energy make any precise evaluation almost impossible. Therefore, the Tevatron limits are in fact weaker than suggested above.

In passing, we note that the bounds on a fourth generation of particles from Higgs searches at the Tevatron do not apply to heavy fermions that get only part of their mass from electroweak symmetry breaking, such as the quirks in our work. For an additional pair of fermions that get most of their mass from electroweak symmetry breaking, the Higgs production cross-section $\sigma_{gg\to H}$ is known to increase by a factor of roughly 9, making a dramatic effect on Higgs physics [55]. This allowed CDF and D0 to rule out fourth generation quarks for a Higgs mass in the window 145 GeV $< m_H <$ 185 GeV. However, for heavy particles that get only part of their mass by electroweak symmetry breaking, their contribution to the cross-section $\sigma_{gg\to H}$ decreases and the bounds are generally much weaker or absent.

Before moving on to the discussion of electroweak precision constraints we should briefly comment on the possibility of producing v-glueballs in Higgs decays. Up to now we have considered the production of v-glueballs as a by-product of quirkonium annihilation and relaxation. However, there is another possibility for this production to occur. For sufficiently small v-glueball masses, the interaction (3.2) can also mediate processes such as $h \to \Theta_\kappa\Theta_\kappa$ and $h \to \Theta_\kappa\Theta_\kappa\Theta_\kappa$. Assuming only minor phase space suppression, the branching ratio to v-glueballs for a SM Higgs below 140 GeV and $n_v = 2-4$ is of order $(\alpha_v y^2 v_h^2 m_h/3\pi M^2 m_b)^2 \sim 10^{-3} - 10^{-2}$. This implies a cross-section for producing v-glueballs at the Tevatron of order a few fb. Even though the cross-section is small, when combined with quirkonium annihilations, the production of v-glueballs in Higgs decays may be useful in the low mass range $m_0 \simeq 1 - 70$ GeV. The produced v-glueballs can then decay to a wide variety of final states, including b quarks, τ leptons, and multiple photons, among others; for small v-glueball masses, a significant fraction of these decays may occur with displaced vertices. At the Tevatron, there may be potential to observe a few events in the $b\bar{b}\tau^+\tau^-$ or $b\bar{b}b\bar{b}$ channels, although with limited statistics. In the case of displaced vertices, the D0 collaboration has searched for pair production of neutral long-lived particles decaying to a $b\bar{b}$ pair, and found no significant excess above the background [56]. This search could only exclude branching fractions of order 1, so that in our case it does not imply any bounds. At the LHC, the background problem is more severe, but with a larger cross-section and a larger integrated luminosity than at the Tevatron, the observation of a few v-glueball events may

also be possible. Depending on kinematics, the case of photons that originate away from the primary interaction point may also play an interesting role. A search for displaced photons has been done at D0 [57], and may be possible at ATLAS, due to the longitudinal structure of the electromagnetic calorimeter (ECAL). Besides, CDF and CMS allow the identification of delayed photons from long-lived particles using ECAL timing information (see [54] for results obtained using the CDF detector). The question then is whether at a branching ratio $\sim 10^{-3} - 10^{-2}$ the LHC will have some sensitivity. Keeping these non-standard Higgs decays in mind we leave the analysis of the discovery reach for future work.

5.3 LHC searches for prompt v-glueballs

5.3.1 Colored quirks

A priori, the most spectacular signal is from high p_T photons from the v-glueball decays, which typically have p_T of order 100 GeV or more. The search strategy would be to detect at least two photons and reconstruct their invariant mass.

Given the high p_T of the photons and the simplicity of the measurement, detection could be possible, but challenging. The effects of parton showering, hadronization, initial and final state radiation, and the underlying event impact this measurement in reducing the efficiency for photon detection through the failure of a photon isolation criterion. We should impose a rather simple photon isolation cut, demanding any photon be isolated from any gluon from the second v-glueball decay, to account for the largest effect. Some small efficiency loss should be expected mainly due to ISR and FSR jets, to the underlying event, and to particles emitted in quirkonium relaxation, such as discussed in [13, 49, 50].

To study the signal, we have to choose a fragmentation model; in the last chapter we described a simple way to compute the fragmentation probabilities in the case they are described by a thermal model. Then we allow the v-glueballs to decay according to the branching fractions given in chapters 2 and 3. An important point to note is that only the color singlet states, $\eta_{\mathbf{1}}$ and $\psi_{\mathbf{1}}$, are expected to annihilate significantly into v-glueballs, and only a fraction of the decays will produce the $0^{\pm+}$ and $2^{\pm+}$ states. The color octet states, $\eta_{\mathbf{8}}$ and $\psi_{\mathbf{8}}$, will decay mostly to gg or g^*, but the backgrounds will be larger in this case. Therefore, even if a small fraction of events leads to final states with the $0^{\pm+}$ and $2^{\pm+}$ states, the diphoton decay mode might still be the cleanest signature.

Since the signal photons are very high-p_T, we believe (based on conversations with LHC experimental experts, and on the fact that fake and real photons play a comparable role in the

lower-p_T light-Higgs search) that the contribution to the background from fake photons is probably comparable to or smaller than the real-photon background. The real-photon background arise from production of two photons plus two quarks or gluons. In the case that M/m_0 is very large, the two gluons from a v-glueball decay will merge into a single very-high-p_T jet, so we also should consider backgrounds from two photons plus one higher-p_T quark or gluon.

Since we will be relying on very crude estimates, in a first attempt signal and background can be both computed at leading order. Next-to-leading-order corrections are likely to increase both signal and background by a comparable amount. Since we do not count the number of jets or impose a jet veto, initial and final state radiation should not significantly change the acceptance or efficiency. The extra radiation and the underlying event will slightly reduce our photon isolation efficiency.

The abundance of radiative decays also leads to new signatures, which might not not be the discovery modes, but which will nevertheless be of great interest, and should be studied further if any excess of multi-photon events or two photon plus Z events are observed at the LHC. First, there is the possibility of three-photon resonances in the decays such as $1^{+-} \to \gamma 0^{++}$ followed by $0^{++} \to \gamma\gamma$. Of course the branching fraction of this process may be low, but the signal has very low background, so a few events may suffice. Other $+-$ and $--$ states may also have radiative decays, giving three-photon resonances. These states may also decay to γgg, which may provide a third photon in events where some other v-glueball decays to $\gamma\gamma$; again this may help separate the signal from backgrounds. Second, there is the possibility of double-radiative decays such as $3^{++} \to 1^{-+}\gamma$ followed by $1^{-+} \to \gamma 0^{++}$. Even if the 0^{++} state decays to jets, one expects an edge in the two photon invariant mass, and rare three- and four-photon events will show additional kinematic structure. Radiative decays of v-glueballs to Z bosons may not always be kinematically allowed, and even when present, the small branching fraction to dileptons makes leptonic Z's relatively rare compared to photons. Nevertheless, they should clearly be included in this search, since $\ell^+\ell^-\gamma\gamma$ events with jets are rare, and since kinematic features in this channel would not only help identify the signal but would constrain the effective action generating the radiative decay.

5.3.2 Uncolored quirks

Uncolored quirks are produced with much lower rates, and colored quirks will dominate over uncolored ones unless the mass of the colored quirks is of order 3 times larger than that of the uncolored ones. In this case, decays to gluons are no longer dominant, as we showed in

the section 3.4.3. The lower rates for quirkonium production are somewhat compensated by the higher rate for two and even four photons. Also, the v-glueball lifetimes are longer. Since $m_0 < M$, the regime for m_0 in which all v-glueballs decay promptly is much reduced.

Annihilation to W plus one or more v-glueballs will consume a substantial fraction of the quirkonium states. This in turn can lead to final states with two photons plus jets, or to events with two photons, a lepton, missing transverse momentum, and possibly jets. Although it is plausible that this channel will be sufficient for a discovery, the probability of four-photon events is not negligible. For heavier v-glueballs ($m_0 > 160$ GeV) these make up of order 4 percent or more of v-glueball-pair final states, while for light v-glueballs ($m_0 < 160$ GeV) they will make up as many as 60 percent, enough that a simple counting of 3- and 4-photon events may reveal a signal without kinematic constraints. (However in this case the photons may also be highly displaced, undermining kinematic reconstruction; we will comment on this in more detail below.) If the decays are prompt, a four-photon signal from a two-glueball final state would be fully reconstructable with high resolution, and the spectrum of quirkonium would be identified much more clearly and precisely than in the $W\gamma$ final states from charged quirkonium.

More precisely, the ratio of charged quirkonium prodution to neutral quirkonium production is about 4. Even if the branching fraction of charged quirkonium annihilation to $W\gamma$ is 1/3 (the other 2/3 going to WZ), the branching fraction of the W to an electron or muon is 2/9, and measurement of a structure in transverse mass requires more than a few events. Meanwhile, the probability of neutral pseudoscalar quirkonium production to produce v-glueballs is about 70%. Thus the four-photon signal, with a tiny background and a spectacular signature, is likely to be at least 15 percent as large as the $W\gamma$ signal, and possibly larger. Geometrical acceptance will reduce the four photon signal, but its special nature still probably makes it the best target for a search — assuming the v-glueballs are long-lived enough to decay within the detector. If the v-glueballs decay invisibly, the $W\gamma$ signal reemerges as the ideal approach. And if the decays are displaced, other issues arise, to which we now turn.

5.4 Signal and Background for Displaced Decays

Despite a long history of theoreticians predicting the possibility of new long-lived particles at the Tevatron or LHC, displaced vertices from new particles are often treated as unlikely exotica to be searched for when all else has failed. Few Tevatron studies of displaced particle decays have been performed until very recently, and few LHC studies were performed until this past year. No Tevatron triggers are optimized for signatures of displaced vertices, and until recently

there was no discussion of adding trigger pathways at the LHC. Specialized tracking algorithms could only be applied at the Tevatron through full reconstruction of very large event samples. Recently this has changed [94–96].

Of course if m_0 is small, there are a variety of states to consider, with a wide variety of lifetimes. Only one of these need be both long-lived and regularly produced to provide a strong signature for new physics.

New long-lived particles, though they have no standard model backgrounds, pose special challenges at the Tevatron and the LHC. The ATLAS and CMS detectors were not designed to detect displaced vertices beyond the beampipe; indeed, they are designed with so much material that they create displaced vertices from secondary pion-detector interactions at a distressingly large rate. Even CDF and D0, with less material, have very substantial detector backgrounds from secondary vertices.

The LHCb detector may have an interesting role to play if there are new particles with displaced vertices in the 1 to 100 cm range [7]. It has a material-free region extending out to tens of centimeters, somewhat compensating for the small angular acceptance of the detector. However, it can only handle an instantaneous luminosity of $3 \times 10^{32}\text{cm}^{-2}\text{s}^{-1}$, a tenth of the moderate-luminosity running expected in the early years of the LHC. Even the colored quirkonium production process is typically too small, unless $M \ll 1$ TeV, to contribute many v-glueballs into the LHCb detector.

In models with a single new metastable resonance (such as the next-to-lightest supersymmetric particle in gauge-mediated models) it is somewhat fine-tuned for this single long-lived state to have a lifetime between picoseconds and microseconds, so that it has a reasonable chance of decaying with a displaced vertex inside the detector. However, in many hidden valley models, there are multiple metastable states, making this possibility much less fine-tuned. In our current case, there are numerous v-glueball states with quite different lifetimes, and at least one is long-lived in a wide range of the parameter space. The v-glueballs decay to a wide variety of final states, all of which might appear at displaced vertices. These include

- jet pairs (from gg, or from ZZ with one Z decaying to neutrinos)
- jet quartets (from WW or ZZ),
- photon pairs,
- lepton pairs ($\mu^+\mu^-, e^+e^-, \mu^\pm e^\mp$) (from ZZ with one Z decaying to neutrinos, or from WW leptonic decays),

- jets and photons (from radiative decays such as γgg or $Z\gamma\gamma$)
- leptons and photons (from γWW, γZZ, $Z\gamma\gamma$)
- jets and leptons (from Zgg, WW, ZZ)

Here we view taus as either jets or leptons, since their displacement is far more striking than their identity.

All of these signatures are easy in principle — there are no standard model backgrounds — but all are challenging in practise, with the possible exception of displaced muon pairs. For this reason, along with the various possible arrangements of branching fractions, it is by no means obvious which of the various final states is best for an analysis. Moreover the optimal choices are likely to vary from detector to detector. We limit ourselves, therefore, to comments that may be useful to an experimentalist considering this type of signature.

If only colorless quirks are light and $m_\Theta < 2m_W$, then, as we saw in chapter 2 and chapter 3, decays to $\gamma\gamma$ will dominate. Four-photon events are sufficiently striking that discovery with few events may not require observation of displacement; whether and how to measure the long lifetime is a subtle issue we will discuss further below. For $m_\Theta > 2m_W, 2m_Z$ the WW and ZZ signals come into play. There are several possible strategies. The first would be to select events with two photons and look for displaced jets from WW or ZZ; nearly half of the quirkonium annihilations would be of this type. But displaced jet pairs have large backgrounds, depending on the precise kinematics, from secondary interactions (hard hadrons striking the beampipe, detector material, or even air molecules), which will be all too common at the LHC detectors. A second approach would be to select events with two hard (possibly non-isolated) leptons and see if they reconstruct a displaced Z boson, possibly with additional tracks (from the second Z emerging from the same vertex.) The rate for this process could be of order 2.5% per glueball, or 5% per quirkonium annihilation. This signal is technically easier, much cleaner, and has much lower background, so it might be an earlier priority and perhaps is better overall than the displaced-jet signature. One could also drop the mass constraint and look merely for two leptons from WW, with a large opening angle and invariant mass larger than the Z, that reconstruct a vertex.

If the colored quirks are sufficiently light compared to their colorless partners, jet pairs will dominate. The first non-pure-jet signals by branching fraction are di-photon and lepton-plus-jets (from WW). For di-photon signals, the displacement hurts twice; it is hard to detect the displacement, unless it is quite substantial, and it will also degrade the di-photon mass resolution since the reconstructed photon three-momenta will be incorrect. Meanwhile it is far

from obvious that a vertex with two jets and a lepton is much easier to reconstruct than a vertex with two jets alone. The first ultra-clean signature is again e^+e^- or $\mu^+\mu^-$ (plus two neutrinos) from WW or ZZ. Unfortunately the branching fraction is now quite small, approximately 0.06 percent of all v-glueball decays, and thus perhaps 0.12 percent of all quirkonium annihilations. Moreover, this signal is only present for those v-glueballs with mass well above $2m_Z$. Thus one may try to find displaced Z bosons, but one must also be prepared to observe displaced jets or photons.

An event with two pairs of displaced jets may not even pass jet triggers in some cases. New trigger strategies for events in which one of the v-glueballs decays in the calorimeters or muon system are under development [94, 95] but their effectiveness and practicality are not yet demonstrated. Moreover, this strategy is only useful if one of the v-glueballs serves as a trigger, in which case it is unlikely to be reconstructable, and at least one other v-glueball has decayed sufficiently early in the tracker that its tracks can be reconstructed convincingly. Even then, there will be backgrounds from secondary interactions.

Fortunately, the reasonable rate for photon pairs will ensure some fraction of quirkonium events are captured. An interesting strategy, therefore, will be to take two-photon-plus-jets events and search for a displaced vertex involving pairs of jets. (One should also remember that the jets might merge, if M/m_0 is large enough, so vertices involving single high-p_T jets must also be considered.) An intermediate step would be to detect the presence of a high-p_T jet with no normal tracks, for which outside-in tracking and calorimetry information might detect charged tracks entering at unusual angles.

Eventually, one would hope to maximize the ability to detect displaced jets, especially ones with high p_T. For instance, if $m \sim 1.5$ TeV and $m_0 \sim 300$ GeV, then the number of quirkonium events may be quite small. In this case the diphoton events will be very few. The jets, meanwhile, will have p_T above 500 GeV. Thus one might also consider looking at the tracking in events with three or four jets at high p_T. Such high-p_T jets in QCD events will unfortunately have a high hadron multiplicity and a corresponding high probability of high-energy secondary interactions [96]. However, the signal will have special characteristics unlike most QCD events: no hard primary tracks near the secondary vertex; two or more such secondary vertices; a possible large opening angle at the vertex. One would hope that such a signal could be extracted from the background of secondary interactions, but this requires a detailed study, and probably some actual LHC data, as opposed to mere simulation.

Chapter 6
Conclusion and open problems

We discussed the importance and relevance of hidden valley models in the realm of Beyond the Standard Model physics. To ensure that such physics does not go undiscovered requires precise understanding of how new physics will reveal itself in the current and future generation of particle-physics experiments. This thesis discussed various aspects of collider phenomenology in the quirk and hidden valley scenario, and its implications for undergoing experiments at the LHC.

We considered a hidden valley that at low energy is a pure-Yang-Mills theory, a theory that has numerous metastable v-glueballs built from the hidden valley gluons. A v-glueball can decay into a set of SM particles through a loop of heavy charged or colored particles. We constructed the $D = 8$ effective action coupling the two sectors. We considered the phenomenology of this scenario, and found formulas for the lifetimes and branching ratios of the most important of these states. The dominant decays are to two standard model gauge bosons, or by radiative decays with photon emission, leading to jet- and photon-rich signals.

With the similar objective of studying phenomenologically rich models, we considered models in which glueballs may be able to decay inside inside the detectors even for low confinement scale. Our scenario is motivated by Higgs portal hidden valleys models , in which the hidden glueballs interact with the SM sector through Higgs interactions. One of the most remarkable features of this scenario is the large spread in v-glueball lifetimes, even for a fixed choice of the parameters. The formalism of Peskin and Takeuchi was employed to show that operators considered in this work are not heavily constrained by precision electroweak physics, therefore leaving plenty of room in the parameter space to be explored by the future experiments at the LHC. We further investigated its phenomenology and possible discovery signatures.

In order to determine whether the aforementioned signatures are likely to be detectable at the LHC, it remains to investigate the dynamics of the production process. We studied several aspects of v-glueball production and discussed in some detail the dynamics of colored quirkonia. It would be interesting to extend these results by determining whether the energy lost during quirk relaxation may contribute with another discovery channel for glueballs and

quirks in other regions of parameter space. It remains an open problem to determine the non-perturbative couplings of glueballs to quirks and whether the amplitudes for glueball emission are further suppressed.

We also commented on the issue of hadron collider searches and discussed briefly the most likely strategies for discovery. For promptly decaying v-glueballs, the di-photon resonance from C-even glueball decays is likely to be the discovery channel for these glueballs at the LHC. The case of late decaying v-glueballs deserves further investigation.

Our models predict that a significant amount of energy is lost during quirkonium decay to v-glueballs and/or perturbative gluons. The latter will affect photon isolation, potentially increasing the backgrounds and lowering the sensitivity. It would be interesting to determine the effect on photon isolation of the quirkonium relaxation in order to get concrete predictions for the background. To accomplish this task, it is near certainty that new MonteCarlo tools will have to be designed or modified from existing ones to deal with backgrounds from multijets signal events.

We have seen that the pure-glue hidden valley scenario gives rise to spectacular phenomenology at hadron colliders. These phenomena are sufficiently exotic that they could be missed unless a reasonable strategy is designed to search for them. Given the simple nature of these models, it is worthwhile to put some effort in this direction. We plan to continue our investigations by doing an analysis of signal to background ratios. The next step will be to produce event generators for this exotic physics that can be used to develop concrete search strategies. It is important in this data driven era, however, to continue to take a pragmatic and impartial approach and investigate both minimal and non-minimal theories. It remains for the LHC to confirm whether there is a role for any of these particular theories in what physics lies beyond the SM.

References

[1] C. Amsler *et al.* [Particle Data Group], Phys. Lett. B **667**, 1 (2008).

[2] D. Feldman, Z. Liu and P. Nath, Phys. Rev. D **75**, 115001 (2007) [arXiv:hep-ph/0702123].

[3] K. Cheung and T. C. Yuan, JHEP **0703**, 120 (2007) [arXiv:hep-ph/0701107].

[4] Y. Gershtein, F. Petriello, S. Quackenbush and K. M. Zurek, Phys. Rev. D **78**, 095002 (2008) [arXiv:0809.2849 [hep-ph]].

[5] Y. Li, F. Petriello and S. Quackenbush, Phys. Rev. D **80**, 055018 (2009) [arXiv:0906.4132 [hep-ph]].

[6] M. J. Strassler and K. M. Zurek, Phys. Lett. B **651** (2007) 374 [arXiv:hep-ph/0604261].

[7] M. J. Strassler and K. M. Zurek, Phys. Lett. B **661**, 263 (2008) [arXiv:hep-ph/0605193].

[8] M. J. Strassler, arXiv:hep-ph/0607160.

[9] M. J. Strassler, arXiv:0801.0629 [hep-ph].

[10] T. Han, Z. Si, K. M. Zurek and M. J. Strassler, JHEP **0807**, 008 (2008) [arXiv:0712.2041 [hep-ph]].

[11] M. J. Strassler, arXiv:0806.2385 [hep-ph].

[12] Z. Chacko, H. S. Goh and R. Harnik, Phys. Rev. Lett. **96**, 231802 (2006) [arXiv:hep-ph/0506256].

[13] G. Burdman, Z. Chacko, H. S. Goh and R. Harnik, JHEP **0702**, 009 (2007) [arXiv:hep-ph/0609152].

[14] K. M. Zurek, arXiv:1001.2563 [hep-ph].

[15] K. S. Babu, I. Gogoladze and C. Kolda, arXiv:hep-ph/0410085.

[16] J. Schwinger, Phys. Rev. 82, 664 (1951); A. Casher, H. Neuberger and S. Nussinov, Phys. Rev. D **20**, 179 (1979).

[17] K. M. Zurek, arXiv:0811.4429 [hep-ph]; J. March-Russell, S. M. West, D. Cumberbatch and D. Hooper, JHEP **0807** (2008) 058 [arXiv:0801.3440 [hep-ph]]; N. Arkani-Hamed and N. Weiner, JHEP **0812**, 104 (2008) [arXiv:0810.0714 [hep-ph]]; A. E. Nelson and C. Spitzer, arXiv:0810.5167 [hep-ph].

[18] R. Blumenhagen, M. Cvetic, P. Langacker and G. Shiu, Ann. Rev. Nucl. Part. Sci. **55**, 71 (2005) [arXiv:hep-th/0502005].

[19] J. E. Juknevich, D. Melnikov and M. J. Strassler, JHEP **0907**, 055 (2009) [arXiv:0903.0883 [hep-ph]].

[20] J. E. Juknevich, JHEP **1008**, 121 (2010) [arXiv:0911.5616 [hep-ph]].

[21] B. Grinstein and L. Randall, Phys. Lett. B **217**, 335 (1989).

[22] R. Tarrach, Nucl. Phys. B **196**, 45 (1982).

[23] A.Y. Morozov, Sov. J. Nucl. Phys. 40 (1984), p. 505.

[24] C. J. Morningstar and M. J. Peardon, Phys. Rev. D **60** (1999) 034509 [arXiv:hep-lat/9901004].

[25] Y. Chen *et al.*, Phys. Rev. D **73** (2006) 014516 [arXiv:hep-lat/0510074].

[26] V. A. Novikov, M. A. Shifman, A. I. Vainshtein and V. I. Zakharov, Nucl. Phys. B **165**, 67 (1980).

[27] V. A. Novikov, M. A. Shifman, A. I. Vainshtein and V. I. Zakharov, Nucl. Phys. B **165**, 55 (1980); V. A. Novikov, M. A. Shifman, A. I. Vainshtein and V. I. Zakharov, Phys. Lett. B **86**, 347 (1979) [JETP Lett. **29**, 594.1979 ZFPRA,29,649 (1979 ZFPRA,29,649-652.1979)].

[28] J. F. Donoghue, K. Johnson and B. A. Li, Phys. Lett. B **99** (1981) 416.

[29] J. M. Cornwall and A. Soni, Phys. Lett. B **120** (1983) 431.

[30] J. Kuti, Nucl. Phys. Proc. Suppl. **73** (1999) 72 [arXiv:hep-lat/9811021]

[31] M. Loan and Y. Ying, Prog. Theor. Phys. **116**, 169 (2006) [arXiv:hep-lat/0603030].

[32] S. Gao and C. Gale, Phys. Rev. C **57**, 254 (1998) [arXiv:nucl-th/9711006].

[33] R. Rapp and C. Gale, Phys. Rev. C **60**, 024903 (1999) [arXiv:hep-ph/9902268].

[34] V. A. Novikov, M. A. Shifman, A. I. Vainshtein and V. I. Zakharov, Nucl. Phys. B **165**, 67 (1980).

[35] V. A. Novikov, M. A. Shifman, A. I. Vainshtein and V. I. Zakharov, Nucl. Phys. B **165**, 55 (1980); V. A. Novikov, M. A. Shifman, A. I. Vainshtein and V. I. Zakharov, Phys. Lett. B **86**, 347 (1979) [JETP Lett. **29**, 594.1979 ZFPRA,29,649 (1979 ZFPRA,29,649-652.1979)].

[36] N. Kaiser and U. G. Meissner, Nucl. Phys. A **519** (1990) 671.

[37] V. Mathieu, N. Kochelev and V. Vento, Int. J. Mod. Phys. E **18**, 1 (2009) [arXiv:0810.4453 [hep-ph]].

[38] R. Delbourgo and D. s. Liu, Phys. Rev. D **51**, 118 (1995) [arXiv:hep-ph/9403372].

[39] A. E. Faraggi and M. Pospelov, Astropart. Phys. **16**, 451 (2002) [arXiv:hep-ph/0008223].

[40] A. Falkowski, J. Juknevich and J. Shelton, arXiv:0908.1790 [hep-ph].

[41] G. D. Kribs, T. S. Roy, J. Terning and K. M. Zurek, arXiv:0909.2034 [hep-ph].

[42] V. A. Novikov, L. B. Okun, M. A. Shifman, A. I. Vainshtein, M. B. Voloshin and V. I. Zakharov, Phys. Rept. **41**, 1 (1978).

[43] M. J. Strassler, SLAC-PUB-5978

[44] S. Groote and A. A. Pivovarov, Eur. Phys. J. C **21**, 133 (2001) [arXiv:hep-ph/0103313].

[45] For a review on Higgs Physics, see: J. F. Gunion, H. E. Haber, G. Kane, S. Dawson, *The Higgs Hunter's guide* (Addison-Wesley, Reading Mass., 1990)

[46] R. L. Jaffe, K. Johnson and Z. Ryzak, Annals Phys. **168** (1986) 344.

[47] L. B. Okun, JETP Lett. **31** (1980) 144 [Pisma Zh. Eksp. Teor. Fiz. **31** (1979) 156], Nucl. Phys. B **173** (1980) 1.

[48] S. Gupta and H. R. Quinn, Phys. Rev. D **25** (1982) 838.

[49] J. Kang, M. A. Luty and S. Nasri, JHEP **0809**, 086 (2008) [arXiv:hep-ph/0611322].
J. Kang and M. A. Luty, JHEP **0911**, 065 (2009) [arXiv:0805.4642 [hep-ph]].

[50] R. Harnik and T. Wizansky, Phys. Rev. D **80**, 075015 (2009) [arXiv:0810.3948 [hep-ph]].

[51] T. Appelquist and H. D. Politzer, Phys. Rev. Lett. **34**, 43 (1975).

[52] A. Abulencia *et al.* [CDF Collaboration], Phys. Rev. D **75**, 112001 (2007) [arXiv:hep-ex/0702029].

[53] T. Aaltonen *et al.*, arXiv:0910.5170 [hep-ex].
R. Culbertson *et al.*,[CDF Collaboration], Public note

[54] T. Aaltonen *et al.* [CDF Collaboration], Phys. Rev. D **78**, 032015 (2008) [arXiv:0804.1043 [hep-ex]].

[55] G. D. Kribs, T. Plehn, M. Spannowsky and T. M. P. Tait, Phys. Rev. D **76**, 075016 (2007) [arXiv:0706.3718 [hep-ph]].

[56] V. M. Abazov *et al.* [D0 Collaboration], Phys. Rev. Lett. **103**, 071801 (2009) [arXiv:0906.1787 [hep-ex]].

[57] V. M. Abazov *et al.* [D0 Collaboration], Phys. Rev. Lett. **101**, 111802 (2008) [arXiv:0806.2223 [hep-ex]].

[58] B. W. Lynn, G. Penso and C. Verzegnassi, Phys. Rev. D **35**, 42 (1987).

[59] M. E. Peskin and T. Takeuchi, Phys. Rev. D **46**, 381 (1992).

[60] J. E. Juknevich, D. Melnikov and M.J. Strassler, in preparation.

[61] H. Georgi, A. Manohar and G. W. Moore, Phys. Lett. B **149**, 234 (1984).

[62] H. Georgi and L. Randall, Nucl. Phys. B **276**, 241 (1986).

[63] A. V. Manohar and M. B. Wise, Phys. Lett. B **636**, 107 (2006) [arXiv:hep-ph/0601212].

[64] S. Weinberg, Phys. Rev. Lett. **63**, 2333 (1989).

[65] S. Chang, P. J. Fox and N. Weiner, Phys. Rev. Lett. **98**, 111802 (2007) [arXiv:hep-ph/0608310].

[66] R. Dermisek and J. F. Gunion, Phys. Rev. D **77**, 015013 (2008) [arXiv:0709.2269 [hep-ph]].

[67] B. A. Dobrescu, G. L. Landsberg and K. T. Matchev, Phys. Rev. D **63**, 075003 (2001) [arXiv:hep-ph/0005308].

[68] G. 't Hooft and M. J. G. Veltman, Nucl. Phys. B **153**, 365 (1979).

[69] J. M. Maldacena, Adv. Theor. Math. Phys. **2**, 231 (1998) [Int. J. Theor. Phys. **38**, 1113 (1999)] [arXiv:hep-th/9711200]; for a review see O. Aharony, S. S. Gubser, J. M. Maldacena, H. Ooguri and Y. Oz, Phys. Rept. **323**, 183 (2000) [arXiv:hep-th/9905111].

[70] S. S. Gubser, I. R. Klebanov and A. M. Polyakov, Phys. Lett. B **428**, 105 (1998) [arXiv:hep-th/9802109]; E. Witten, Adv. Theor. Math. Phys. **2**, 253 (1998) [arXiv:hep-th/9802150].

[71] E. Witten, Adv. Theor. Math. Phys. **2**, 505 (1998) [arXiv:hep-th/9803131].

[72] C. Csaki, H. Ooguri, Y. Oz and J. Terning, JHEP **9901**, 017 (1999) [arXiv:hep-th/9806021]; also see R. C. Brower, S. D. Mathur and C. I. Tan, Nucl. Phys. B **587**, 249 (2000) [arXiv:hep-th/0003115] and references therein.

[73] M. Berg, M. Haack and W. Mueck, Nucl. Phys. B **789**, 1 (2008) [arXiv:hep-th/0612224]; A. Dymarsky and D. Melnikov, JHEP **0805**, 035 (2008) [arXiv:0710.4517 [hep-th]]; M. K. Benna, A. Dymarsky, I. R. Klebanov and A. Solovyov, JHEP **0806**, 070 (2008) [arXiv:0712.4404 [hep-th]]; A. Dymarsky, D. Melnikov and A. Solovyov, arXiv:0810.5666 [hep-th].

[74] N. Brambilla *et al.* [Quarkonium Working Group], arXiv:hep-ph/0412158.

[75] W. Lucha and F. F. Schoberl, Int. J. Mod. Phys. C **10**, 607 (1999) [arXiv:hep-ph/9811453].

[76] T. Appelquist and H. D. Politzer, Phys. Rev. D **12**, 1404 (1975).

[77] E. C. Poggio, H. R. Quinn and S. Weinberg, Phys. Rev. D **13**, 1958 (1976).

[78] H. Fritzsch, Phys. Lett. B **67**, 217 (1977).

[79] J. S. Bell and J. Pasupathy, Phys. Lett. B **83**, 389 (1979).

[80] C. Quigg, Acta Phys. Polon. B **15**, 53 (1984).

[81] M. Beneke, arXiv:hep-ph/9703429.

[82] K. Igi and S. Ono, Phys. Rev. D **33**, 3349 (1986).

[83] T. Appelquist, M. Dine and I. J. Muzinich, Phys. Lett. B **69**, 231 (1977).

[84] E. Eichten and K. Gottfried, Phys. Lett. B **66**, 286 (1977).

[85] J. L. Richardson, Phys. Lett. B **82**, 272 (1979).

[86] V. D. Barger, E. W. N. Glover, K. Hikasa, W. Y. Keung, M. G. Olsson, C. J. . Suchyta and X. R. Tata, Phys. Rev. D **35**, 3366 (1987) [Erratum-ibid. D **38**, 1632 (1988)] [Phys. Rev. D **38**, 1632 (1988)].

[87] C. Quigg and J. L. Rosner, Phys. Lett. B **71**, 153 (1977).

[88] K. Cheung, W. Y. Keung and T. C. Yuan, Nucl. Phys. B **811**, 274 (2009) [arXiv:0810.1524 [hep-ph]].

[89] Y. P. Kuang, Front. Phys. China **1**, 19 (2006) [arXiv:hep-ph/0601044].

[90] Y. P. Kuang,

[91] N. Brambilla and A. Vairo, Acta Phys. Polon. B **38**, 3429 (2007) [arXiv:0711.1328 [hep-ph]].

[92] P. L. Cho and A. K. Leibovich, Phys. Rev. D **53**, 150 (1996) [arXiv:hep-ph/9505329].

[93] K. J. Juge, J. Kuti and C. J. Morningstar, arXiv:hep-ph/9711451.

[94] O. Harris [ATLAS Collaboration], PoS **HCP2009**, 076 (2009).

[95] A. Policicchio [ATLAS Collaboration], PoS E **PS-HEP2009**, 423 (2009).

[96] V. M. Abazov *et al.* [D0 Collaboration], Phys. Rev. Lett. **103**, 071801 (2009) [arXiv:0906.1787 [hep-ex]].

Appendix A

A.1 Three-body decays

In the main body of the text we have argued that three-body decays of states in the C-odd sector are largely suppressed as compared to their radiative decays to light C-even states. As an example, here we consider a three-body decay $1^{--} \to 1^{+-}gg$ and demonstrate that there is a substantial suppression of its rate. We will restrict ourselves to consider the case of the s-wave decay mode since this is expected to give the highest contribution to the decay rate in a partial wave expansion. In this approximation only P and $L_{\mu\nu\alpha\beta}$ operators contribute (table 2.2). This corresponds to the amplitude

$$\frac{\alpha_s\alpha_v}{M^4}\,\chi_s\left[C_P\langle g^a,g^b|\,\mathrm{tr}\;G_{\mu\nu}\tilde{G}^{\mu\nu}|\,0\rangle\,\langle 1^{+-}|\,P|1^{--}\rangle\,+\right.$$
$$\left.+C_L\langle g^a,g^b|\,\mathrm{tr}\;G_{\mu\nu}G_{\alpha\beta}|\,0\rangle\langle 1^{+-}|\,L^{\mu\nu\alpha\beta}|1^{--}\rangle\right],$$

where the s-wave approximation implies the following form of the matrix elements;

$$\langle 1^{+-}|\,P|1^{--}\rangle = \frac{\epsilon^+\cdot\epsilon^-}{m_{1^-}}\,\mathbf{M^P_{1^{--}1^{+-}}},$$

$$\langle 1^{+-},q|\,L_{\mu\nu\alpha\beta}|1^{--},p\rangle = \frac{\mathbf{M^L_{1^{--}1^{+-}}}}{m_{1^-}^3}\,(\epsilon_{\mu\nu\rho\sigma}p^\rho\epsilon^{-\sigma}(p_\alpha\epsilon^+{}_\beta - p_\beta\epsilon^+{}_\alpha)+$$
$$+\,\epsilon_{\alpha\beta\rho\sigma}p^\rho\epsilon^{-\sigma}(p_\mu\epsilon^+{}_\nu - p_\nu\epsilon^+{}_\mu) - \text{traces}) + \dots\,,$$

The above amplitude gives a decay rate

$$\Gamma_{1^-\to 1^+gg} = \frac{\alpha_s^2\alpha_v^2}{2^9\pi^3M^8}\frac{1}{3}(N_c^2-1)\chi_s^2m_{1^-}^3\,\left(4C_L^2(\mathbf{M^L_{1^{--}1^{+-}}})^2\,f_L(a)+\right.$$
$$\left.+C_P^2(\mathbf{M^P_{1^{--}1^{+-}}})^2\,f_P(a)\right)+\dots\,, \quad \text{(A.1)}$$

where we define the dimensionless functions $f_L(a)$ and $f_P(a)$ of $a\equiv m_{1^+}^2/m_{1^-}^2$ as

$$f_L(a) = -\frac{1}{15120a}(171a^7 - 1295a^6 + 4410a^5 - 9450a^4 + 11025a^3-$$
$$-\,4221a^2 - 630a - 10) - \frac{1}{36}\,a(5a-9)\log(a),$$

$$f_P(a) = -\frac{1}{120a}\left(a^6 + 36a^5 + 1305a^4 - 1305a^2 - 36a - 1\right) + \\ + \frac{1}{2}\,a\left(9a^2 + 28a + 9\right)\log(a).$$

For the values of v-glueball masses from the spectrum in figure 2.1, $a \simeq 0.6$, $f_L(0.6) \simeq 3 \times 10^{-5}$ and $f_P(0.6) \simeq 7 \times 10^{-5}$.

The ratio of the decay rate (A.1) to the radiative two-body decay (3.18) is

$$\frac{\Gamma_{1^-\to 1^+gg}}{\Gamma_{1^-\to 0^+\gamma}} = 6 \times 10^{-6}\frac{\alpha_s^2}{\alpha\alpha_v}\,\frac{\chi_s^2}{\chi^2}\left(\frac{4C_L^2(\mathbf{M^L_{1^{--}1^{+-}}})^2 + \frac{f_P}{f_L}C_P^2(\mathbf{M^L_{1^{--}1^{+-}}})^2}{(\mathbf{M^\Omega_{1^{--}0^{++}}})^\mathbf{2}}\right).$$

Unless there is an extreme degeneracy in the $SU(5)$ multiplet of X particles, which is unnatural due to $SU(5)$-asymmetric renormalization of the masses, we expect χ is at least of order 0.1, so the coefficient in front of the ratio of the form-factors will be around 10^{-2} or smaller.

For other states in the C-odd sector, a rough estimate confirms that the ratio of the three-body decays to the radiative decays is never greater than 1/10 and is typically much smaller. Thus, we conclude that the three-body decays in this sector are never dominant. Since most such decays are to gluons, and are therefore very difficult to observe, the three-body processes can for current purposes be ignored.

A.2 Computation of $\mathcal{L}^{(6)}_{eff}$

Definitions

In the following the momenta of the initial gluons (p_1, p_2) and final Higgs bosons (k_1, k_2) are all chosen to be incoming. We make use of the following invariants

$$s = (p_1 + p_2)^2 \quad t = (p_1 + k_4)^2 \quad u = (p_1 + k_3)^2 \tag{A.2}$$

obeying the condition

$$s + t + u = k_3^2 + k_4^2 \tag{A.3}$$

where we have assumed that the gluons are massless, $p_1^2 = p_2^2 = 0$.

Pasarino-Veltman functions C_0 and D_0

The computation of the Feynman graphs is performed using the Passarino-Veltman decomposition of the one-loop tensor integrals [68]. For our results below we will make use of the 3 and 4 point scalar functions C_0 and D_0. The explicit expressions are rather lengthy and have to be

handled numerically. However, one can derive an integral representation

$$C_0(r_1, r_2, s, M_1, M_2, M_3) = \int_0^1 \int_0^x \left[-r_2 x^2 - r_1 y^2 + (-s + r_1 + r_2)xy + \right. \\ \left. + (M_3 - M_2 + r_2)x + (M_2 - M_1 + s - r_2)y - M_3\right]^{-1} dy dx \quad \text{(A.4)}$$

$$D_0(r_1, r_2, r_3, r_4, s, t, M_1, M_2, M_3, M_4) = \int_0^1 \int_0^x \int_0^y \left[-r_3 x^2 - r_2 y^2 - r_1 z^2 + \right. \\ + (-t + r_1 + r_4)xy + (s + t - r_2 - r_4)xz + (-s + r_1 + r_2)yz + (M_4 - M_3 + r_3)x + \\ \left. + (M_3 - M_2 + t - r_3)y + (M_2 - M_1 + r_4 - t)z - M_4\right]^{-2} dz\, dy\, dx \quad \text{(A.5)}$$

Fermion loop

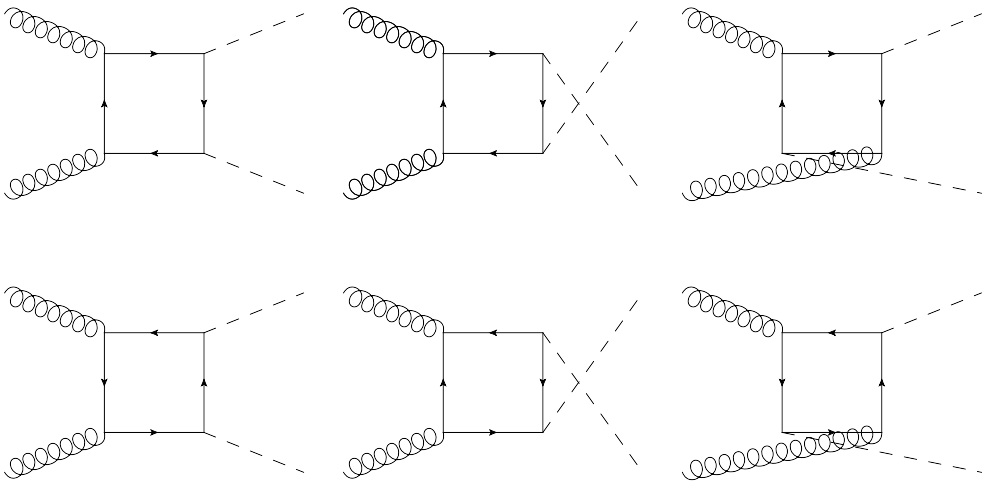

Figure A.1: Graphs contributing to $gg \to HH$

The amplitude for the fusion of two massless v-gluons into a pair of Higgs boson fields arises at lowest order in perturbation theory from a loop of heavy particles. The relevant graphs are depicted in figure A.1. We assume that there is a pair of vector-like fermion fields, a doublet and a singlet of $SU(2)_L$, transforming under the fundamental representation of $SU(n_v)$. The doublet and singlet have masses M and m, respectively. Gauge invariance constrains the amplitude to be

$$\mathcal{M}_\Box = \frac{y^2 g_v^2}{8\pi^2} \left(p_1^\nu p_2^\mu - p_1 \cdot p_2 g^{\mu\nu}\right) F_\Box \, \epsilon_\mu^1 \epsilon_\nu^2 \delta_{ab} + \cdots \quad \text{(A.6)}$$

where ϵ_μ^1, ϵ_μ^2 are the polarization vectors of the incoming v-gluons. The form factor $F_\Box$ is given by:

$$F_\Box = f(s, t, u, k_3^2, k_4^2, m, M) + f(s, t, u, k_4^2, k_3^2, m, M) + (M \leftrightarrow m) \quad \text{(A.7)}$$

where

$$
\begin{aligned}
&f(s,t,u,k_3^2,k_4^2,m,M) = \\
&-\frac{1}{s^2}(k_3^2+k_4^2-2(M+m)^2)\left[(k_4^2-u)C_0(0,k_4^2,u,M^2,M^2,m^2)+(k_4^2-t)C_0(0,k_4^2,t,m^2,m^2,M^2)\right. \\
&\left.+(k_3^2-u)C_0(0,u,k_3^2,m^2,m^2,M^2)+(k_3^2-t)C_0(0,t,k_3^2,u,M^2,M^2,m^2)\right] \\
&+8\frac{m^2}{s}C_0(0,0,s,m^2,m^2,m^2) \\
&-2\frac{m^2}{s}(-2(m+M)^2+k_3^2+k_4^2+\frac{M}{m}s)\left[D_0(0,0,k_3^2,k_4^2,s,t,m^2,m^2,m^2,M^2)\right. \\
&\left.+D_0(0,0,k_4^2,k_3^2,s,u,m^2,m^2,m^2,M^2)\right]+ \\
&\frac{1}{s^2}\left(2m^4s+4m^3Ms+m^2(s(4M^2-k_4^2)+2k_3^2k_4^2-k_3^2(2k_4^2+s))+2mM(2M^2s-2k_3^2(k_4^2-t)\right. \\
&+2k_4^2t-s^2-2st-2t^2)+(2M^2-k_3^2-k_4^2)(sM^2+k_3^2k_4^2-k_3^2k_4^2) \\
&\left.+s(2m^2+2M^2-k_3^2-k_4^2)p_t^2\right)D_0(0,k_4^2,0,k_3^2,t,u,m^2,m^2,M^2,M^2)+4 \qquad \text{(A.8)}
\end{aligned}
$$

with $p_t = 2(p_1k_3)(p_2k_3)/(p_1p_2) - k_3^2$.

Large fermion mass limit and effective Lagrangian

The form factor can be evaluated by taking the limit $M, m \gg s, t, u, k_3^2, k_4^2$. At leading order in the mass splitting of the heavy fermions $M \approx m$, the form factor reads

$$F_\Box = \frac{8}{3Mm} + \mathcal{O}(s/M^2). \qquad \text{(A.9)}$$

The matrix element for $g_a g_b \to HH$ can be obtained in perturbation theory from the following non-renormalizable interaction

$$\mathcal{L}_{eff}^{(6)} = \frac{y^2\alpha_v}{3\pi Mm} H^\dagger H \text{tr}\ \mathcal{F}_{\mu\nu}\mathcal{F}^{\mu\nu}. \qquad \text{(A.10)}$$

A.3 The form factors $\mathcal{M}_{JJ'}^{(i)}$

In addition to the momenta p and q, we introduce a pair of tensors $\epsilon_{\mu_1,\cdots,\mu_J}(p)$ and $\tilde{\epsilon}_{\mu_1,\cdots,\mu_{J'}}(q)$ to represent the polarizations of the spin-J and spin-J' states respectively. It will be convenient to define "reduced" polarization tensors by contracting some of the indices with the vectors p and q,

$$\epsilon_{\mu_1,\cdots,\mu_{J-K}}(p) = \epsilon_{\mu_1,\cdots,\mu_J}(p)q^{\mu_{J-K+1}}\cdots q^{\mu_J} \qquad \tilde{\epsilon}_{\mu_1,\cdots,\mu_{J'-K'}}(q) = \tilde{\epsilon}_{\mu_1,\cdots,\mu_J}(q)p^{\mu_{J'-K'+1}}\cdots p^{\mu_{J'}}. \qquad \text{(A.11)}$$

The invariant form factors are constructed from the reduced polarization tensors and the vectors p and q. For the simplest $J \to 0$ case, the only form factor is obtained when all the indices of

the polarization tensor are fully contracted with q,

$$\epsilon(p) = \epsilon_{\mu_1,\cdots,\mu_J}(p)\, q^{\mu_0}\cdots q^{\mu_J}. \tag{A.12}$$

This gives the matrix element

$$\langle 0, q|S|J, p\rangle \;=\; \mathbf{M^S_{0J}}\, \epsilon_{\mu_1,\cdots,\mu_J}(p)\, q^{\mu_0}\cdots q^{\mu_J} \tag{A.13}$$

where now $\mathbf{M^S_{0J}}$ is the transition matrix which depends on the transferred momentum. For the more complex $J \to J' = 1$ case, there are two form factors parametrizing the matrix element,

$$\epsilon_{\mu,\mu_2\cdots,\mu_J}(p)\, q^{\mu_2}\cdots q^{\mu_J}\, \tilde{\epsilon}^{\mu}(q), \qquad \epsilon_{\mu_1,\mu_2\cdots,\mu_J}(p)\, q^{\mu_1}\cdots q^{\mu_J}\, \tilde{\epsilon}_{\nu}(q)\, p^{\nu}. \tag{A.14}$$

In the reduced notation, these are simply $\epsilon_\mu\, \tilde{\epsilon}^\mu =$ and $\epsilon\, \tilde{\epsilon}$. In addition, we can contract the polarization tensors with a Levi-Civita tensor as follows,

$$\epsilon^{\mu\nu\rho\sigma}\epsilon_{\mu}(p)\, p_\rho\, q_\sigma \tilde{\epsilon}_\nu(q) = \epsilon^{\mu\nu\rho\sigma}\epsilon_{\mu,\mu_2\cdots,\mu_J}(p)\, q^{\mu_2}\cdots q^{\mu_J}\, p_\rho\, q_\sigma \tilde{\epsilon}_\nu(q) \tag{A.15}$$

Collecting all terms, we obtain the following matrix element

$$\begin{aligned}\langle 1, q|S|J, p\rangle = \mathbf{M^S_{1J}}\epsilon_{\mu,\mu_2\cdots,\mu_J}(p)\, q^{\mu_2}\cdots q^{\mu_J}\, \tilde{\epsilon}^{\mu}(q) + \mathbf{M^{S'}_{1J}}\epsilon_{\mu_1,\mu_2\cdots,\mu_J}(p)\, q^{\mu_1}\cdots q^{\mu_J}\, \tilde{\epsilon}_{\nu}(q)\, p^{\nu} + \\ \mathbf{M^{S''}_{1J}}\epsilon^{\mu\nu\rho\sigma}\epsilon_{\mu,\mu_2\cdots,\mu_J}(p)\, q^{\mu_2}\cdots q^{\mu_J}\, p_\rho\, q_\sigma \tilde{\epsilon}_\nu(q)\end{aligned} \tag{A.16}$$

We next turn to the more complicated matrix element for the $J \to J' = 2$ transition. Firstly, we define the auxiliary tensors

$$\epsilon_{\mu\nu}(p) = \epsilon_{\mu,\nu,\mu_3\cdots,\mu_J}(p)\, q^{\mu_3}\cdots q^{\mu_J}, \quad \epsilon_{\mu}(p) = \epsilon_{\mu,\mu_2\cdots,\mu_J}(p)\, q^{\mu_2}\cdots q^{\mu_J} \tag{A.17}$$

and

$$\tilde{\epsilon}_\mu(q) = \tilde{\epsilon}_{\mu\nu}(q)\, p^{\nu}. \tag{A.18}$$

From $\epsilon_{\mu\nu}(p)$, $\epsilon_\mu(p)$, $\tilde{\epsilon}_{\mu\nu}(q)$ and $\tilde{\epsilon}_\mu(q)$ we can form the following three invariants

$$\epsilon_{\mu\nu}(p)\, \tilde{\epsilon}_{\mu\nu}(q), \quad \epsilon_\mu(p)\, \tilde{\epsilon}_\mu(q), \quad (\epsilon_\mu(p)\, q^\mu)\, (\tilde{\epsilon}_\nu(q)\, p^\nu) \tag{A.19}$$

In addition, contracting with the Levi-Civita tensor gives two more invariants,

$$\epsilon^{\mu\nu\rho\sigma}\epsilon_\mu(p)\, p_\rho\, q_\sigma \tilde{\epsilon}_\nu(q), \quad \epsilon^{\mu\nu\rho\sigma}\epsilon_{\mu\lambda}(p)\, p_\rho\, q_\sigma \tilde{\epsilon}_\nu{}^{\lambda}(q). \tag{A.20}$$

Therefore, there are five form factors in the $J \to J' = 2$ case. The general rule to find all the form factors in the case $J \to J'$ case is now clear. Without loss of generality we can assume $J > J'$. First we construct the reduced spin-J tensor with J' indices,

$$\epsilon_{\mu_1,\cdots,\mu_{J'}}(p) = \epsilon_{\mu_1,\cdots,\mu_J}(p) q^{\mu_{J-J'}}\cdots q^{\mu_J} \tag{A.21}$$

so that we have two tensors with J' indices. Then we form the invariants

$$\epsilon_{\mu_1,\cdots,\mu_{J'}}(p)\tilde{\epsilon}^{\mu_1,\cdots\mu_{J'}}(q),\ \cdots,\ \epsilon_{\mu}(p)\,\tilde{\epsilon}^{\mu}(q),\ \epsilon(p)\,\tilde{\epsilon}(q), \tag{A.22}$$

for a total of $J'+1$ invariant form factors. Secondly, there are contractions with the Levi-Civita tensor as follows

$$\epsilon_{\mu\nu\rho\sigma}p^{\rho}q^{\sigma}\epsilon_{\mu,\mu_2,\cdots,\mu_{J'}}(p)\tilde{\epsilon}^{\nu\mu_2,\cdots\mu_{J'}}(q),\ \cdots,\ \epsilon_{\mu\nu\rho\sigma}p^{\rho}q^{\sigma}\epsilon_{\mu}(p)\,\tilde{\epsilon}^{\nu}(q) \tag{A.23}$$

giving J' additional invariants. Hence, the total number of Lorentz invariant form factors is $2J'+1$ for the transitions $J \to J'$, $J' < J$. To see that this contemplate all the possibilities, we can apply angular momentum counting rules. By composing the spin J and spin J' states we obtain total spin $|J-J'|,\cdots,J+J'$. For a scalar operator, these have to be combined with total angular momentum $L = |J-J'|,\cdots,J+J'$ in order to give total spin 0. So for $J' < J$ we get $2J'+1$ form factors associated with the different values of L.

i	1	2	3	4	5
$\mathcal{M}^{(2,i)}_{\alpha\beta\rho\sigma}$	$g_{\alpha\rho}\,g_{\beta\sigma}$	$g_{\alpha\rho}\,\hat{q}_{\beta}\,\hat{p}_{\sigma}$	$\hat{q}_{\alpha}\hat{p}_{\rho}\,\hat{q}_{\beta}\,\hat{p}_{\sigma}$	$g_{\beta\rho}\,\epsilon_{\alpha\sigma zw}\,\hat{p}^{z}\,\hat{q}^{w}$	$\hat{q}_{\beta}\,\hat{p}_{\rho}\,\epsilon_{\alpha\sigma zw}\,\hat{p}^{z}\,\hat{q}^{w}$
$\mathcal{M}^{(1,i)}_{\alpha\rho}$	$g_{\alpha\rho}$	$q_{\alpha}\,\hat{p}_{\rho}$	$\epsilon_{\alpha\rho zw}\,\hat{p}^{\,z}\hat{q}^{\,w}$	-	-

Table A.1: The auxiliary tensors $\mathcal{M}^{(J,i)}$. Here $\hat{q}_{\alpha} = q_{\alpha}/\sqrt{q^2}$ and $\hat{p}_{\alpha} = p_{\alpha}/\sqrt{p^2}$.

To summarize, we show the matrix elements up to spin 3 that are needed to compute the decays of the v-glueballs in figure 2.1. In terms of the auxiliary tensors shown in table A.1, the matrix elements read,

$$\mathcal{M}^{(i)}_{32} = \hat{q}_{\gamma}\,\epsilon^{\alpha\beta\gamma}(p)\,\tilde{\epsilon}^{\,\rho\sigma}(q)\,\mathcal{M}^{(2,i)}_{\alpha\beta\rho\sigma} \tag{A.24}$$

$$\mathcal{M}^{(i)}_{31} = \hat{q}_{\gamma}\,\hat{q}_{\beta}\,\epsilon^{\alpha\beta\gamma}(p)\,\tilde{\epsilon}^{\,\rho}(q)\,\mathcal{M}^{(1,i)}_{\alpha\rho} \tag{A.25}$$

$$\mathcal{M}_{30} = \hat{q}_{\alpha}\,\hat{q}_{\beta}\ \hat{q}_{\gamma}\,\epsilon^{\alpha\beta\gamma}(p) \tag{A.26}$$

$$\mathcal{M}^{(i)}_{22} = \epsilon^{\alpha\beta}(p)\,\tilde{\epsilon}^{\,\rho\sigma}(q)\,\mathcal{M}^{(2,i)}_{\alpha\beta\rho\sigma} \tag{A.27}$$

$$\mathcal{M}^{(i)}_{21} = \hat{q}_{\beta}\,\epsilon^{\alpha\beta}(p)\,\tilde{\epsilon}^{\,\rho}(q)\,\mathcal{M}^{(1,i)}_{\alpha\rho} \tag{A.28}$$

$$\mathcal{M}_{20} = \hat{q}_{\alpha}\,\hat{q}_{\beta}\ \epsilon^{\alpha\beta}(p) \tag{A.29}$$

$$\mathcal{M}^{(i)}_{11} = \epsilon^{\alpha}(p)\,\tilde{\epsilon}^{\,\rho}(q)\,\mathcal{M}^{(1,i)}_{\alpha\rho} \tag{A.30}$$

$$\mathcal{M}_{10} = \hat{q}_{\alpha}\ \epsilon^{\alpha}(p) \tag{A.31}$$

where we denote $\hat{q}_\alpha = q_\alpha/\sqrt{q^2}$. For the sake of brevity, we have not shown the seven matrix elements that correspond to the $3 \to 3$ transition. These can be obtained along the same line that led to (A.24)-(A.31).

A.4 The virial theorem and related theorems

Two results of considerable general utility for the study of bound states in a central potential are the virial theorem,

$$\langle T\rangle = E = \langle V\rangle = \langle \frac{r}{2}\frac{dV}{dr}\rangle \tag{A.32}$$

and the connection between the s-wave wave function at the origin and the gradient of the potential,

$$|\psi(0)|^2 = \mu\,\langle \frac{dV}{dr}\rangle, \tag{A.33}$$

where $\mu = M/2$ is the reduced mass, T, V and E are the kinetic, potential and total energy, respectively. An important case occurs for power law potential of the form

$$V(r) = \lambda\, r^\nu, \tag{A.34}$$

for which kinetic, potential and total energy are related by

$$\langle T\rangle = \frac{\nu}{2}\langle V\rangle = \frac{\nu}{\nu+2}E, \tag{A.35}$$

or equivalently,

$$< V >= \frac{2}{\nu+2}E. \tag{A.36}$$

Thus for the linear potential ($\nu = 1$) we find

$$\langle r\rangle = \frac{2E}{3\lambda}. \tag{A.37}$$

The mass and coupling strength dependences of the level spacings are prescribed by the Schrödinger equation as

$$\Delta E \propto (2\mu)^{-\nu/(2+\nu)}\,|\lambda|^{2/(2+\nu)}. \tag{A.38}$$

Thus for the Coulomb potential ($\nu = -1$), $\Delta E \propto \mu|\lambda|^2$, while for the linear potential ($\nu = 1$),$\Delta E \propto (\lambda^2/\mu)^{1/3}$.

According to the scaling rules of the Schrödinger equation, quantities with the dimensions of length scale as

$$L \propto (\mu/|\lambda|)^{1/(2+\nu)}. \tag{A.39}$$

An important quantity is the probability density at the origin, $|\psi(0)|^2$, which has dimensions of inverse volume and so scales as

$$|\psi(0)|^2 \propto (\mu|\lambda|)^{3/(2+\nu)}. \tag{A.40}$$

For a Coulomb potential, therefore, $|\psi(0)|^2 \propto (\mu|\lambda|)^3$, while for a linear potential $|\psi(0)|^2 \propto \mu\lambda$. Transition matrix elements of electric and magnetic multipole operators and sizes of bound states with given quantum numbers are other examples of quantities to which the scaling rule (A.39) may be applied. Electric dipole matrix elements scale as

$$\langle n' \,|\, \mathcal{E} \,|\, n\rangle \propto L \tag{A.41}$$

while the magnetic dipole matrix element behaves as

$$\langle n' \,|\, \mathcal{M} \,|\, n\rangle \propto 1. \tag{A.42}$$

Since radiative widths are given by

$$\Gamma(\mathcal{E} \text{ or } \mathcal{M}) \propto \omega^3 \langle n' \,|\, \mathcal{E} \text{ or } \mathcal{M} \,|\, n\rangle \tag{A.43}$$

with $\omega \sim \Delta E$, we find

$$\Gamma(\mathcal{E}) \propto \mu^{-(2+3\nu)/(2+\nu)} \lambda^{4/(2+\nu)} \tag{A.44}$$

and

$$\Gamma(\mathcal{M}) \propto \mu^{-(4+5\nu)/(2+\nu)} \lambda^{6/(2+\nu)}. \tag{A.45}$$

The WKB approximation is a very useful and powerful method to solve bound state problems for highly excited states. An useful result is

$$|R_{n,0}(0)|^2 = \frac{(2\mu)^{3/2}}{\pi}\, E_n^{1/2}\, \frac{dE_n}{dn}, \tag{A.46}$$

where $R_{n,0} \equiv \sqrt{4\pi}\psi(0)$ is the S-wave radial wavefunction. This expression has been generalized to include higher angular momentum waves,

$$\left|\frac{d^l}{dr^l} R_{nl}(0)\right|^2 = \frac{1}{\pi}\left[\frac{l!}{(2l+1)!!}\right]^2 (2\mu E_{n,l})^{l+1/2}\, \frac{\partial(2\mu E_{n,l})}{\partial n}. \tag{A.47}$$

For a potential (A.34) the energy eigenvalues in the WKB approximation are given by

$$E_{nl} = \lambda^{2/(2+\nu)}\, (2\nu)^{-\nu/(2+\nu)} \left[A(\nu)\left(n + \frac{l}{2} - \frac{1}{4}\right)\right]^{2\nu/(2+\nu)}, \tag{A.48}$$

$$A(\nu) = \frac{2\nu\sqrt{\pi}\,\Gamma(\frac{3}{2} + \frac{1}{\nu})}{\Gamma(\frac{1}{\nu})}, \qquad \nu > 0. \tag{A.49}$$

Plugging (A.48) into (A.50) one can show that the squares of S-wave radial wavefunctions at the origin are given by

$$|R_{n,0}(0)|^2 = \frac{2}{\pi}\,(2\mu\lambda)^{3/(2+\nu)}\, \frac{\nu}{2+\nu}\, [A(\nu)]^{3\nu/(2+\nu)} \left(n - \frac{1}{4}\right)^{2(\nu-1)/(2+\nu)} \tag{A.50}$$

with $A(\nu)$ given by (A.49).

Vita

Jose Juknevich

EDUCATION

2010 **Rutgers University**, Department of Physics, New Jersey, USA
PhD in Physics. Advisor: Prof. Matthew J. Strassler
Thesis topic: Phenomenology of Pure-Gauge Hidden Valleys at Hadron Colliders

2003 **Balseiro Institute**, Bariloche, Argentina *M. S. in Physics*
Advisor: Prof. Gerardo Aldazabal
Thesis topic: String Theory on Orientififolds and Gepner points

2002 **Balseiro Institute**, Bariloche, Argentina *B. S. in Physics*

PUBLICATIONS

1. J. E. Juknevich, *"Pure-Glue Hidden Valleys through the Higgs Portal,"* JHEP **1008**, 121(2010) arXiv:0911.5616 [hep-ph]
2. J. E. Juknevich, D. Melnikov and M. J. Strassler, *"A Pure-Glue Hidden Valley I. States and Decays,"* JHEP **0907**, 055 (2009) arXiv:0903.0883 [hep-ph].
3. A. Falkowski, J. Juknevich and J. Shelton, *"Dark Matter Through the Neutrino Portal,"* arXiv:0908.1790 [hep-ph].
4. G. Aldazabal, E. Andres and J. E. Juknevich, *"On SUSY standard-like models from orbifolds of D = 6 Gepner orientifolds,"* JHEP **0607**, 039 (2006) [arXiv:hep-th/0603217].
5. G. Aldazabal, E. C. Andres and J. E. Juknevich, *"Particle models from orientifolds at Gepner-orbifold points,"* JHEP **0405**, 054 (2004) [arXiv:hep-th/0403262].

ACADEMIC EXPERIENCE

2008-2010 **Graduate Assistant**, New High Energy Theory Center, Rutgers

2007-2008 **Teaching Assistant**, Department of Physics and Astronomy, Rutgers, *General Physics Lab 205, General Physics Lab 206.*

2004-2005 **Reseach Assistant**, University of Buenos Aires